REPORT DOCUMENTATION PAGE

Form Approved OMB No. 0704-0188

1. AGENCY USE ONLY (Leave blank)	2. REPORT DATE	3. REPORT TYPE AND DATES COVERED
	1-February 2000	Final Report, Jul 99 – Dec 99

4. TITLE AND SUBTITLE

Testing And Analysis Of Complex Structures To Improve CalcuRep

5. FUNDING NUMBERS

F61775-99-WE044

6. AUTHOR(S)

Mr. Stephan Verhoeven

7. PERFORMING ORGANIZATION NAME(S) AND ADDRESS(ES)

Delft University of Technology
Faculty of Aerospace Engineering; Kluyverweg 1
Delft 2629 HS
The Netherlands

8. PERFORMING ORGANIZATION REPORT NUMBER

N/A

9. SPONSORING/MONITORING AGENCY NAME(S) AND ADDRESS(ES)

EOARD
PSC 802 BOX 14
FPO 09499-0200

10. SPONSORING/MONITORING AGENCY REPORT NUMBER

SPC 99-4044

11. SUPPLEMENTARY NOTES

12a. DISTRIBUTION/AVAILABILITY STATEMENT

Approved for public release; distribution is unlimited.

12b. DISTRIBUTION CODE

A

13. ABSTRACT (Maximum 200 words)

This report results from a contract tasking Delft University of Technology as follows: The contractor shall investigate the performance of bonded composite repairs to complex metal aircraft structures in comparison with analytical predictions in order to verify new analytical models. Specifically, the contractor shall compare the performance of bonded composite repairs to cracked wide stiffened wing panels with unstiffened panels. Experimental results will also be compared with new analytical model predictions. The contractor's experimental data will aid the USAF Academy Center for Aircraft Structural Life Extension (CAStLE) in developing a more powerful version of the bonded repair program CalcuRep.

14. SUBJECT TERMS

EOARD, Aging Aircraft, Fatigue, Bonded Repair

15. NUMBER OF PAGES

117

16. PRICE CODE

N/A

17. SECURITY CLASSIFICATION OF REPORT	18. SECURITY CLASSIFICATION OF THIS PAGE	19. SECURITY CLASSIFICATION OF ABSTRACT	20. LIMITATION OF ABSTRACT
UNCLASSIFIED	UNCLASSIFIED	UNCLASSIFIED	UL

NSN 7540-01-280-5500

Standard Form 298 (Rev. 2-89)
Prescribed by ANSI Std. 239-18
298-102

TESTING AND ANALYSIS OF COMPLEX STRUCTURES TO IMPROVE CALCUREP SPC 99-4044

FINAL REPORT

EOARD CONTRACT: F61775-99-WE044

DATE: FEBRUARY 1, 2000

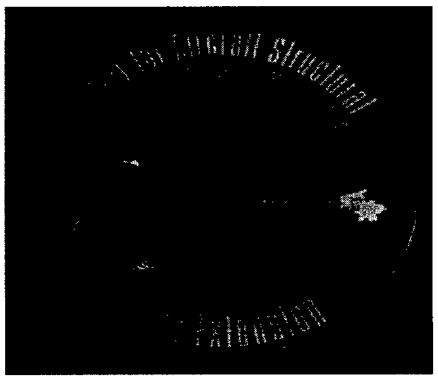

AUTHOR: S. VERHOEVEN

HQ USAFA/DFEM
CENTER FOR AIRCRAFT
STRUCTURAL LIFE EXTENSION
2354 FAIRCHILD DR., STE 6H2
USAF ACADEMY, CO 80840-6240
TELEPHONE: +1-719-333-2531
FAX: +1-719-333-2944
E-MAIL: STEPHAN.VERHOEVEN@USAFA.AF.MIL

PREFACE

In the following report the results of static and fatigue tests on integrally stiffened unpatched and patched wing panels are presented. The stiffened panels simulate C-141 lower wing skin panels. This report is the final deliverable for EOARD contract F61775-99-WE044.

It was the intention to use actual C-141 lower wing skin panels but, due to export restrictions and equipment limitations, this was not possible. It was therefore decided to use integrally stiffened panels simulating the C-141 panels.

The work on the machined panels started at USAFA before the start of the current EOARD contract, and data collection for the static tests and spectrum tests on unpatched panels was done at USAFA, Colorado. Preparations for the spectrum tests on the patched panels were performed at Delft University, and the actual spectrum tests were finished at USAFA.

United States Air Force Academy, Colorado

SUMMARY

The goal of this research was to obtain test data for crack growth in both unpatched and patched complex structures, in order to verify new and improved bonded repair analysis software, CalcuRep2000.

It was decided to consider the case of an integrally stiffened lower wing panel, similar to wing skin panels from the C-141. The example of the C-141 was chosen because this is one of the most well known cases of bonded repairs to complex structures. The repairs on the C-141 weep holes required extensive analytical as well as FE-modeling, and it is the intention to implement the capability of analyzing complex structures such as these in CalcuRep2000, combined with a spectrum loading capability. However, no test data are available to compare the new program to, and tests had to be carried out. This report will give the results of static and fatigue tests on integrally stiffened patched and unpatched panels.

Two different integrally stiffened panels were considered, a narrow panel with one central stiffener and a wide panel with three stiffeners. Static analyses of these panels showed that the grips introduce the loads satisfactorily. By measuring the strains on top of the stiffeners, it is evident that the load introduction into the stiffeners occurs over a small distance and that there is secondary bending in the panel. Comparison of the strains in the wide and the narrow panel showed that the strains are similar. It should be kept in mind that the panels did not have cracks at this point, which could change the stress distribution.

Testing the narrow panel in compression showed some non-linear behavior. This is due to the nature of the panel dimensions, which are not equivalent to the actual C-141 wing panel dimensions. Although the narrow panel can carry the maximum compressive load in the C-141 spectrum, the buckling characteristics of the narrow panel require reducing the maximum compressive spectrum load. Compressive testing of the wide panels resulted in compressive failure, possibly due to the fact that the total length of the specimen, including grips, is larger for the wide panel than for the narrow panel, and thus reduces the critical buckling load of the panel.

Two narrow and two wide unpatched panels were tested under spectrum loading. Two different spectra were used for testing: the original C-141 spectrum including compressive loads, and a modified spectrum in which the compressive loads are replaced by zero. Testing of two narrow unpatched panels showed larger crack growth rates in both skin and stiffener for the specimen loaded by the spectrum including the compressive loads. This is a direct cause of the compressive loads that reduce the effect of plastic zones that are formed by tensile loads. When testing a wide panel with a spectrum including compressive loads with a

maximum of -100 MPa, failure of the panel occurred in compression. This was expected from the static analysis. It was decided to use a spectrum with maximum compressive loads of –40 MPa on the wide panels. The specimen loaded by a spectrum with only tensile loads had significantly lower crack growth rates in both skin and stiffener, compared to the specimen that was loaded by a spectrum including compressive loads.

Four patched narrow panels were tested: two panels with boron-epoxy patches and two panels with Glare patches. Comparing specimens loaded by spectra including compressive loads to specimens loaded only by a tensile spectrum showed only marginal differences. The omission of compressive loads has no significant effect on crack growth under patches. This can be explained by the fact that high tensile loads cannot cause significant plastic zones at the crack tip due to the large reduction in stress intensity factor underneath the patch. Because of the relatively small plastic zones, the compressive stresses cannot cause a large difference in crack growth rates by decreasing the effect of plastic zones that are not present to begin with. No significant difference in performance between Glare and boron-epoxy patches, both in tension and in compression, was found. Possible splitting of the boron-epoxy patch does not seem to be of concern, and the difference in performance due to the different coefficients of thermal expansion of boron-epoxy and Glare seems to be compensated by other effects, possibly shear lag in the thicker Glare patches and a difference in bending behavior between the thick Glare patches and the thin boron-epoxy patches. The difference in starter crack size does not influence the crack growth rates significantly, as can be expected from the Rose model. Comparing crack growth rates of narrow patched and unpatched panels showed that the crack growth is significantly reduced by the presence of the patches, and the stiffeners did not fail in any of the patched specimens. The repairs easily withstand one full C-141 life.

Four wide patched panels were tested: two with Glare patches and two with boron-epoxy patches. There was no significant difference in crack growth rates between the specimens loaded by a spectrum including compressive loads and by a spectrum without compressive loads. As was the case with the narrow panels, there appears to be no significant difference in crack growth behavior between the specimens with boron-epoxy patches and the specimens with Glare patches. Possible splitting of the patch does not seem to be of any concern and differences in the coefficients of thermal expansion seem to be overruled by other effects, possibly shear lag and differences in bending behavior between the Glare and boron-epoxy patches. By comparing the crack growth rates for the skin cracks of the patched and unpatched panels, it can be seen that the patched cracks grow at a significantly lower rate than the unpatched cracks. During the tests, the center stiffeners did not fail in any of the specimens, and the repairs easily withstood one full life.

Comparison of the crack growth rates of the patched narrow and wide panels, tested under the C-141 spectrum with only tensile loads, showed that the crack growth rates for the skin cracks were all of the same order of magnitude, and apparently load attraction does not play a significant role in these panels. Therefore, it appears to be valid to use the narrow panels for fatigue crack growth experiments of patched cracks.

The data obtained during this research can be readily used for verification of the new and/or improved models in CalcuRep2000 (scheduled for release in summer 2000). It will be straightforward to generate stress intensity files for each block by using these spectrum files as input files in CalcuRep2000. Output files containing K values or ΔK values can be generated, and by using a crack growth prediction code, the crack extension can be calculated for each block and direct comparison with the results in this report will be possible.

TABLE OF CONTENTS

LIST OF FIGURES

LIST OF TABLES

1. INTRODUCTION

1.1 PROJECT BACKGROUND

As is described in the EOARD contract, the goal of this research is to obtain test data for crack growth in both unpatched and patched complex structures. The data that will be obtained during this test program will be used for verification of the new and improved models that will be implemented in a new version of CalcuRep: CalcuRep2000. In this chapter a short description will be given of the current capabilities and limitations of CalcuRep, as well as the planned improvements. Also a description of the structure tested, simulating an actual repair on a C-141, is given.

1.1.1 Current version of CalcuRep

Before airlines and airworthiness authorities will consider crack patching a viable repair alternative, it is important that the analysis can be performed in the field by an aircraft maintenance engineer. This implies that the complex analysis must be transformed to a user-friendly and easy-to-use software package for design and analysis with conservative engineering guidelines so that acceptable repairs can be designed. Until recently, the detailed design and analysis of bonded repairs could only be performed by specialist teams, due to the complexity of the analyses.

In close cooperation, the United States Air Force Academy and Delft University of Technology developed a software package, CalcuRep [1], that allows non-specialists, such as maintenance engineers with limited knowledge of bonded repair analysis, to design and analyze bonded repairs. CalcuRep contains pull-down menus of material, mechanical and physical properties that are easy to use, and the output consists of acceptability guidelines.

The analytical model in CalcuRep is based on the Rose model [2], developed at the Aeronautical and Maritime Research Laboratories (AMRL) in the early 1980's. The Rose-model accounts for stress reduction under the patch and load attraction to the patch due to a stiff inclusion. The Rose model is a continuum two-dimensional model that considers only elliptical patches, bonded to infinite flat sheets under bi-axial loading. In CalcuRep, the Rose model has been extended to include important thermal effects. These effects are induced by curing of the adhesive and by operating temperatures but in CalcuRep, the thermal model was slightly modified from that of the original Rose model. The second extension that was added calculates the effect of secondary bending induced by a single-sided repair.

With CalcuRep it is possible to quickly optimize the patch material and geometry with respect to the stress intensity reduction at the crack tip and the adhesive shear strain, for a given skin thickness, adhesive system and cruise temperature.

1.1.2 Planned improvements in CalcuRep2000

Although the models that are incorporated in CalcuRep are already extensive, CalcuRep has some limitations in its current version which make the development of a new version, CalcuRep2000, necessary in order to make the program more useful for USAF applications. A demonstration version of the new program was presented at the Aircraft Structural Integrity Program 1999 conference in San Antonio, Texas [3].

As was mentioned in the previous paragraph, the current version of CalcuRep is based on the Rose model. The Rose model is valid for elliptical patches, bonded to infinite flat sheets under bi-axial loading. Although this model is satisfactory for flat specimens that are being tested in the laboratory, previous research using a more realistic barrel test set-up [4] showed that CalcuRep was less accurate in predicting stresses underneath and around bonded repairs in a more realistic structure. Measured stresses and stress intensity factors did not match the predictions made by CalcuRep. Another reason for developing CalcuRep2000 is the fact that there are some errors in the current version in the thermal model as well as in the model for secondary bending.

As was mentioned before, the first CalcuRep for Windows version allowed the user to make quick and simple design studies. The version was geared towards maintenance personnel designing simple fuselage repairs. Despite the fact that the program had limited capabilities, it could still cover a majority of the expected repairs. However, one of the most likely locations for cracks to occur is in and around stress concentrations, instead of in the middle of a undisturbed sheet. Although the influence of the rivet hole itself on the crack intensity factor at the crack tip is not assumed to be large, one should keep in mind that the presence of rivets indicates the presence of structural members such as stiffeners and frames. The substructures can have a large influence on, for example, secondary bending and can change thermal constraints and thus the effective coefficient of thermal expansion (CTE), changing thermal residual stresses underneath and around the repair. This can significantly affect the stresses at the crack tips and at the patch tips.

The major effort in developing CalcuRep2000 is focussed on expanding the model to be capable of designing more complex bonded repairs. Much of this effort is performed in Australia at Monash University and the Aeronautical and Maritime Research Laboratory (AMRL). It involves a parametric Finite Element Method (FEM) as well as an analytical study of different design variables such as: stiffener spacing, stiffener height, ratio of stringer stiffness vs. skin thickness, broken stiffeners, cracked skin, riveted vs. integral stiffeners, etc. One possibility to incorporate this data is a lookup table with correction factors if more complex geometries are to be repaired .

DERA (Defence Evaluation and Research Agency) and AFRL (Air Force Research Laboratory) are expanding the database of the effects of crack growth under spectrum fatigue loading. DERA studies the effects of spectrum loading and overloads when bonded repairs are used. Some of these effects were studied earlier for the application and verification of the C-5A repair performed in 1995. CAStLE (Center for Aircraft Structural Life Extension) and Delft University are implementing the new knowledge and models into the new computer code which will be released in 2000. However, CalcuRep2000 will not be a crack growth prediction program. Through input and output files the user can combine the repair results with a crack-growth program of choice.

Of course these new and improved models need verification using test data. Monash University is performing tests on riveted stiffened panels and the research presented in this report is focusing on integrally stiffened panels. It was decided to consider the case of an integrally stiffened lower wing panel, similar to wing skin panels from the C-141. The example of the C-141 was chosen because this is one of the most well known cases of bonded repairs to complex structures. The repairs on the C-141 weep holes required extensive analytical as well as FE-modeling and it is the intention to implement the capability of analyzing complex structures such as these in CalcuRep2000. However, no test data is available to compare to the new and improved models and tests need to be carried out. More on the C-141 can be found in the next paragraph.

Although actual C-141 panels were available for testing at the Center for Aircraft Structural Life Extension (USAFA), these panels could not be tested at the Academy labs due to equipment limitations, and due to export restrictions it was not possible to perform these tests outside the United States. Therefore it was decided to test generic stiffened panels that simulate the C-141 panels.

1.2 BACKGROUND OF TESTED STRUCTURE: THE C-141

1.2.1 History of the C-141

The C-141A (Fig.1.1) was designed and manufactured by Lockheed as a long-range, heavy logistics transport aircraft and was entered into service in January 1964. The primary materials in the aircraft are the 7000-series aluminum alloys heat-treated to the T6 condition, an alloy well known for its sensitivity to fatigue. The original design life goal for the aircraft was 30,000 flight hours, and a full-scale fatigue test was performed to validate this design goal. In addition, the aircraft was designed to be fail-safe for a single-element failure (e.g., a single wing plank), which was then the standard for commercial aircraft design.

Ten years after the aircraft had been in service, it was evident that the fuselage was volume-limited for a number of logistic missions. By 1974 a decision was made to add approximately 22 ft. to the length of the fuselage and to add in-flight refueling capability to the aircraft. Due to the increased weight of the aircraft, the

loading of the wing also increased. An assessment was made in 1977 to find out if there was enough remaining life to justify the modifications. It was found that the lower-bound economic service life was 45,000 hours of the then-current use spectrum modified by addition of in-flight refueling missions (called the SLA-IIB spectrum). After the fuselage extension the aircraft were re-designated as the C-141B.

1.2.2 Weep hole problem

By late 1992 the aircraft had reached an average of about 35,000 equivalent SLA-IIB spectrum hours, with some higher-time aircraft approaching the 45,000-hour economic service life estimate. Because of delays and uncertainty about the future of the C-17 (the replacement for the C-141B), Congress decided that a committee had to determine the technical feasibility of extending the service life of the aircraft. As part of this study, directly after operation Desert storm in which the C-141 fleet was heavily used, teardown inspections of the wings were done for two service aircraft, which had about 45,000 equivalent SLA-IIB spectrum hours. These teardown inspections showed evidence of wide spread fatigue damage (WFD) in the fuel drain holes (the so-called "weep holes") in the integral stiffeners in the lower wing skins. The C-141 has lower wing skins that are made of aluminum 7075-T6 with integral stiffeners. In order to use the full fuel capacity of the wing, weep holes were drilled in the bottom of the risers near the skin at the time of production of the aircraft. In that way, fuel is able to flow from one side of the stiffener to the other side and it is possible to move the fuel between the stiffeners towards the fuel pumps. However, these weep holes caused stress concentrations and, since the lower wing skins are predominantly in tension, cracks started to occur in the stiffeners, growing from the weep holes upward to the top of the stiffener and from the weep holes downward to the skin. The actual stiffeners in the C-141 did not break.

Methods to protect the structural safety until aircraft retirement or replacement of the lower wing skins were investigated and included: increased inspections, expansion of the holes in order to introduce compressive residual stresses, and the use of bonded composite doublers (patches). As of 1993, the weep hole cracking problem was brought successfully under control through a combination of inspections, the use of bonded boron/epoxy repair doublers, the cold working of holes where possible, and in some cases the replacement of wing panels. This took a joint effort by Warner-Robins ALC and their supporting contractors, with assistance from the Air Force's Wright Laboratories.

1.2.3 Future plans for fleet

The C-141B's are now in the process of being retired and replaced by the C-17, but they will not be completely phased out of the inventory for several more years. Plans for the C-141 fleet are to convert 63 aircraft to the C-141C. The major work in this conversion will be the installation of a glass cockpit and new avionics. Plans are to retire the C-141B by the end of FY2002 and to retire the

C-141C by the end of FY2006. Until it is retired, the structural management of the C-141 force will continue to be a significant challenge, emphasizing the need for safe and economical repairs for aging aircraft.

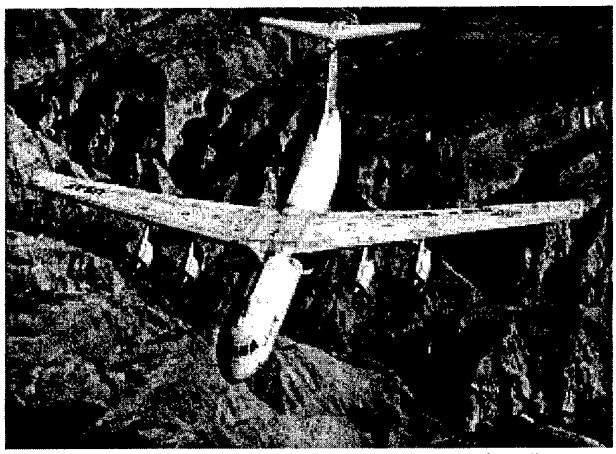

Fig.1.1 : The C-141B "Starlifter".

2. TEST APPROACH

This chapter will describe the test plan, test methods and specimens used in this research.

2.1 LOADS ON LOWER WING SKIN

Tests that were done by CAStLE (Center for Aircraft Structural Life Extension) in the past were mainly on thin flat aluminum sheet specimens under constant amplitude loading. In the case of a fuselage skin, the actual loads can be approximated by constant amplitude loading, but the loading conditions for a lower wing skin of a large transport are dominated by atmospheric turbulence, and thus variable amplitude loads, also called spectrum loads, are required.

In the recent past some qualification tests were done at USAFA and Delft University of Technology under more realistic variable amplitude loading conditions for a prototype bonded Glare (fiber metal laminate) repair on the aft crown section of a C-5A. This repair was performed in 1995. The repair that was applied was a thin skin repair, although some frames and stiffeners were present underneath the structure. However, only the skin showed stress corrosion cracking and needed repair, the underlying structure remained intact.

As was the case with the C-5A, the loading conditions of the C-141 lower wing skin cannot be simulated realistically using constant amplitude loading, and information was requested from Warner-Robins ALC to obtain the fatigue spectrum of the C-141 lower wing skin. The following paragraphs describe the methods of preparing the spectrum, as were used in the case of the C-5A. Although further information on the C-141 spectrum cannot be given, it is assumed that this procedure was also used by Warner Robins in preparation of the spectrum data for the C-141.

Generation of spectrum data

The spectrum data that were supplied by Warner-Robins ALC are based on statistical data. The spectrum data is obtained by statistical determination of the cyclic loading that the aircraft structure will experience during its service life. The basic ingredients required in this statistical process are repeated loads, environmental criteria, and aircraft usage [5]. This paragraph will give a short background description of the spectrum data that were used.

Repeated loads and environmental criteria

The terminology "repeated loads" is used in describing the external loads experienced by the aircraft. Since these loads vary with the aircraft's operating conditions (for example, fuel weight, cargo weight, speed, altitude, etc.), unit loads are calculated at increments of these operational parameters throughout the normal operating envelope. The resulting unit loads, stored in grid form, are

directly convertible to stresses by use of the stress-to-load ratios induced at specific aircraft locations. These stress grids are structured in order to allow linear interpolation between grids in order to match input mission segment conditions. These stress grids are known as a "loads system".

In the same way, statistical definitions of the aircraft's operating environment, determined from recorded data, are stored in grid format to allow interpolation to the required conditions. For a flight condition, these statistical definitions of the aircraft response to its environment include parameters such as the percentage of time spent in atmospheric turbulence of a defined intensity, or the number and magnitude of maneuvers that are expected as a function of mission or segment type. These statistical definitions of the operating environment are known as the "environmental criteria".

Mission profiles and utilization

Usage for repeated loads or stress spectra computation is analytically defined by "mission profiles". A mission profile is a collection of individual mission segments, properly sequenced, which define the fuel weight, cargo weight, altitude, speed, and aircraft configuration throughout a complete flight from ramp to final taxi in a chronological order. A mission segment is one portion of a mission profile during which the external 1.0 g loads and incremental loads are considered constant for analysis purposes. The number of segments required to define a mission profile is determined by the complexity of the scenario itself (e.g. number of configuration changes, flight duration, weight changes during flight, etc.) and by engineering judgment as to how much variation of external loads within a segment can be tolerated without adversely influencing analysis results.

Similarly, a "mission profile set" is a collection of mission profiles which, when utilization weighted, define the projected overall usage throughout the service life. The number of profiles required to define the mission profile set is determined by the complexity of the overall usage.

Spectrum Development Program

The data obtained by the procedures in the previous paragraphs are the input data for the P6049 Spectra Development Program. The main function of the P6049 Spectra Development Program is to write discrete pairs of min-max stresses representing stresses which are expected to occur during each segment of a specified mission profile at a specified structural location under average environmental conditions. More information about these functions of the P6049 program can be found in [5].

The output of the P6049 program contains a non-integer number of cycles that can be used for a crack growth prediction program but not for usage on fatigue machines that require an integer number of cycles. Further editing, using software developed at Delft University, is necessary. Each pass (also called a

"block") represents 504.5 flight hours. Fractional occurrences are summed and when an occurrence value of 1 is reached they are placed in the spectrum. Hence there are a different number of cycles in each pass. Also, the spectrum is filtered to remove cycles with $\Delta\sigma$'s of less than 3500 psi to reduce the number of cycles for testing. More information about the C-141 spectrum can be seen in Table 2.1. Whereas the actual C-141 spectrum contains compressive loads up to –100 MPa, there will also be a modified C-141 spectrum, in which the compressive loads are replaced by loads equivalent to zero. A total of 60 blocks represents one C-141 lifetime.

PASS #	MIN STRESS (PSI)	MAX STRESS (PSI)	NUMBER OF CYCLES	PASS #	MIN STRESS (PSI)	MAX STRESS (PSI)	NUMBER OF CYCLES
1	-14182.230	16387.051	5637	31	-14182.230	19374.359	6854
2	-14182.230	16387.051	5666	32	-14817.160	17893.750	6829
3	-14171.050	17108.199	6699	33	-14734.200	17893.750	6847
4	-14182.230	16387.051	6180	34	-15567.160	18631.480	6881
5	-14182.230	17108.199	6670	35	-14182.230	17879.420	6893
6	-14182.230	17028.650	6602	36	-14932.230	18264.590	6822
7	-14734.200	16395.100	6799	37	-14921.050	18629.420	6848
8	-14817.160	17893.750	6612	38	-14182.230	17108.199	6714
9	-14932.230	16803.160	6789	39	-14817.160	17129.420	6966
10	-14182.230	17108.199	6435	40	-14734.200	17893.750	6759
11	-14182.230	17108.199	6833	41	-14921.050	18286.170	6668
12	-14182.230	17028.650	6695	42	-14942.710	17688.500	7035
13	-14182.230	17108.199	6852	43	-14182.230	18643.750	6794
14	-14921.050	16952.221	6684	44	-14579.000	17319.820	6777
15	-14192.710	17199.570	6689	45	-14932.230	17610.400	6883
16	-14817.160	17893.750	6810	46	-15682.230	18010.240	6692
17	-14182.230	16803.160	6858	47	-14817.160	17131.480	6855
18	-14932.230	17879.420	6695	48	-15671.050	18049.730	6875
19	-14182.230	18629.420	6803	49	-14669.650	17659.760	6783
20	-14734.200	17129.420	6680	50	-14182.230	17494.631	6883
21	-14817.160	17514.590	6893	51	-14182.230	17199.570	6761
22	-14182.230	18643.750	6739	52	-14192.710	17879.420	6879
23	-14895.790	17610.400	6782	53	-14782.230	18060.160	6963
24	-14932.230	17893.750	6818	54	-14932.230	18052.080	6692
25	-14182.230	17659.760	6766	55	-14817.160	19308.609	6816
26	-14182.230	16980.869	6926	56	-14182.230	18624.359	6813
27	-14932.230	18052.080	6862	57	-14182.230	18609.980	6915
28	-14032.230	17142.930	6694	58	-14171.050	17299.730	6828
29	-14182.230	18452.221	6840	59	-15484.200	19393.750	6687
30	-15484.200	17199.570	6603	60	-14895.790	18529.340	6869

Table 2.1: Minimum and maximum stress, number of cycles per pass for C-141 spectrum [6].

2.2 TEST PLAN

Several different types of tests are done during this program. Two different panels were used, a narrow panel (designated with N) with one central stiffener and a wide panel (designated with W) with three stiffeners, of which only the center stiffener contains a weep hole.

The first tests are static tests using strain gages. Both a narrow as well as a wide panel are equipped with strain gages and tests are done to check whether the grips are loading the panels accurately. Strains should be symmetric over the panels and, in order to use the narrow panels for research purposes, the strain distribution in the narrow panel should be similar compared to those in the wide panel. A comparison with a FE-model is also made. Static tests are done both in tension and in compression.
After the static tests, two narrow panels are loaded in fatigue using constant amplitude (CA) loads to look at the crack initiation behavior of the panels. This is important because the panels have to be pre-cracked before the patches can be applied. The remainder of the tests are all fatigue tests using the original C-141 spectrum with a maximum compressive load of –100 MPa, and the modified C-141 spectrum from which the compressive loads are removed (set at zero MPa). For some specimens the compression loads are eliminated to see if this causes any difference in the crack growth behavior between Glare and boron-epoxy patches. The test overview can be seen in Table 2.2. As can be seen, the compressive loads with the C-141 spectrum for the wide panels are limited to –40 MPa whereas the narrow panels are loaded by spectra with compressive loads up to –100 MPa (this is the original C-141 spectrum, more about this can be found in Paragraph 3.4). Both panel types are also loaded with a C-141 spectrum where all the compressive loads are replaced by zero MPa.

The loading ramp rates at which the spectrum tests are carried out, are 90 kN/sec for the narrow panels and 270 kN/sec for the wide panels. Because the cross sectional area of the wide panel is three times the cross sectional area of the narrow panel, the resulting frequencies are identical for both types of specimens.

Panel designation	Pre-crack load (MPa)	Loading condition, max. compression loads (MPa)	Patch material	Weep hole diameter and distance from center of hole to inside of skin (mm)
N1	60-3	Static analysis/ Crack initiation test CA	No patches	6.35/5.97
N2	60-3	Crack initiation test CA	No patches	3.18/5.97
N3	60-3	C-141 spectrum, -100	No patches	6.35/7.35
N4	60-3	C-141 spectrum, 0	No patches	6.35/7.35
N5	60-3	C-141 spectrum, 0	Boron-epoxy	6.35/7.35
N6	60-3	C-141 spectrum, -100	Boron-epoxy	6.35/7.35
N7	60-3	C-141 spectrum, -100	Glare	6.35/7.35
N8	60-3	C-141 spectrum, 0	Glare	6.35/7.35
Extra test	60-3	C-141 spectrum, 0	Boron-epoxy	6.35/7.35
W1	60-3	Static analysis/ C-141 spectrum, -100	No patches	6.35/7.35
W2	60-3	C-141 spectrum, 0	No patches	6.35/7.35
W3	60-3	C-141 spectrum, -40	No patches	6.35/7.35
W4	60-3	C-141 spectrum, -40	Boron-epoxy	6.35/7.35
W5	60-3	C-141 spectrum, 0	Boron-epoxy	6.35/7.35
W6	60-3	C-141 spectrum, -40	Glare	6.35/7.35
W7	60-3	C-141 spectrum, 0	Glare	6.35/7.35

Table 2.2: Overview of test specimens.

2.3 SPECIMENS

The dimensions of the integrally stiffened panels as well as the repair description will be given in the following paragraphs.

2.3.1 Panel description

The panels that are used are machined from 1-inch thick aluminum 7075-T6. Although the C-141 panels have stiffeners of approximately 2-inch height, 1-inch thick plate material was used to limit material and machining costs. A complication when machining integrally stiffened panels from thick plate material is that the removing of material can result in a change of the internal stress state, resulting in warping of the panel. This can adversely affect the accuracy of the panel dimensions.

Two different panels were used, a narrow panel with one central stiffener and a wide panel with three stiffeners of which only the center stiffener contains a weep hole. The dimensions of these two different configurations can be seen in Fig.2.1. and Fig.2.2. The narrow panel was chosen to limit material and equipment requirements, as well as to study the width effect on crack growth. Verification is necessary to see whether the usage of narrow panels is justified.

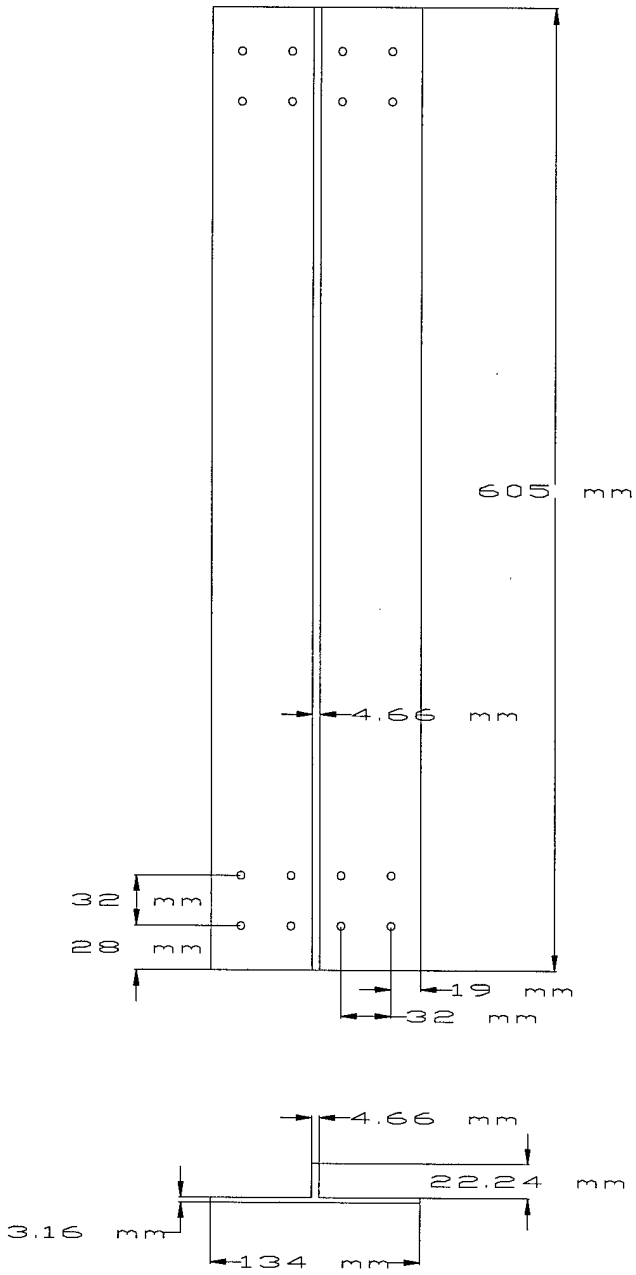

Fig.2.1: Dimensions of narrow panel with one center stiffener.

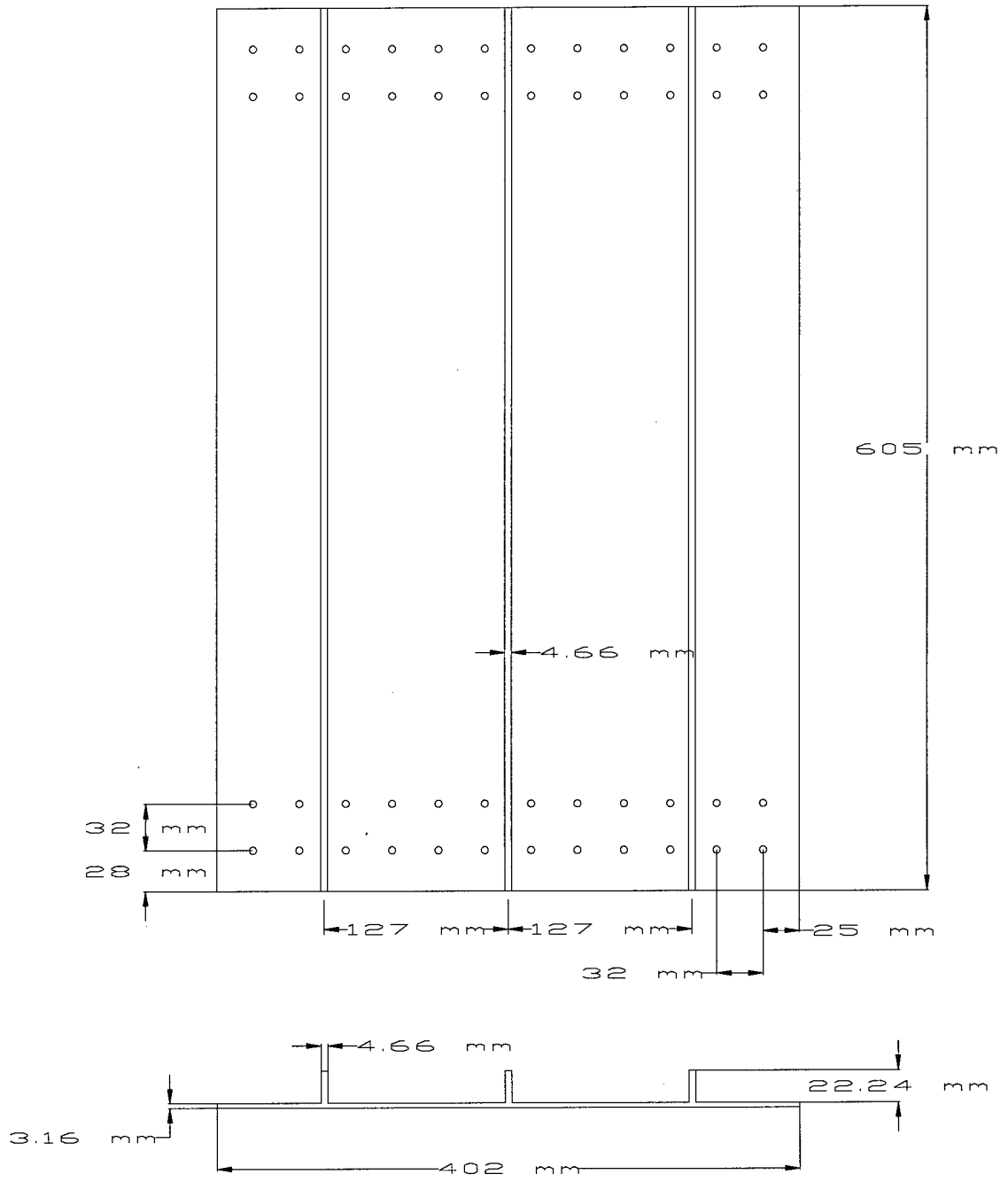

Fig.2.2: Dimensions of wide panel with three stiffeners.

Fig.2.3 shows a 3D picture of the panel with 3 integral stiffeners and weep holes. Only the center stiffener has a weep hole in the panels tested. The weep holes in the wide panels are made by using an electric discharge machine. For the narrow panels it is possible to use a conventional drill.

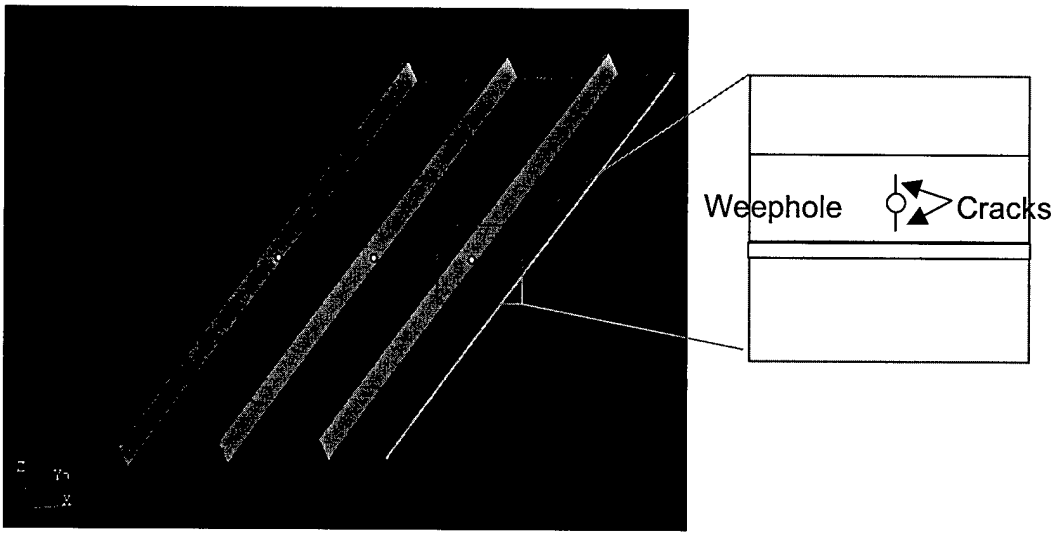

Fig.2.3: 3D picture of stiffened panel with weep holes [7].

For the C-141 weep hole repairs, the fatigue cracking problem is predominantly in the integral stiffeners. Cracks emanating from the weep hole grow towards the top of the stiffener (not reaching the top), away from the skin, and from the weep hole towards the skin.

2.3.2 Gripping of the panels

To be able to load the panels in the fatigue machine, it is necessary to use grips. The grips consist of two flat plates on each side of the panel. The stiffeners run to the end of the panel and thus one side of the grips has milled slots to accommodate the ends of the stiffeners.

It was decided only to grip the skin and not the stiffeners. The stiffeners are loaded through the skin. Some distance is needed before the stiffener is completely loaded over the entire height. This way of loading also introduces a problem: the load that is introduced is not located at the neutral line of the panel, hence secondary bending occurs. This might result in problems with crack initiation in the weep hole. In the actual C-141 structure cracks tend to grow from both sides of the weep hole, but in the case of the panel it is possible that the crack will initiate at one side of the weep hole edge, closest to the skin.

Fig.2.4 shows the grips of the wide panel, and specifically the side with the slots in the grips. The other side of the grips, the skin side, has no slots. Also grips with hole-pin connections instead of wedge grips were used during the tests.

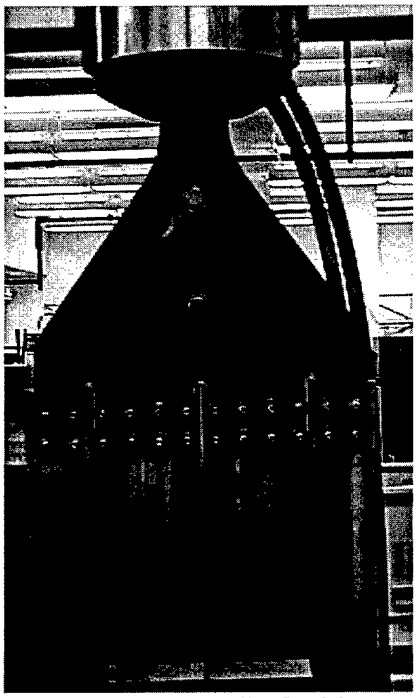

Fig.2.4: Grip detail of wide panel.

2.3.3 Patches: material choice

Two different patching materials were used in this research: boron-epoxy, as was used in the actual weep hole repairs, and the fiber metal laminate (FML) Glare. FML's consist of thin 0.2 to 0.5 mm aluminum alloy sheets, adhesively bonded in alternating layers with fiber/epoxy prepregs. A coding system is used to describe the lay-up of the laminate. For example, Glare2-3/2-0.2 has a 3/2 lay-up, i.e. 3 layers of Al 2024-T3, each with a thickness of 0.2 mm, separated by two unidirectional S2-glass fiber/epoxy prepreg layers (each with a thickness of 0.25 mm) that are both in the same direction (Glare2 has unidirectional fiber layers). There are several reasons why it is interesting to use different patch materials for this research. The first reason is the difference in Coefficient of Thermal Expansion (CTE) between the patching material and the structure that is being repaired.

The CTE in the longitudinal direction of boron ($4.5x10^{-6}/°C$) is low compared to the CTE of the aluminum ($22.5x10^{-6}/°C$). During the cure cycle in the unconstrained situation, as is the case when applying a patch to a relatively small test specimen, both materials are able to expand freely. The uncured adhesive is no restriction to both materials expanding. After curing at elevated temperatures, the adhesive will change into the cured state and bond the two materials. When the temperature decreases after curing, the aluminum will contract more than the boron and, since the adhesive is set, the parts cannot contract unrestricted, and the boron patch will put tensile stresses on the repaired crack in the panel (i.e. the patch tries to open the crack).

Glare2 has a thermal coefficient of expansion of $16.3x10^{-6}/°C$, which is still lower than the CTE of aluminum. This means that by cooling down from the cure temperature of 120°C, the aluminum still contracts more than the Glare patch. Again, this will cause residual thermal tensile (crack opening) stresses on the crack, but they will be lower than in the case of the boron patch.

If these panels, which are repaired in an unconstrained condition, are cooled down to cruise altitude temperatures, the aluminum will still contract more than the patches, resulting in additional tensile thermal stresses on the crack faces. Repairs made in an unconstrained situation, tested at the lowest service temperature, represent the worst case scenario with regards to thermal stresses, and will result in conservative test results.

Another reason for using different patch materials is to see whether both materials perform similarly in compression. The boron patches that are used are almost completely uni-directional, whereas the Glare patches are more "bi-axial" due to the aluminum layers. Compression loading might cause patch-splitting in the boron-epoxy patches.

2.3.4 Patches: dimensions

For each of the weep hole repairs, three patches are applied to the stiffened panel. A double sided repair is applied to the cracked stiffener and a single sided repair is applied to the flat skin side of the panel (which would be the outside of the actual C-141 wing, see Fig.2.9 for more details).

Boron-epoxy patches

The boron-epoxy skin patches are made out of 13 plies of Textron Specialty Materials 5521/4, with a thickness of 0.13 mm per ply, resulting in a total patch thickness of 1.69 mm. The stiffener patches have 8 plies with a total thickness of 1.04 mm. These lay-ups were chosen to keep the extensional stiffness (the Youngs modulus multiplied by the thickness) as close as possible to the extensional stiffness of the Glare patches. The stiffness ratio of the repairs, this is the extensional stiffness of the repairs divided by the extensional stiffness of the structure, is 1.2.

An inverted wedding cake lay-up was used, i.e. the largest ply is on the outside of the repair and the smallest ply is closest to the specimen. The advantage of the inverted wedding cake is that the number of exposed ply edges is reduced. Only the edge of the largest ply is exposed to the environment, the other plies are protected by this outer layer.

Tapering of the boron patches, in order to reduce stresses in the skin and adhesive at the patch tip, is accomplished by stepping down the length of the plies. The taper ratio is approximately 1:30. The dimensions of the boron-epoxy

patches can be seen in Fig.2.5 and Fig.2.6. The loading direction is parallel to the long side of the patches.

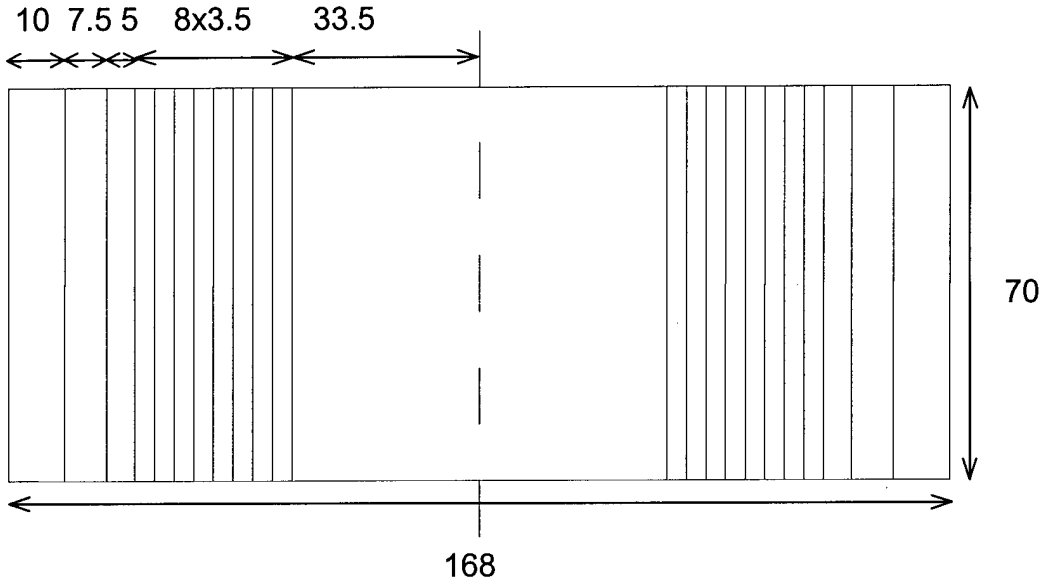

Fig.2.5: Boron-epoxy patch for skin side (all dimensions in mm).

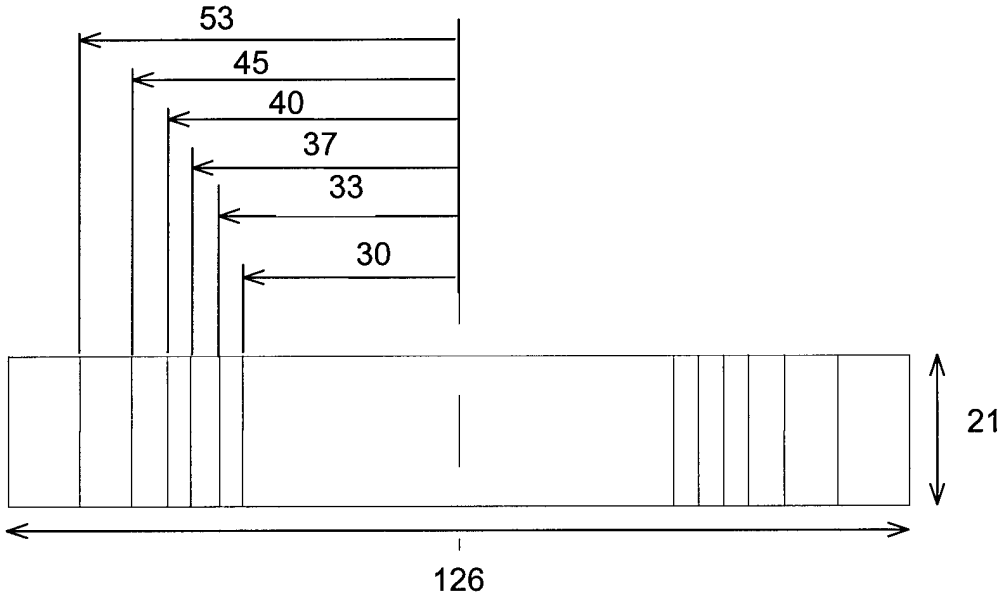

Fig.2.6: Boron-epoxy patch for stiffener (all dimensions in mm).

Glare patches

The Glare patches are made out of two different custom made Glare2 lay-ups: Glare2 8/7 0.3 with a thickness of 4.15 mm for the skin patches and Glare2 6/5 0.3 with a thickness of 3.05 mm for the stiffener patches. The stiffness ratio for these repairs were 1.2, similar to the stiffness ratios for the boron-epoxy repairs. To prevent high skin stresses and adhesive peel stresses, the edges of the Glare patches are tapered. This is accomplished by machining the edges of the patches. The taper ratio in the loading direction is 1:10, no taper is applied in the width direction, as is the case with the boron-epoxy patches. The stiffener patches are only tapered in the loading direction, the taper ratio is 1:10 as well. The outer dimensions of the Glare patches are similar to the boron- epoxy patches, see Fig.2.7 and Fig.2.8, and the loading direction is in the direction of the long side of the patches.

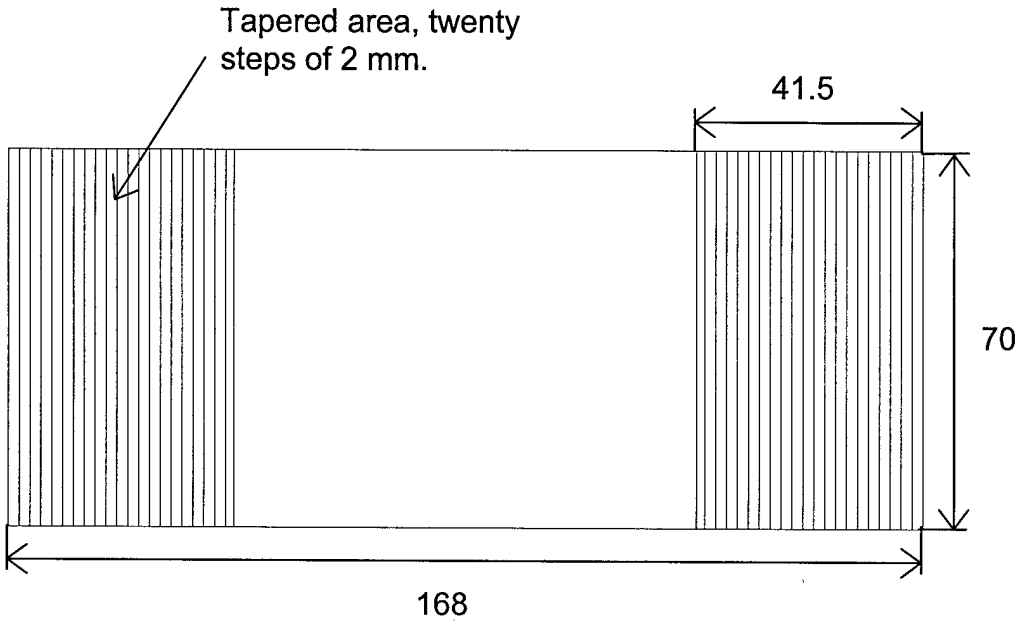

Fig.2.7: Glare2 8/7 0.3 patch for skin side (all dimensions in mm).

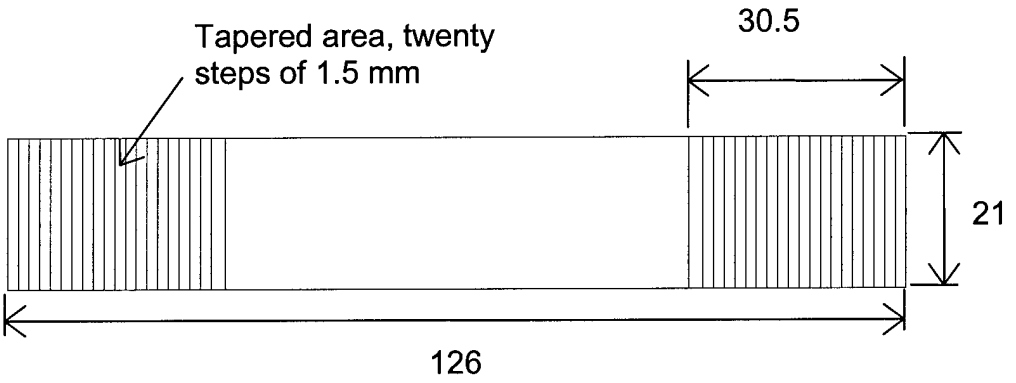

Fig.2.8: Glare2 6/5 0.3 patch for stiffener (all dimensions in mm).

2.3.5 Surface preparation procedure

One of the most important steps in the process of adhesive bonding is the surface pre-treatment. Before the patches can be bonded to the aluminum panels, the surface has to be cleaned of grease, dirt and other contaminants. The panels must have a stable oxide layer for good durability and corrosion resistance.

Two different surface preparations were used in this program:

- Grit blast-silane, followed by priming using BR-127 from Cytec
- Phosphoric acid anodizing (PAA) followed by priming using BR-127 from Cytec

Information about these surface preparation methods can be found in Appendix A.

2.3.6 Bonding of patches

After the surface pre-treatment and pre-cracking, the patches can be bonded to the panels. Before bonding the patches to the stiffener, the weep hole has to be filled to prevent air being trapped in the weep hole underneath the double sided patch. This could cause problems in the bond line. The weep hole is filled using an aluminum plug. FM-73 (Cytec, 0.06 psf) with a mat carrier is used. Two different methods are used for bonding; a hotbonder and autoclave. The cure cycle using the hotbonder is as follows:

- Apply full vacuum, approximately 20" Hg. Keep pressure for 30 minutes to allow all air out of vacuum bag.
- Increase temperature to 50 degrees Celsius at a rate of 3°C per minute. Keep at 50°C for 12 to 30 minutes.
- Decrease vacuum to 11" Hg and then increase temperature to 125°C at a rate of 3°C per minute.
- Cure for 1 hour at 125°.
- Decrease temperature at a rate of 5°C per minute. Do not remove vacuum above 70°C.

Some parts of the patching procedure with the hotbonder can be seen in Fig.2.9 through 2.11.

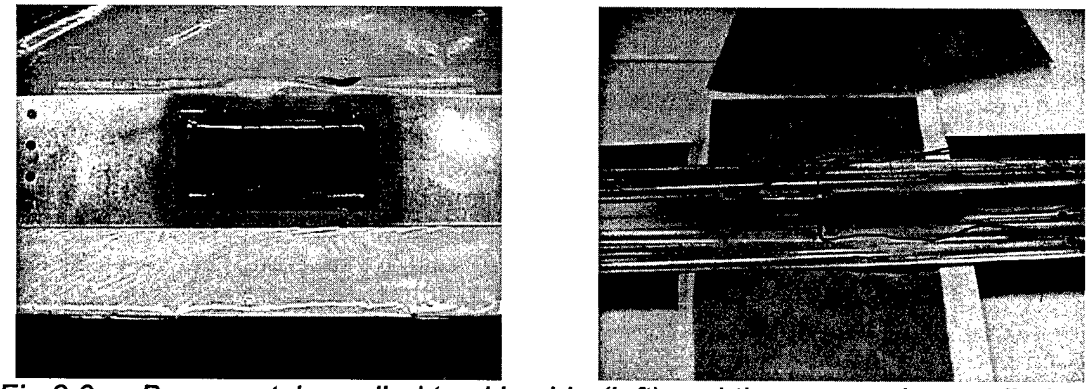

Fig.2.9: Boron patch applied to skin side (left) and thermocouples applied to stiffener side (right).

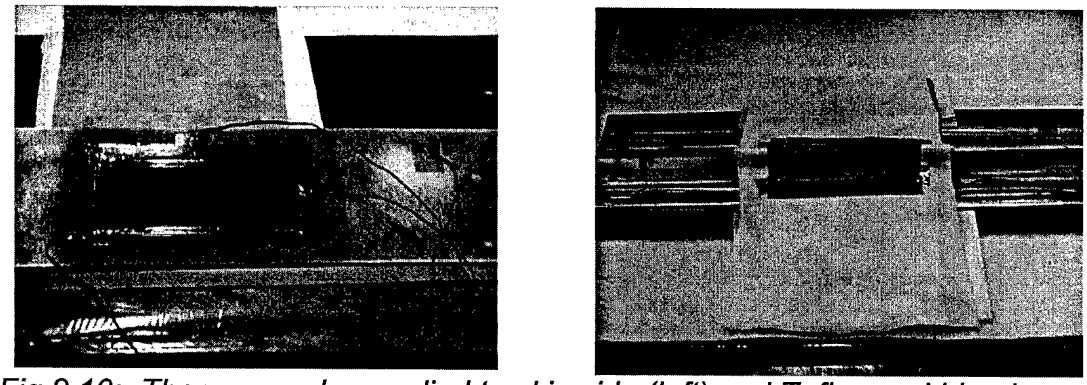

Fig.2.10: Thermocouples applied to skin side (left) and Teflon and bleeder on stiffener side (right).

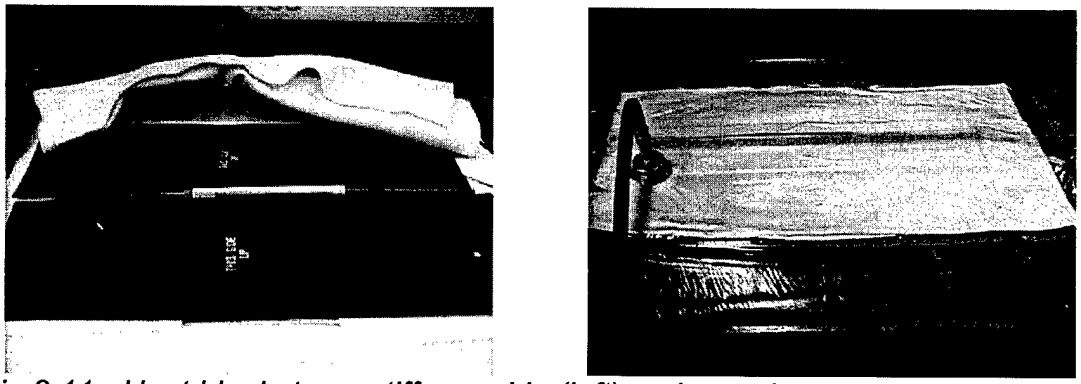

Fig.2.11: Heat blankets on stiffener side (left) and complete vacuum bag (right).

The cure cycle used with the autoclave is shown in Fig.2.12 and is in accordance with the recommended cure cycle from Cytec. It was not possible to use the exact same cycle used with the hotbonder; the autoclave was not able to create these small pressure differences with sufficient accuracy. As can be seen, the vacuum from the vacuum bag itself is released at a temperature of 60 degrees Celsius. The temperature ramp rate is 2.5 degrees Celsius per minute. A maximum of two wide panels and two narrow panels could be cured at the same time with the autoclave, resulting in significant time savings compared to the hotbonder.

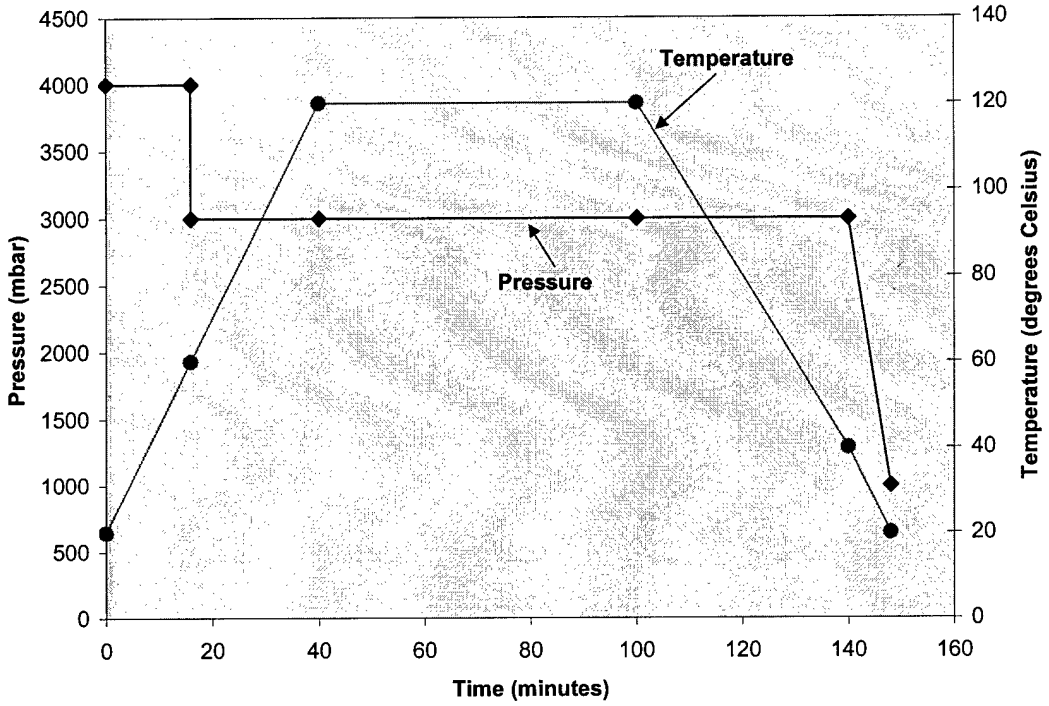

Fig.2.12: Cure cycle for FM-73 using autoclave

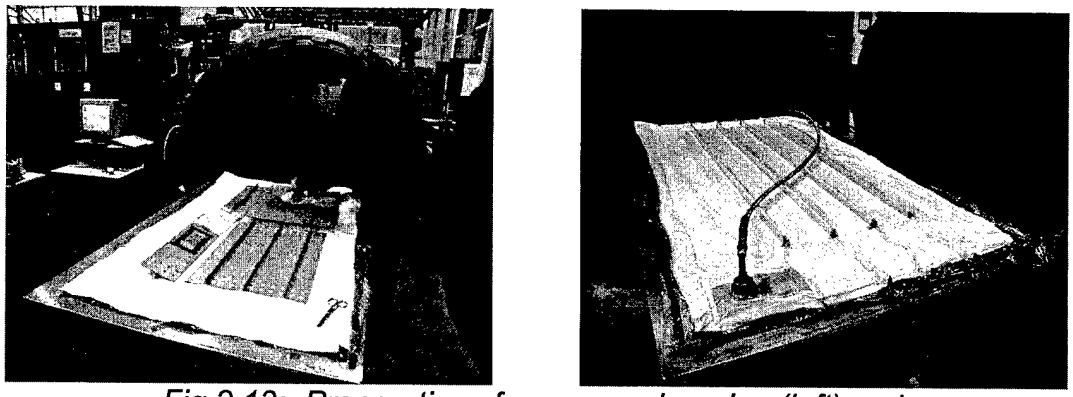

Fig.2.13: Preparations for vacuum bagging (left) and completed vacuum bag (right).

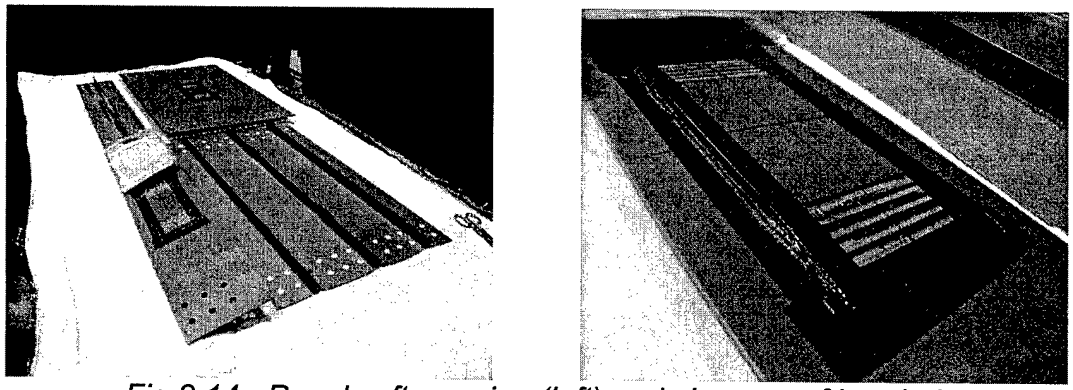

Fig.2.14: Panels after curing (left) and close-up of bonded Glare skin patch (right).

3. STATIC ANALYSES

As was mentioned before, two different panels are used: a narrow and a wide panel. The narrow panels are preferred since they reduce costs, reduce test equipment requirements and are easier to handle during testing. This chapter will describe the static tests. The static tests are done to determine if the panels are loaded correctly by the grips and to verify if the narrow panels can be used instead of the wide panels. The strain gage results are also compared to FE-results.

3.1 STRAIN GAGES ON UNPATCHED PANELS

To obtain the strains in the panels, strain gages were bonded to the surface of two unpatched panels. The strain gages that are used are CEA-13-240UZ-120 by Micro-Measurements Division. They are bonded to the aluminum surface using M-Bond 200.

Both a narrow panel (N1) and a wide panel (W1) are equipped with strain gages (12 gages on the narrow panel and 20 gages on the wide panel). Both the stiffener side (inside of tank), the flat skin side (outside of tank) and the stiffeners are equipped with gages. Fig.3.1 and Fig.3.2 show the locations of the strain gages on the panels. Strain gages that appear to be bonded to the top of the stiffener (1 and 4 for the narrow panel and 2,4,6,8,10 and 12 for the wide panel) are actually bonded on the side surface of the stiffener, as far up on the stiffener as possible. The width of the strain gages does not allow them to be positioned on the narrow side on top of the stiffener. Strain gages that are indicated in bold print are on the flat skin side (outside of tank) of the panel (7 through 12 for the narrow panel and 17 through 20 for the wide panel).

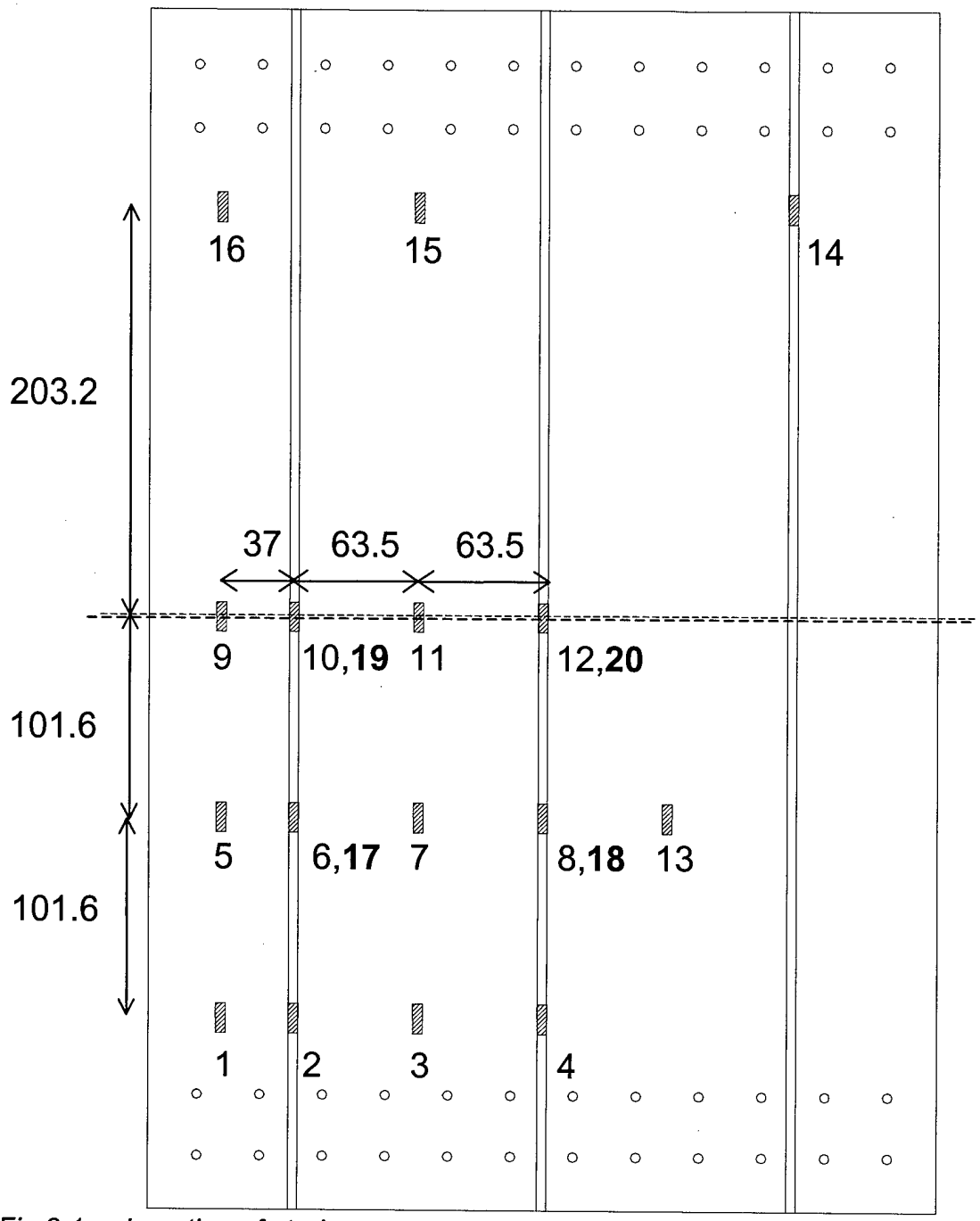

Fig.3.1: Location of strain gages on wide panel W1 (all dimensions in mm), strain gages in bold print are on flat skin side of panel.

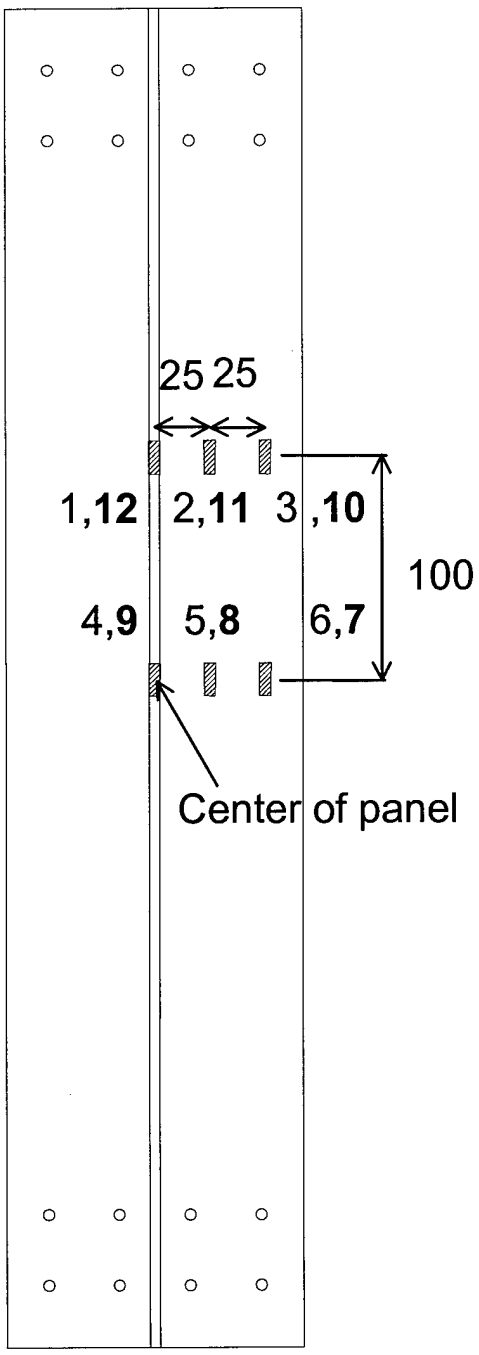

Fig.3.2: Location of strain gages on narrow panel N1 (all dimensions in mm), strain gages in bold print are on flat skin side of panel.

3.2 STRAIN GAGE RESULTS UNDER TENSION

3.2.1 Wide panel

It is preferred to load the panel in steps of 10 MPa up to 140 MPa, but for reasons of comparison with earlier strain gage tests, the panel was loaded in steps of 10 kN up to 220 kN, which is the equivalent of 140 MPa (the maximum load in the C-141 spectrum is approximately 134 MPa). However, the graphs are converted to MPa values to enable comparison with the narrow panel (the cross-sectional area of the wide panel is 1581 mm^2).

The results for the wide panel can be seen in Table 3.1 and Table 3.2. The results from gages 2 and 5 are not listed due to failure of these gages.

Force on panel (kN)	Stress on panel (MPa)	Strain readings (με)								
		1	3	4	6	7	8	9	10	11
10	6.35	106	116	73	53	94	64	102	64	96
20	12.65	201	221	148	118	185	128	196	133	189
30	18.98	290	327	223	184	278	196	291	206	283
40	25.30	384	435	296	253	370	265	386	281	377
50	31.63	478	543	370	324	463	335	482	358	470
60	37.95	567	651	442	394	556	408	577	437	564
70	44.28	656	762	513	465	650	481	672	518	657
80	50.60	746	873	582	538	744	555	768	599	751
90	56.93	832	987	653	611	838	631	864	682	845
100	63.25	922	1097	722	685	933	707	960	766	939
110	69.58	1009	1212	792	760	1028	785	1056	851	1033
120	75.90	1096	1327	863	836	1122	864	1152	937	1126
130	82.23	1185	1441	933	913	1218	945	1249	1024	1222
140	88.55	1272	1553	1004	991	1314	1026	1345	1112	1315
150	94.88	1361	1666	1076	1070	1410	1109	1441	1200	1409
160	101.20	1451	1779	1148	1149	1506	1193	1539	1290	1504
170	107.53	1537	1888	1219	1229	1602	1277	1635	1378	1598
180	113.85	1627	1995	1292	1310	1698	1361	1731	1469	1693
190	120.18	1721	2104	1364	1389	1793	1447	1828	1559	1787
200	126.50	1812	2210	1435	1468	1888	1532	1925	1649	1881
210	132.83	1900	2309	1503	1547	1984	1616	2022	1739	1975
220	139.15	1988	2404	1568	1629	2078	1700	2120	1830	2070

Table 3.1: Strain gage readings of wide panel, gage 1 through 11.

Force on panel (kN)	Stress on panel (MPa)	Strain readings (με)								
		12	13	14	15	16	17	18	19	20
10	6.35	53	99	18	102	103	105	104	100	107
20	12.65	108	193	57	196	196	200	201	194	207
30	18.98	167	288	100	291	290	295	300	288	309
40	25.30	230	383	144	386	384	388	397	380	409
50	31.63	295	478	190	482	477	481	496	473	510
60	37.95	363	574	237	577	571	574	592	564	608
70	44.28	434	670	285	672	665	666	689	655	707
80	50.60	506	766	335	768	759	758	787	746	806
90	56.93	580	862	387	864	853	850	885	837	904
100	63.25	657	958	439	960	948	943	982	927	1002
110	69.58	735	1054	492	1056	1042	1034	1078	1018	1100
120	75.90	815	1149	545	1152	1137	1126	1175	1108	1197
130	82.23	896	1246	599	1249	1232	1219	1274	1200	1296
140	88.55	979	1342	653	1345	1327	1309	1370	1289	1392
150	94.88	1063	1437	707	1441	1421	1401	1467	1380	1490
160	101.20	1149	1535	762	1539	1518	1494	1565	1470	1587
170	107.53	1235	1630	816	1635	1612	1584	1660	1560	1684
180	113.85	1321	1726	870	1731	1707	1676	1757	1652	1781
190	120.18	1408	1823	920	1828	1802	1770	1854	1743	1878
200	126.50	1496	1920	969	1925	1898	1860	1951	1833	1975
210	132.83	1584	2016	1015	2022	1994	1953	2048	1924	2071
220	139.15	1672	2114	1064	2120	2090	2044	2145	2013	2168

Table 3.2: Strain gage readings of wide panel, gage 12 through 20.

Fig.3.3 shows the strain readings of the gages on the skin on the stiffener side of the panel in the outer bays (note that gages 1 and 5 failed). Gage 9, which is located on the horizontal centerline of the panel, shows similar results compared to gage 16, which is located close to the grips, i.e. the load distribution is constant in the loading direction. The maximum strain is approximately 2100 με at 140 MPa applied stress.

Fig.3.4 shows the strain readings of the gages on the skin on the stiffener side of the panel in the inner bays. All gages show similar readings (approximately 2100 με at 140 MPa, except for gage 3 which shows somewhat higher strains. Gage 15, which is at a similar location as gage 3, does show similar readings compared to the other skin gages on the stiffener side of the panel. The only explanation for the divergent results of gage 3 must be error in the gage itself, in the electric circuit of the gage or misalignment of the gage.

Fig.3.5 combines the two previous graphs. It is clear that the load is evenly distributed, both in the width as well as in the loading direction. It can therefore be concluded that the grips introduce the loads satisfactorily as far as distributing the load over the panel is concerned.

Fig. 3.6 shows the strains from the strain gages on the outside of the tank (the flat side of the panel). All these four gages are located on the adjacent side of a stiffener. As can be seen, all four gages show similar results, the maximum strain reading is approximately 2100 με, similar to the readings of skin gages on the stiffener side of the panel. This can be clearly seen from Fig.3.7, which combines all skin gages, both inside and outside of the tank.

Fig.3.8 shows the strain readings of gages that are located on the top of the stiffeners. From gages 4,8 and 12, it is evident that the loading of the stiffeners occurs over a small distance. These gages are all located on the center stiffener and all three show equivalent readings. Two strain gages, 10 and 14, show divergent results. Gage 14 shows results that are significantly too low. Gage 2, which is positioned at a similar location compared to gage 14, failed during the test so no comparison can be made. It is possible that the outer stiffeners are not fully loaded close to the grips but gage 6 on the outer stiffener, which is closer to the center of the panel, shows similar results as the other gages. Gage 10 shows a somewhat higher reading, but the difference with the other gages is not large. Since the test area is in the center area of the panel, the readings of gage 14 are not considered to be an obstruction to testing.

As can be seen in Fig.3.9, the gages that are on top of the stiffener show consistently lower strains than the gages on the outside of the tank on the adjacent side of the stiffeners. The strain difference between skin gages on the outside of the tank and gages on top of the stiffeners is caused by secondary bending of the panel because the panels are not loaded on the neutral line but are only gripped at the skin. It is possible that cracks in the weep hole will initiate and grow towards the skin whereas cracks in the actual C-141 panel grow towards the top of the stiffener, away from the skin. Although there is secondary bending, all gages show linear results.

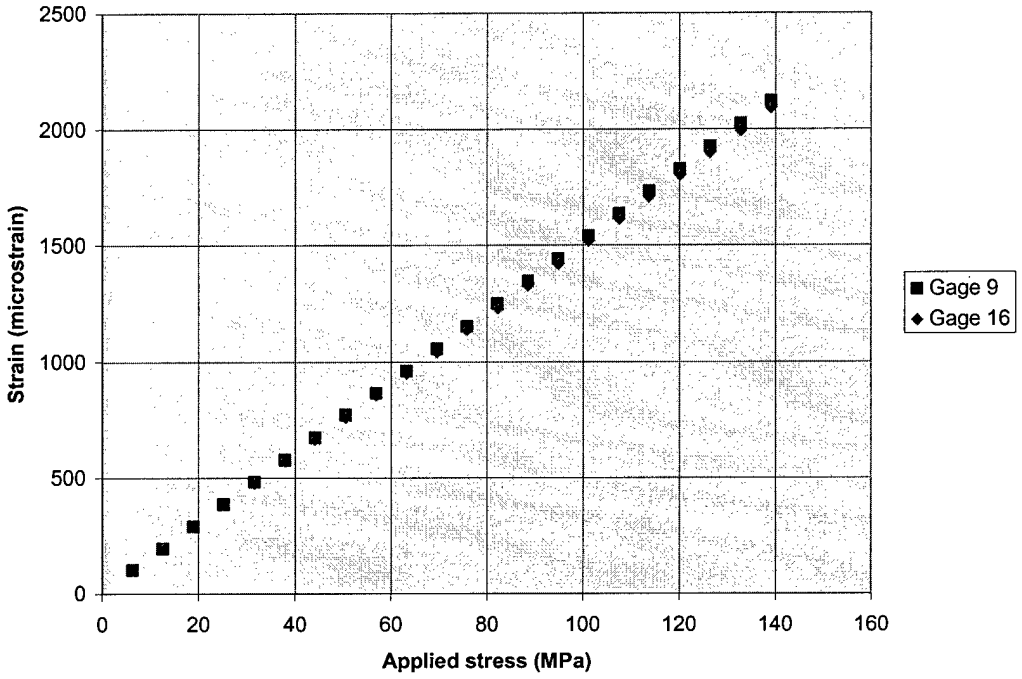

Fig.3.3: Skin gage readings versus applied stress in outer bay on stiffener side of wide panel.

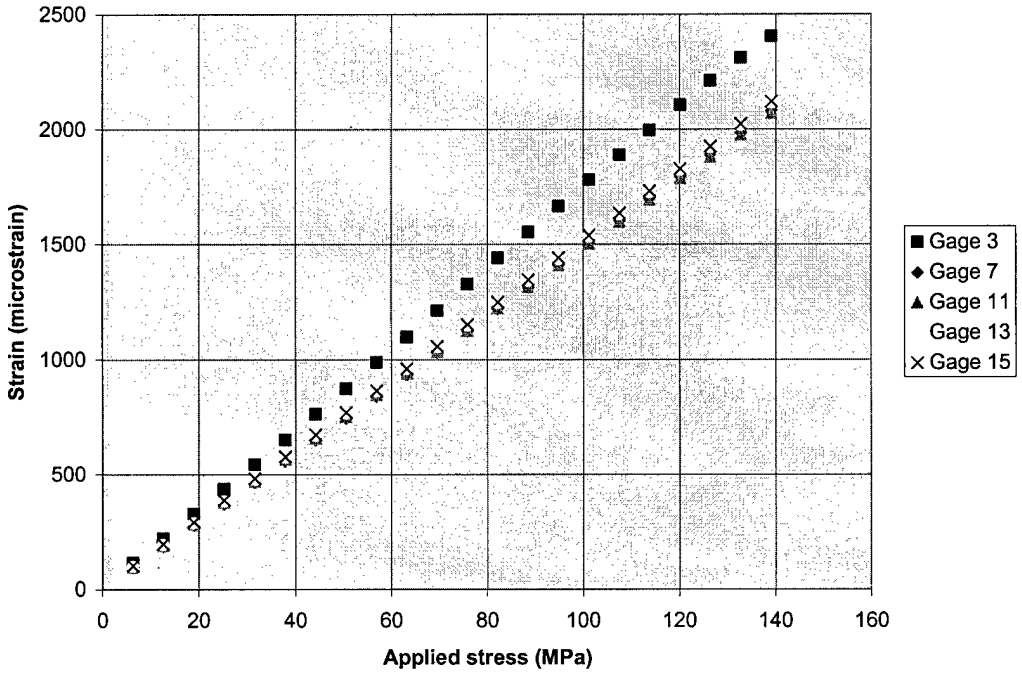

Fig.3.4: Skin gage readings versus applied stress in inner bay on stiffener side of wide panel.

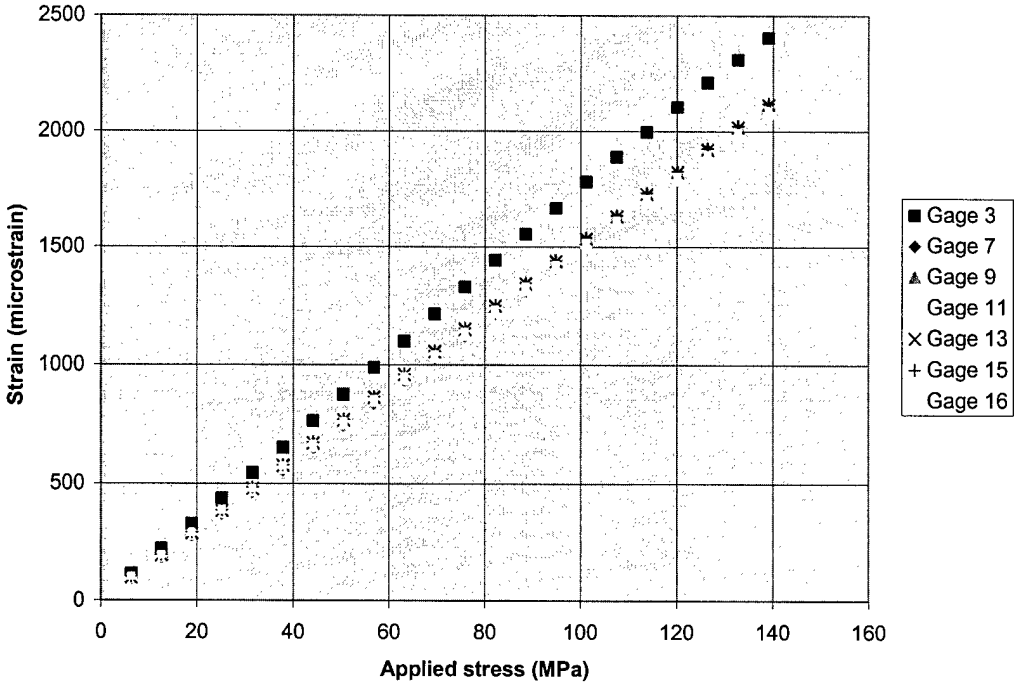

Fig.3.5: Skin gage readings versus applied stress on stiffener side of wide panel.

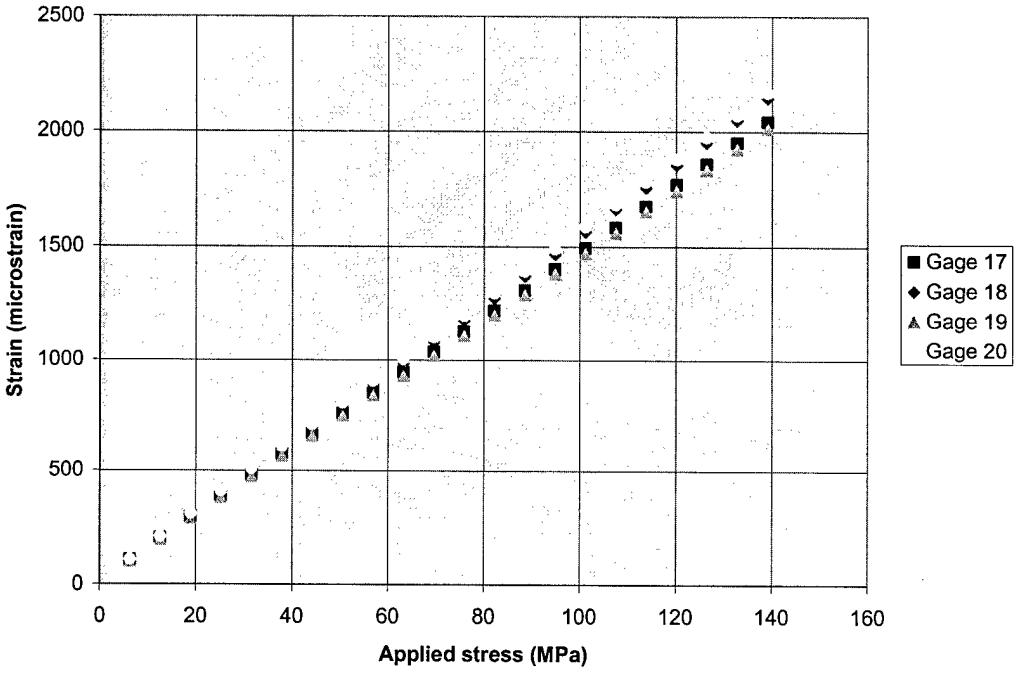

Fig.3.6: Skin gage readings versus applied stress on outside of tank of wide panel.

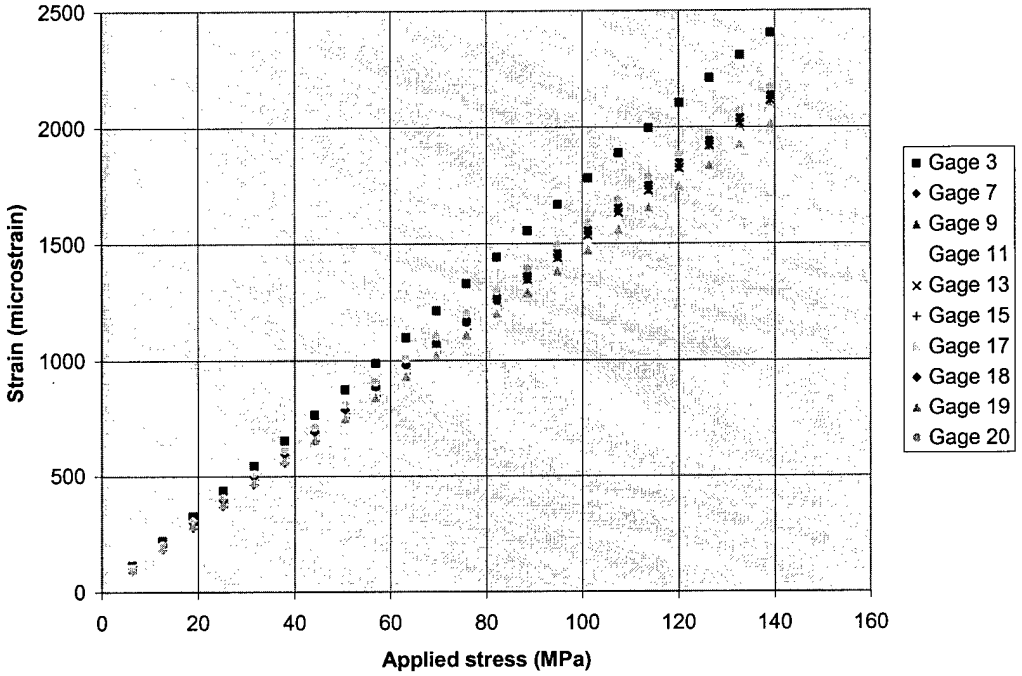

Fig.3.7: Skin gage readings versus applied stress on both the inside and outside of tank of wide panel.

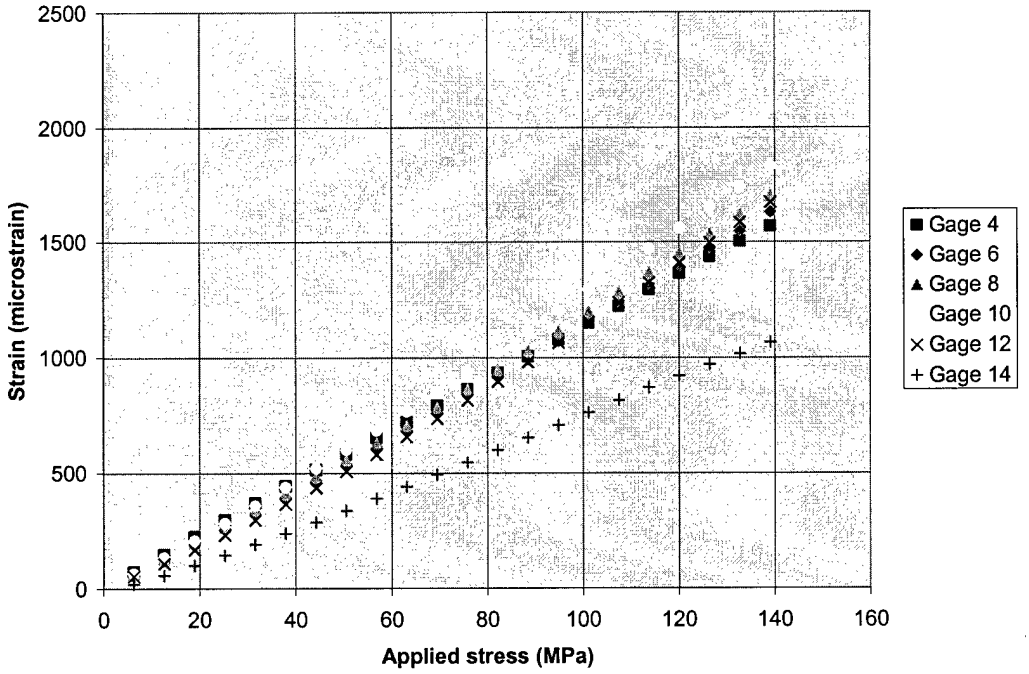

Fig.3.8: Stiffener gage readings versus applied stress on wide panel.

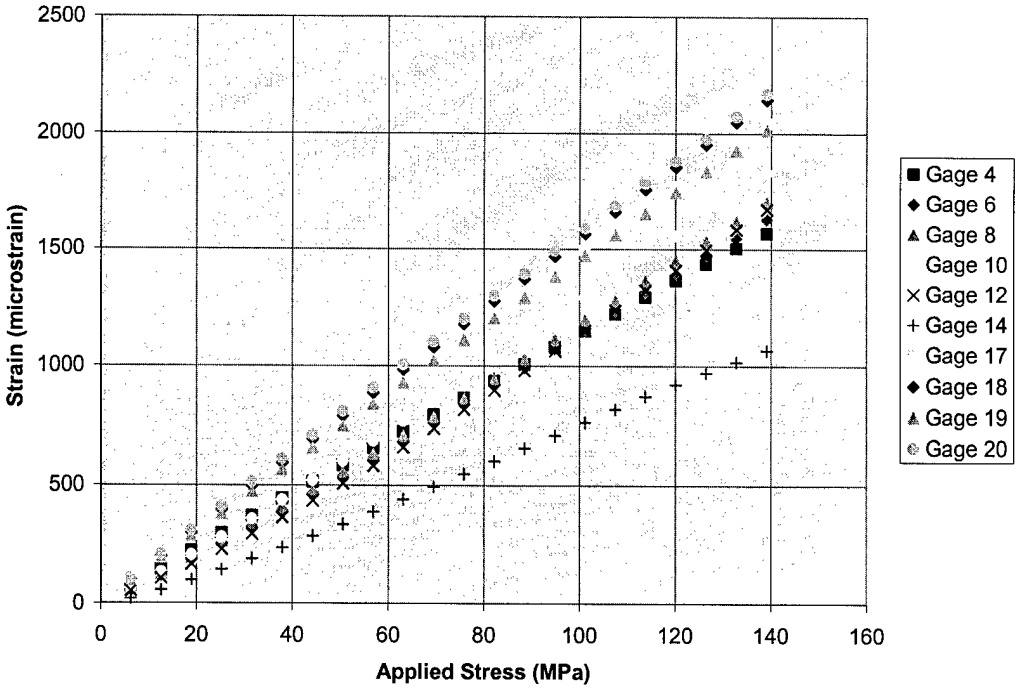

Fig.3.9: Gage readings versus applied stress of stiffener gages and skin gages on outside of tank adjacent to stiffener.

3.2.2 Narrow panel

The panel was loaded in steps of 10 MPa up to 140 MPa (the maximum load in the C-141 spectrum is approximately 134 MPa). The results for the narrow panels can be seen in Table 3.3 and Table 3.4. All strain gages functioned well during the test.

Stress on panel (MPa)	Strain readings (με)					
	1	2	3	4	5	6
10	121	146	151	101	143	142
20	243	293	302	207	287	282
30	367	438	451	317	430	423
40	492	587	601	430	574	564
50	618	733	749	545	718	704
60	745	882	898	663	862	846
70	875	1028	1047	786	1005	988
80	1005	1173	1196	909	1149	1129
90	1137	1325	1346	1035	1295	1272
100	1269	1471	1495	1162	1438	1415
110	1402	1616	1643	1291	1582	1557
120	1536	1762	1792	1421	1726	1699
130	1671	1908	1941	1553	1869	1841
140	1806	2057	2090	1686	2015	1986

Table 3.3: Strain gage readings of narrow panel, gage 1 through 6.

Stress on panel (MPa)	Strain readings (με)					
	7	8	9	10	11	12
10	155	155	158	143	145	146
20	309	308	311	286	290	291
30	462	460	465	429	434	436
40	612	612	619	572	579	581
50	763	762	770	713	723	725
60	912	913	922	856	867	869
70	1062	1063	1074	1000	1012	1014
80	1210	1212	1224	1143	1156	1157
90	1360	1362	1376	1286	1301	1303
100	1507	1511	1526	1430	1445	1445
110	1655	1659	1675	1572	1589	1590
120	1803	1807	1825	1716	1733	1734
130	1950	1955	1974	1859	1877	1877
140	2098	2105	2126	2003	2022	2022

Table 3.4: Strain gage readings of narrow panel, gage 7 through 12.

Fig.3.10 shows the readings of the skin gages on the inside of the tank. All gages show similar results, which means that the panel is evenly loaded in the loading and width directions in the test area.

Fig.3.11 shows the results of the gages on the outside of the tank. Again, all gages show similar readings with approximately the same maximum reading of 2100 με at 140 MPa applied stress.

Fig.3.12 combines the previous two graphs. It is clear than there is no difference between skin gages on the inside and on the outside of the panel.

Fig.3.13 shows the readings of the two gages located on the top of the stiffener. Both gages show similar readings, lower than the strains in the skin of the panel.

Fig.3.14 shows both stiffener gages and skin gages on the outside of the skin adjacent to the stiffener. Again, the stiffener gages show lower strains. As was the case with the wide panel, this is caused by secondary bending of the panel.

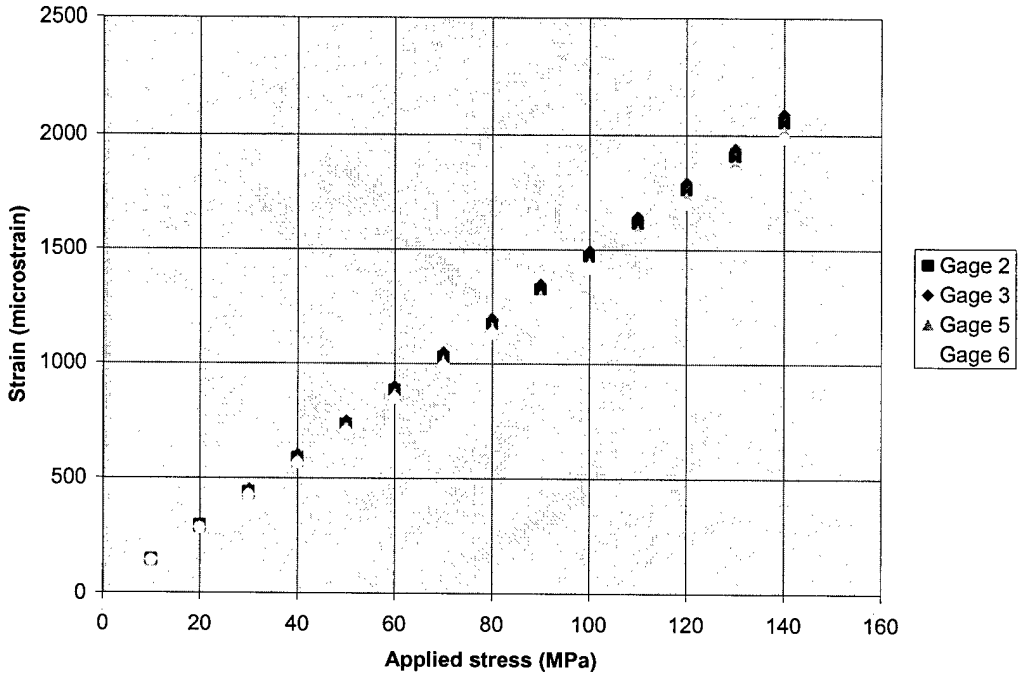

Fig.3.10: Skin gage readings versus applied stress on inside of tank of narrow panel.

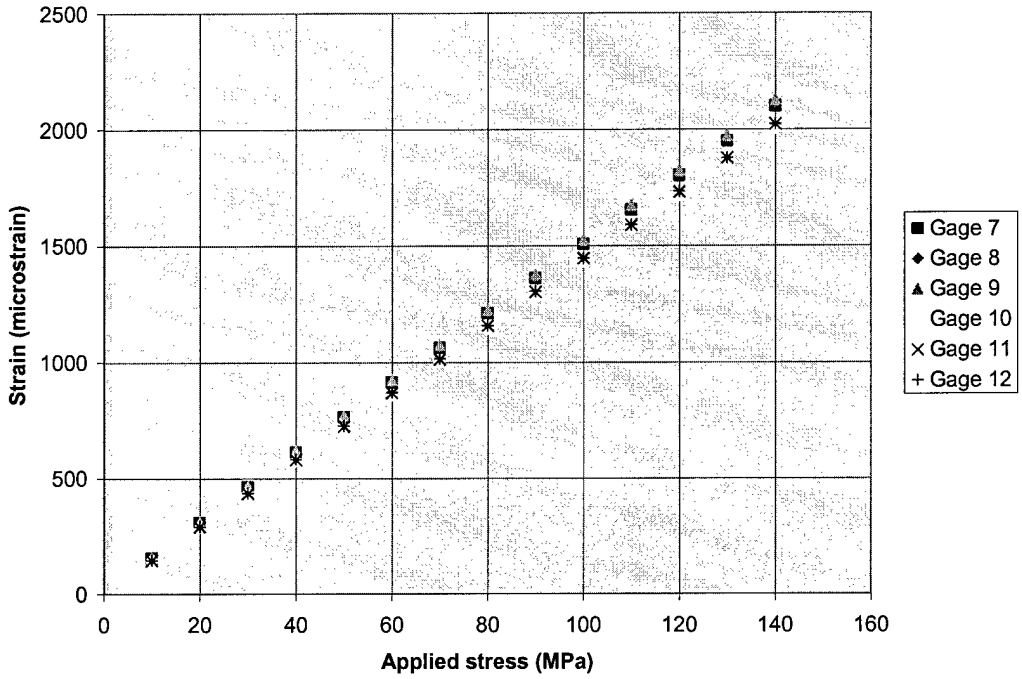

Fig.3.11: Skin gage readings versus applied stress on outside of tank of narrow panel.

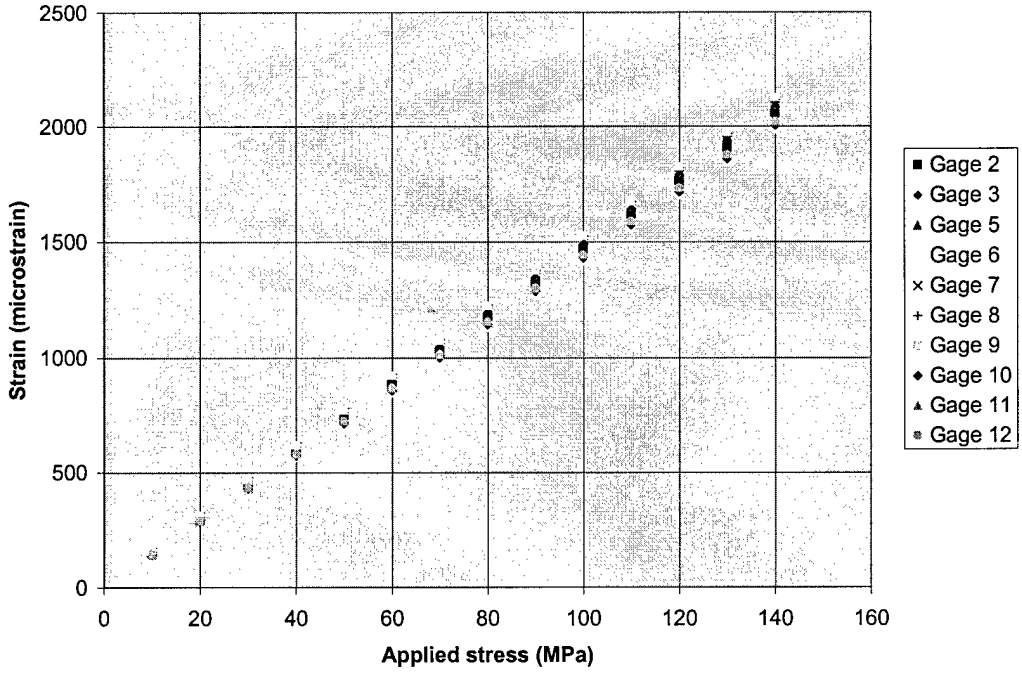

Fig.3.12: Skin gage readings versus applied stress on both the inside and outside of tank of narrow panel.

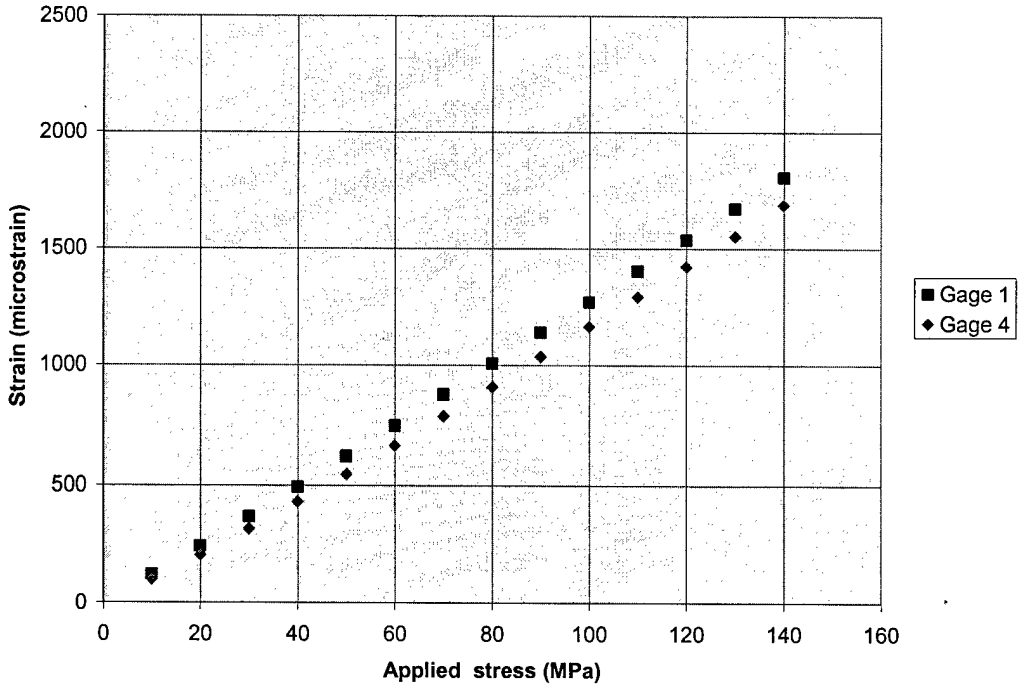

Fig.3.13: Stiffener gage readings versus applied stress on narrow panel.

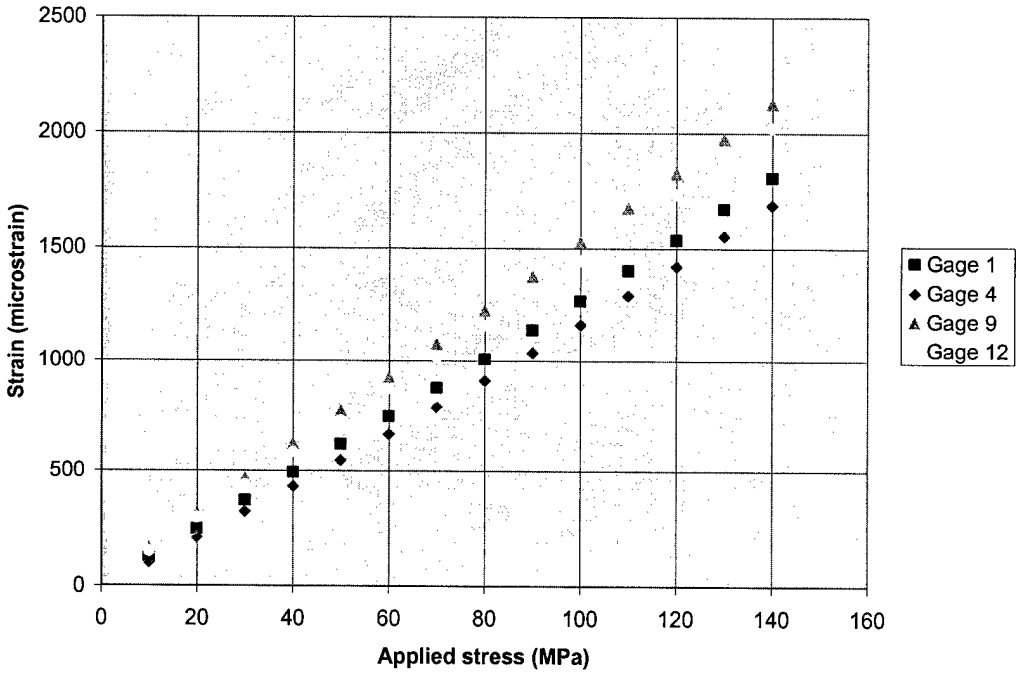

Fig.3.14: Gage readings versus applied stress of stiffener gages and skin gages on outside of tank adjacent to stiffener.

3.2.3 Comparison of wide and narrow panels

This paragraph compares the strains in the wide panel and the narrow panel. The results will be used to determine whether results from testing of the narrow panels can be legitimately compared to that of the wide panels. Strains in the unpatched narrow panel should be similar in magnitude compared to the wide panel.

Fig.3.15 shows the skin gages on the inside of the tank of both the wide and the narrow panels. As can be seen, the strains in the narrow panel are similar to the strains in the wide panel (only gage 3 on the wide panel shows significantly different results).

Fig.3.16 shows the gage readings for the outside of the skin for both the narrow and wide panel. Again, the results are remarkably good; narrow and wide panels give comparable results.

Fig.3.17 shows the stiffener gages of the narrow and wide panel. Only the readings of gage 14 on the wide panel are significantly different, all other gage readings are comparable in magnitude. It can be concluded that the wide and the narrow panels give comparable results when loaded in tension. It should be kept in mind that the panels did not have cracks. The stress distribution can change when cracks develop in the stiffener and skin.

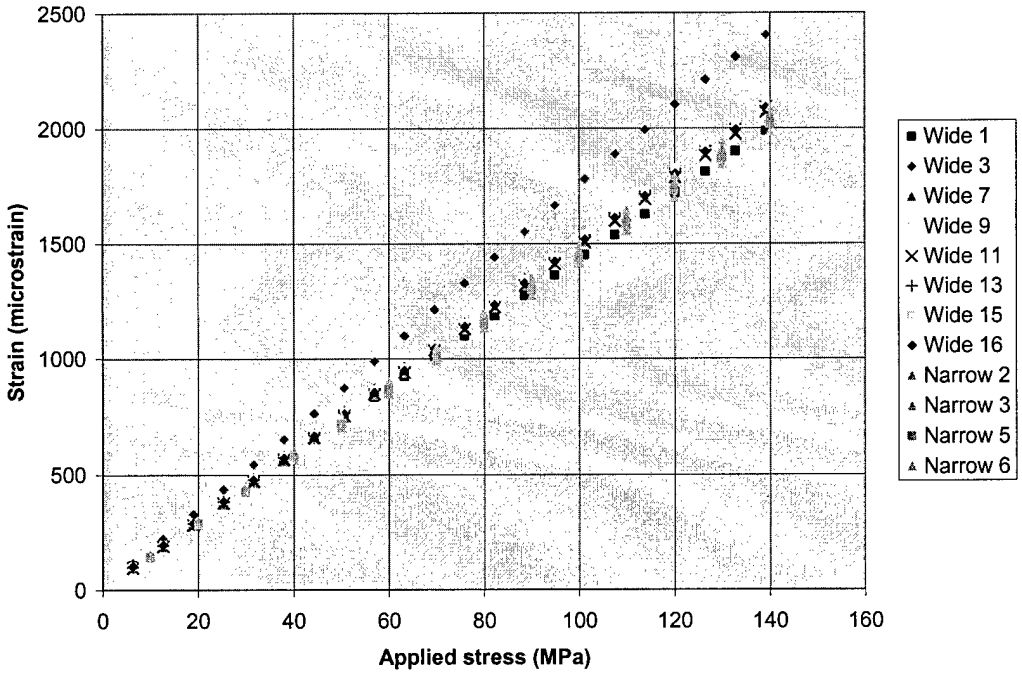

Fig.3.15: Skin gage readings on inside of tank on both the wide and narrow panel.

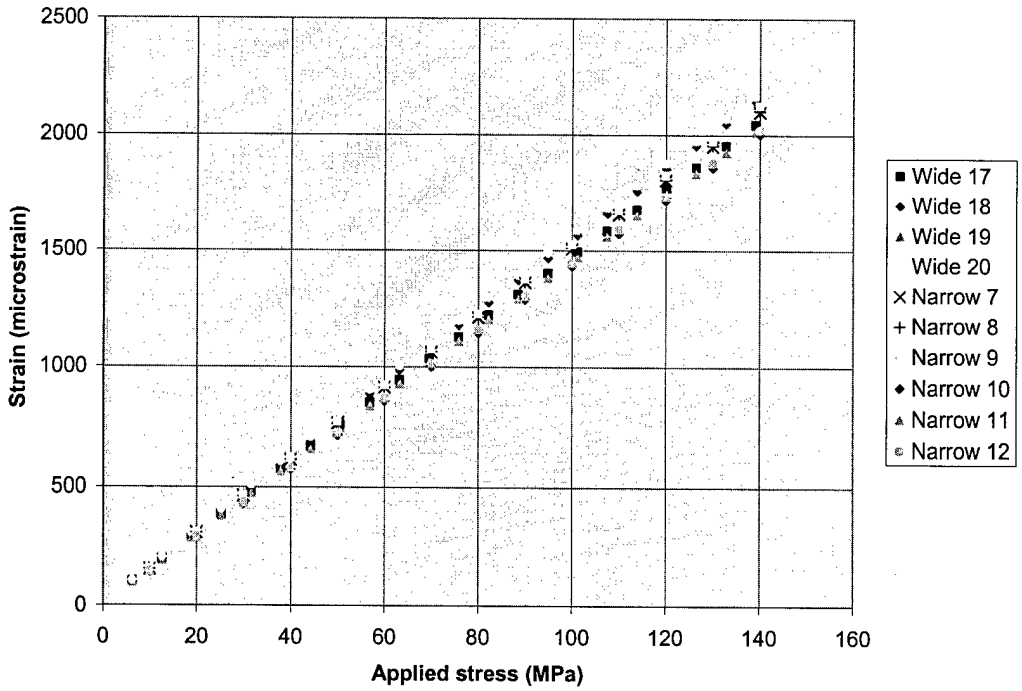

Fig.3.16: Skin gage readings on outside of tank on both the wide and narrow panel.

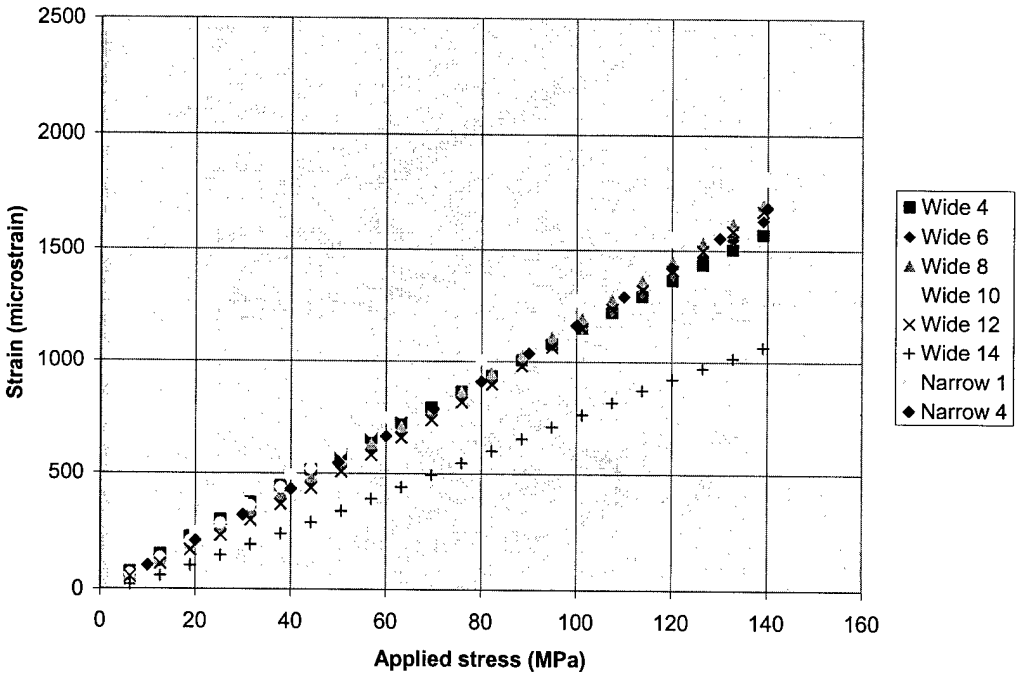

Fig.3.17: Stiffener gage readings on both the wide and narrow panel.

3.3 COMPARISON OF STRAIN GAGE AND FEM RESULTS

3.3.1 Wide panel

The following paragraph will give a comparison between the experimental results from the strain gages and FE-calculations performed by J.J.A. Massar [7].

Due to symmetry, only a quarter of the panels is modeled. Fig.3.18 shows the boundary conditions that are applied to the narrow as well as to the wide panel. Both panels are clamped by grips that are considered infinitely stiff and therefore the rotations in all directions on the top of the panel are suppressed. The displacements in the 1 and 3 direction are suppressed as well. The displacements in the 2 direction and the rotations in 4 and 6 direction are suppressed on the horizontal axis of symmetry. Along the vertical axis of symmetry the displacement in the 1 direction and the rotations in 5 and 6 direction are suppressed. The applied load is modeled as a discrete force at the left side on top of the panel. The enforced boundary conditions along the top of the panel (along the skin and not the stiffeners) ensure equal vertical displacements of the nodes, simulating clamping of the end of the skin. Three-dimensional brick elements (CHEXA elements) are used in the NASTRAN model.

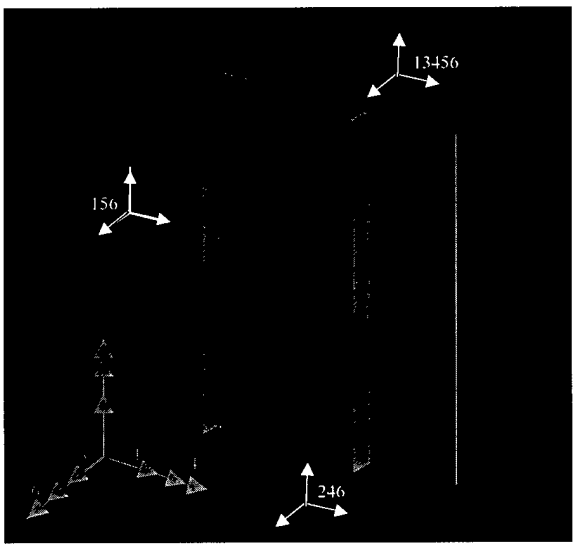

Fig.3.18: Boundary conditions of FE-model (in white). 1,2 and 3 are displacements. 4,5 and 6 are rotations [7].

Four load cases per panel were analyzed to reduce calculation time. As can be seen in Table 3.5 and Table 3.6, the average absolute error decreases with increasing applied load. Note that the average error is significantly influenced by the large error in gage 14. The average error would be significantly lower were this gage excluded.

	P = 20 kN = 12.7 MPa			P = 60 kN = 38 MPa		
Gage #	**FEM (με)**	**Experiment (με)**	**Absolute error (%)**	**FEM (με)**	**Experiment (με)**	**Absolute error (%)**
1	176	201	-12.44	529	567	-6.70
2	153			460		
3	176	221	-20.36	531	651	-18.43
4	153	148	3.38	460	442	4.07
5	176			529		
6	152	118	28.81	455	394	15.48
7	176	185	-4.86	529	556	-4.86
8	152	128	18.75	455	408	11.52
9	176	196	-10.20	529	577	-8.32
10	152	133	14.29	455	437	4.12
11	176	189	-6.88	529	564	-6.21
12	152	108	40.74	455	363	25.34
13	176	193	-8.81	529	574	-7.84
14	153	57	168.42	460	237	94.09
15	176	196	-10.20	531	577	-7.97
16	176	196	-10.20	529	571	-7.36
17	179	200	-10.50	538	574	-6.27
18	179	201	-10.95	538	592	-9.12
19	179	194	-7.73	538	564	-4.61
20	179	207	-13.53	538	608	-11.51
	Average absolute error		**23.59**	**Average absolute error**		**14.93**

Table 3.5: Comparison of strain gage readings and FE-results for 20 and 60 kN for the wide panel.

	P = 130 kN = 82.2 MPa			P = 190 kN = 120 MPa		
Gage #	**FEM (με)**	**Experiment (με)**	**Absolute error (%)**	**FEM (με)**	**Experiment (με)**	**Absolute error (%)**
1	1160	1185	-2.11	1680	1721	-2.38
2	993			1468		
3	1153	1441	-19.99	1690	2104	-19.68
4	993	933	6.43	1468	1364	7.62
5	1153			1687		
6	990	913	8.43	1441	1389	3.74
7	1153	1218	-5.34	1687	1793	-5.91
8	990	945	4.76	1441	1447	-0.41
9	1153	1249	-7.69	1687	1828	-7.71
10	990	1024	-3.32	1441	1559	-7.57
11	1153	1222	-5.65	1687	1787	-5.60
12	990	896	10.49	1441	1408	2.34
13	1153	1246	-7.46	1687	1823	-7.46
14	993	599	65.78	1468	920	59.57
15	1153	1249	-7.69	1690	1828	-7.55
16	1160	1232	-5.84	1680	1802	-6.77
17	1180	1219	-3.20	1714	1770	-3.16
18	1180	1274	-7.38	1714	1854	-7.55
19	1180	1200	-1.67	1714	1743	-1.66
20	1180	1296	-8.95	1714	1878	-8.73
	Average absolute error		**10.72**	**Average absolute error**		**9.73**

Table 3.6: Comparison of strain gage readings and FE-results for 130 and 190 kN for the wide panel.

3.3.2 Narrow panel

As was the case with the wide panels, the average absolute error decreases with increasing applied stress for the narrow panel. Since crack growth after patching is mainly due to the high loads, it is important that predictions in this regime are most accurate, since the smaller loads do not cause any (or very little crack growth). The fact that the average error is decreasing with increasing load is, therefore, favorable for crack growth predictions. Table 3.7 and Table 3.8 shows the results for the narrow panels. It should be noted that the average error for the narrow panel is lower than the average error for the wide panel.

	σ = 10 MPa			σ = 40 MPa		
Gage #	**FEM (με)**	**Experiment (με)**	**Absolute error (%)**	**FEM (με)**	**Experiment (με)**	**Absolute error (%)**
1	120.7	121	-0.25	484	492	-1.63
2	139.7	146	-4.32	556	587	-5.28
3	139.5	151	-7.62	556	601	-7.49
4	120.5	101	19.31	484	430	12.56
5	139.7	143	-2.31	556	574	-3.14
6	139.7	142	-1.62	556	564	-1.42
7	143	155	-7.74	569	612	-7.03
8	143	155	-7.74	569	612	-7.03
9	143	158	-9.49	569	619	-8.08
10	143.3	143	0.21	569	572	-0.52
11	143	145	-1.38	569	579	-1.73
12	143	146	-2.05	569	581	-2.07
	Average absolute error		**5.34**	**Average absolute error**		**4.83**

Table 3.7: Comparison of strain gage readings and FE-results for 10 and 40 MPa for the narrow panel.

	σ = 80 MPa			σ = 120 MPa		
Gage #	**FEM (με)**	**Experiment (με)**	**Absolute error (%)**	**FEM (με)**	**Experiment (με)**	**Absolute error (%)**
1	961	1005	-4.38	1443	1536	-6.05
2	1117	1173	-4.77	1676	1762	-4.88
3	1117	1196	-6.61	1676	1792	-6.47
4	961	909	5.72	1443	1421	1.55
5	1119	1149	-2.61	1680	1726	-2.67
6	1117	1129	-1.06	1680	1699	-1.12
7	1141	1210	-5.70	1713	1803	-4.99
8	1141	1212	-5.86	1713	1807	-5.20
9	1141	1224	-6.78	1713	1825	-6.14
10	1141	1143	-0.17	1713	1716	-0.17
11	1141	1156	-1.30	1713	1733	-1.15
12	1144	1157	-1.12	1718	1734	-0.92
	Average absolute error		**3.84**	**Average absolute error**		**3.44**

Table 3.8: Comparison of strain gage readings and FE-results for 80 and 120 MPa for the narrow panel.

3.4 COMPRESSION ANALYSIS

Both panels are tested in compression up to –100 MPa. It is necessary to verify if these machined panels are capable of carrying this compressive load, which is present in the C-141 spectrum. The dimensions of an actual C-141 lower wing skin are different from the panels used here. The stiffeners of a C-141 panel are almost 2" in height, whereas the height of the stiffeners used here are below 1". This could affect the buckling behavior significantly, as well as the difference in skin thickness between the machined panels and actual C-141 panels.

3.4.1 Narrow panel

The results of the compression test with the narrow panel can be seen in Table 3.9 and Table 3.10.

Stress on panel (MPa)	Strain readings (με)					
	1	2	3	4	5	6
-10	-115	-146	-152	-117	-145	-140
-20	-228	-291	-302	-224	-291	-279
-30	-339	-436	-454	-321	-437	-418
-40	-449	-581	-605	-411	-580	-555
-50	-557	-726	-757	-492	-725	-690
-60	-661	-871	-910	-561	-867	-822
-70	-763	-1019	-1067	-615	-1012	-652
-80	-861	-1166	-1225	-654	-1149	-1068
-90	-967	-1323	-1324	-868	-1160	-865
-100	-1144	-1513	-1242	-1307	-1107	-410

Table 3.9: Strain gage readings of narrow panel in compression, gage 1 through 6.

Stress on panel (MPa)	Strain readings (με)					
	7	8	9	10	11	12
-10	-153	-154	-141	-141	-145	-147
-20	-310	-313	-283	-283	-289	-292
-30	-467	-471	-427	-422	-433	-439
-40	-626	-630	-573	-562	-577	-585
-50	-789	-792	-723	-698	-720	-730
-60	-955	-956	-876	-834	-863	-878
-70	-1127	-1127	-1036	-969	-1007	-1026
-80	-1308	-1302	-1200	-1100	-1150	-1174
-90	-1740	-1631	-1394	-1170	-1301	-1344
-100	-2225	-2047	-1635	-1167	-1522	-1617

Table 3.10: Strain gage readings of narrow panel in compression, gage 7 through 12.

Fig.3.19 through Fig.3.23 show the strain readings for the different strain gages on the narrow panel. Fig.3.19 shows the results for the skin gages on the stiffener side of the panel. It is clear from this graph that the results are not linear over the range of loading. This is due to buckling of the panel. The skin next to the stiffener buckles though the stiffener is still able to carry more load. The skin buckles in a twisting mode: one side buckles towards the stiffener side, whereas the skin on the other side of the stiffener buckles away from the stiffener side.

Fig.3.20 shows the strains on the skin on the outside of the tank. Again, as can be expected from Fig.3.19, gage readings are not linear. Some readings are higher and other readings are lower, especially at high applied stresses when buckling becomes more significant.

Fig.3.21 combines the two previous graphs. As can be seen, the strains from some gages increase whereas other gages show decreasing strains with increasing applied stress. This is due to the twisting buckling mode of the panel.

Fig.3.22 shows the strains from the gages on the stiffener. As can be seen, gage 4 shows non-linear strains whereas gage 1 stays nearly linear with increasing applied stress. Apparently, there is some buckling in the stiffener, but the stiffener is still capable to carry load with increasing applied stress.

Fig.3.23 shows the gage readings of the stiffener gages and the gages on the outside of the tank adjacent to the stiffener. The gages on the top of the stiffener show lower strains than the gages on the skin, as was the case with the panels loaded in tension.

As was mentioned before, the non-linear behavior is due to the nature of the panel, that is not equivalent to the actual C-141 wing panel dimensions. Although the strain gage results show non-linear behavior due to buckling, the narrow panel is still capable of carrying the maximum applied load and the panel does not fail in compression. Although the narrow panel can carry the maximum compressive load in the C-141 spectrum, decreasing the maximum compressive load should be considered and to bring the loads more in accordance with the buckling characteristics of the panel used in this research.

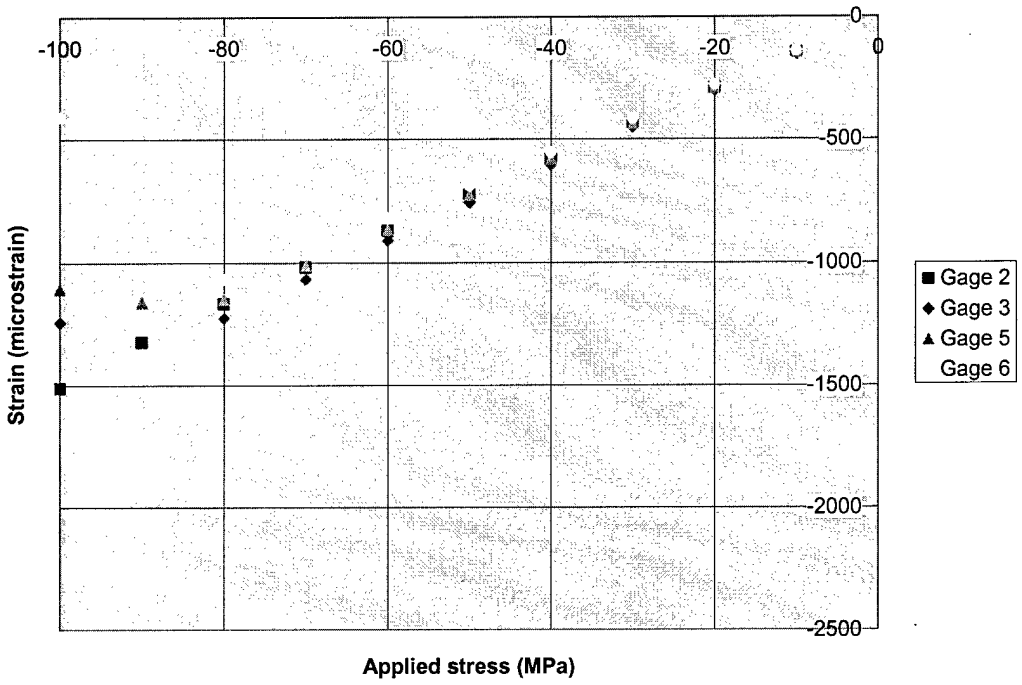

Fig.3.19: Skin gage readings on inside of tank on narrow panel in compression.

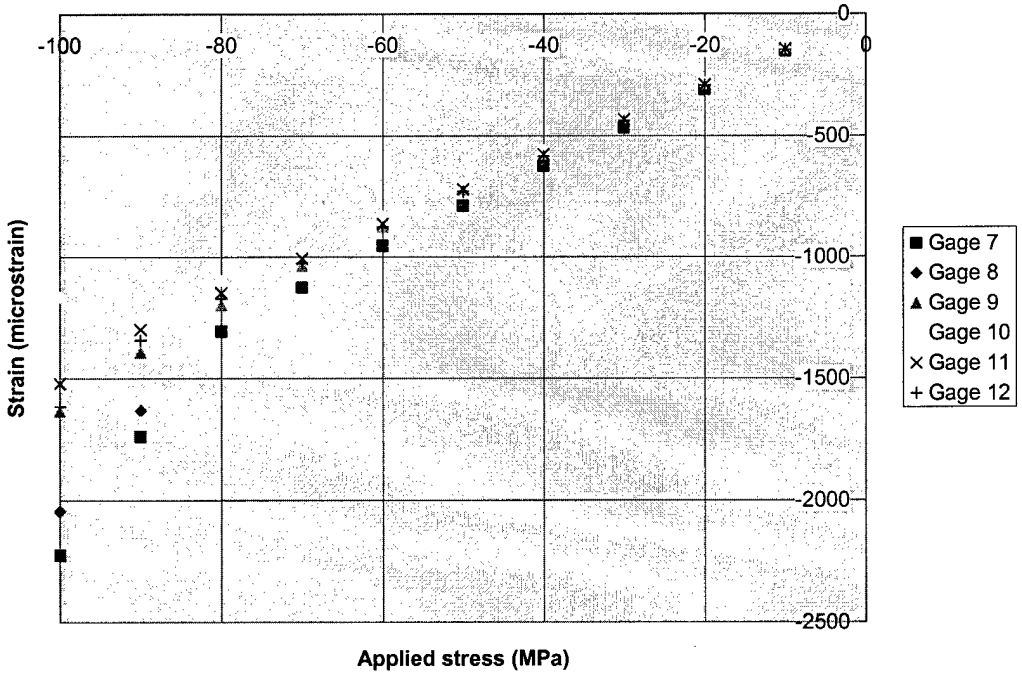

Fig.3.20: Skin gage readings on outside of tank on narrow panel in compression.

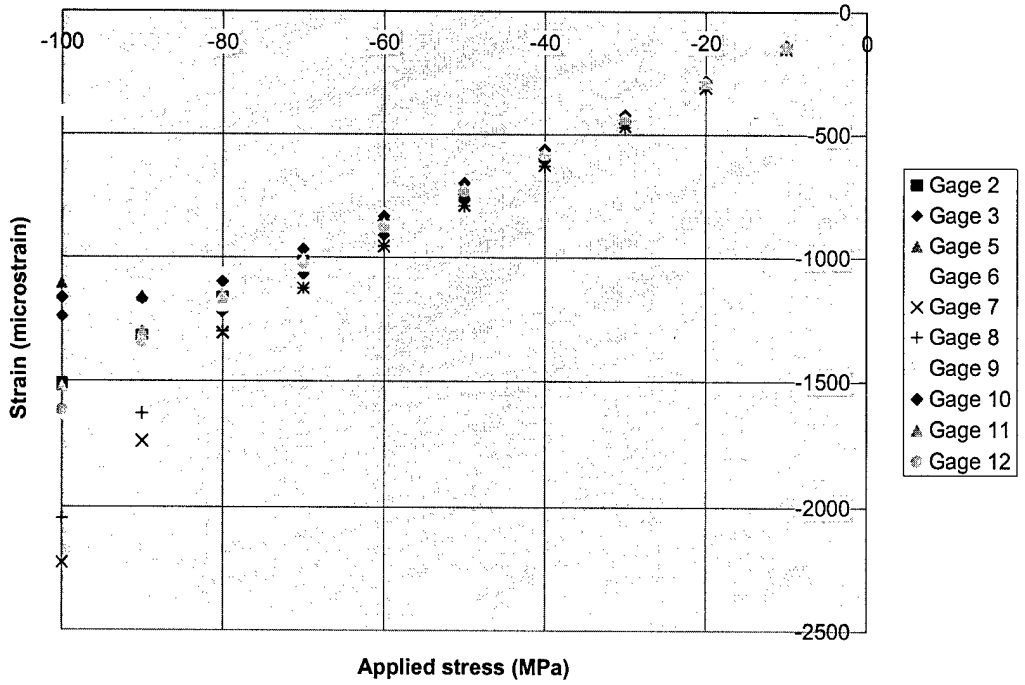

Fig.3.21: Skin gage readings on inside and outside of tank on narrow panel in compression.

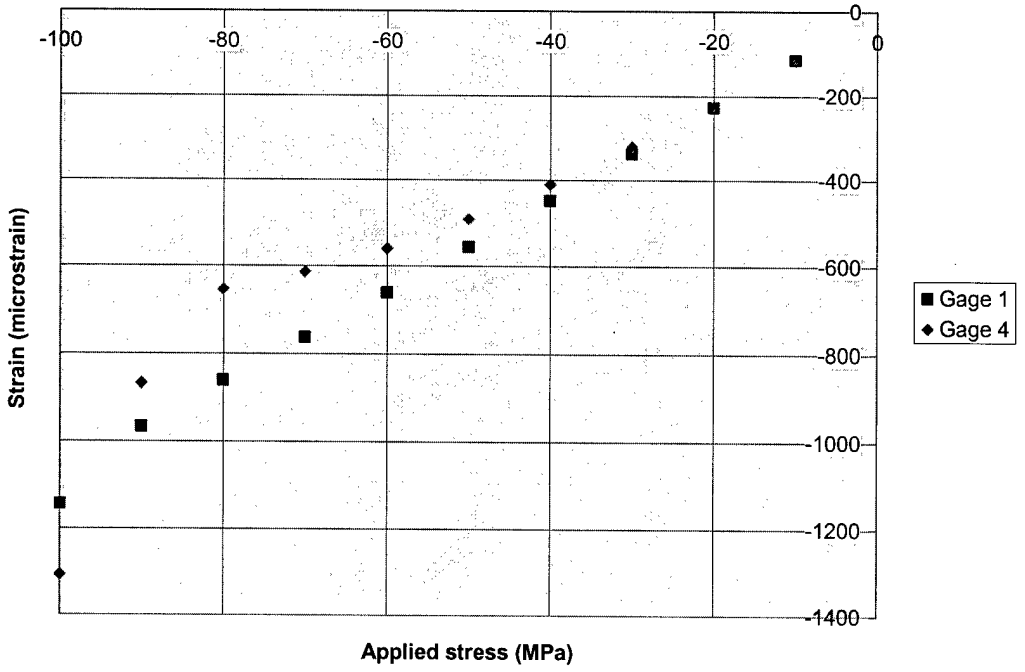

Fig.3.22: Stiffener gage readings on narrow panel in compression.

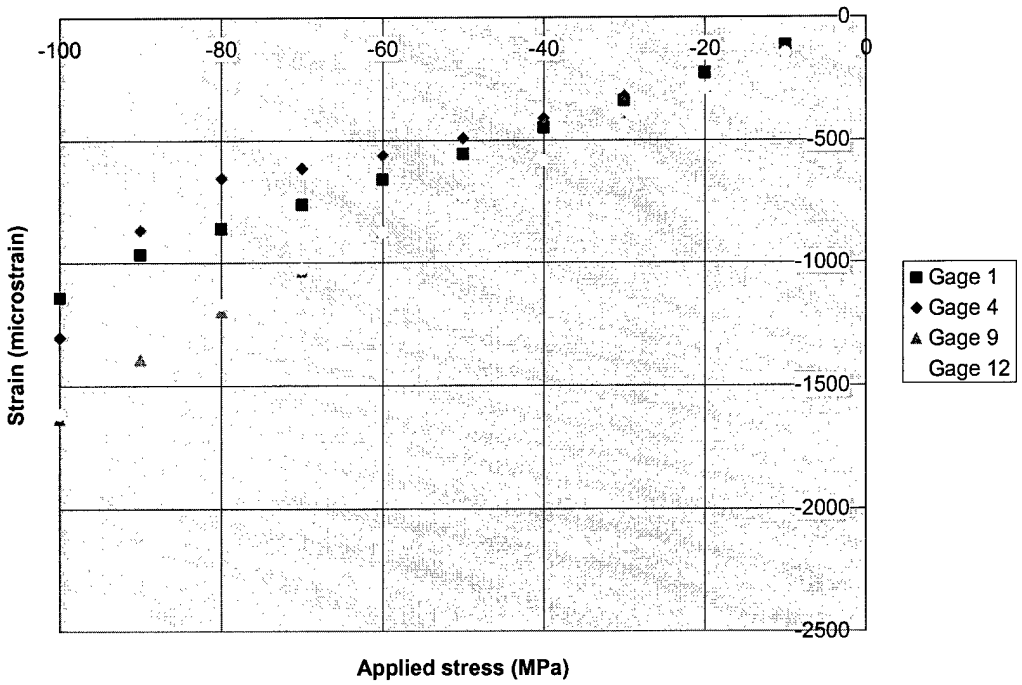

Fig.3.23: Gage readings versus applied stress of stiffener gages and skin gages on outside of tank adjacent to stiffener on narrow panel in compression.

3.4.2 Wide panel

The previous paragraph showed that the narrow panels behave non-linearly in compression, but that the panels are still capable of carrying the maximum compressive load. Preliminary testing of the wide panels in compression resulted in compressive failure. Fig.3.24 shows the load versus displacement curve of the wide panel. As can be seen, the curve becomes non-linear at approximately -50 MPa. A possible explanation for the compressive failure of the wide panel is that the total length of the specimen, including grips, is longer for the wide panel when compared to the narrow panel, and therefore reduces the critical buckling load of the panel. To be able to test the wide panels under spectrum loading including compressive loads, it was decided to limit the compressive loads in the C-141 spectrum to –40 MPa to prevent failure of the wide panels in compression (see test plan in Table 2.2). Note that the narrow panels will be tested with a C-141 spectrum containing compressive loads up to –100 MPa so that a comparison of the wide and narrow panels under compressive spectra cannot be made.

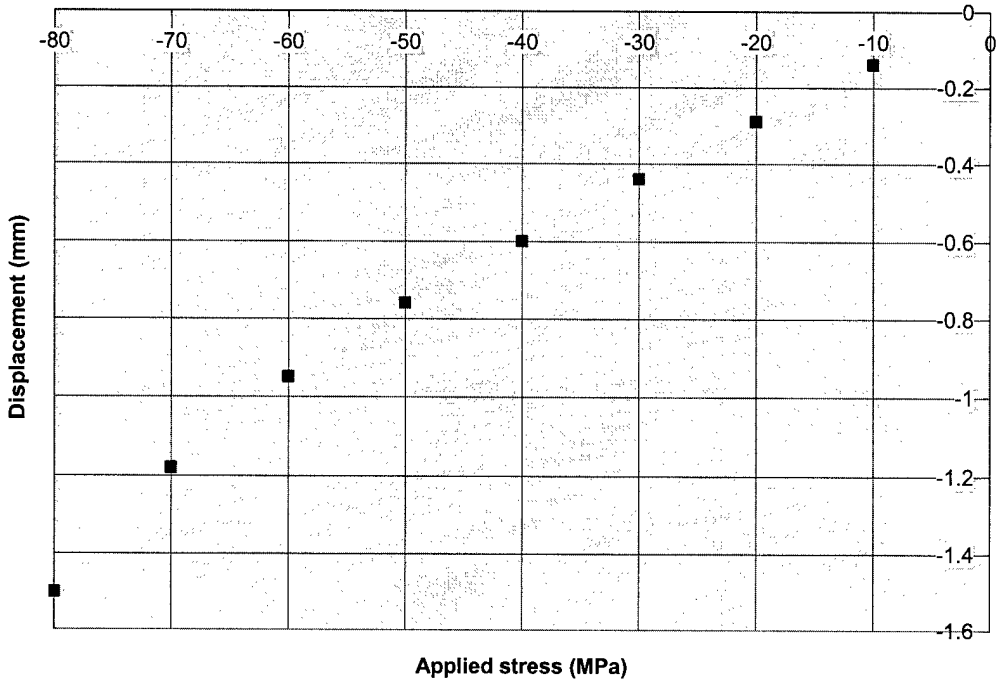

Fig.3.24: Displacement versus applied stress for wide panel in compression.

4. SPECTRUM TESTS ON UNPATCHED PANELS

To obtain a baseline for the patched specimens, it is necessary to test unpatched specimens. This chapter will describe the spectrum tests on unpatched specimens. Specimens will be loaded by spectra both with and without compressive loads.

4.1 PRE-CRACKING OF SPECIMENS

Before the specimens can be tested, it is necessary to pre-crack the panels. Pre-cracking is necessary to obtain a natural crack front from which crack growth can continue. It is important to know the crack growth rate after patching for patched cracks; the crack initiation period from the unpatched weep hole is not interesting since only existing cracks are being considered.

Pre-cracking is done at the lowest stress level possible. If high stress levels are used when pre-cracking unpatched panels, large plastic zones can be created. The large plastic zones create a zone around the crack tip that is in compression and thus lower the effective stress intensity factor, which is undesirable. From previous research [8], it was found that a pre-crack level of 60 MPa results in plastic zones that do not greatly influence the crack re-initiation after patching. However, pre-cracking at this stress level might take a significant amount of time and, during pre-cracking, it was necessary to increase the pre-crack level temporary to 80 MPa in some cases. The pre-crack level is in all cases lowered to 60 MPa after crack initiation was seen at 80 MPa. The pre-cracking was not stopped until crack growth at 60 MPa could be confirmed and the crack had grown through the plastic zone corresponding to the 80 MPa stress level.

Panels N1 and N2 are used, besides for the static analysis, to determine the re-initiation behavior of the stiffened panels. It was found that by making the saw cut first on the tank side of the weep hole, the crack will grow towards the top of the stiffener. It is preferred to have a crack on both sides of the weep hole of 0.1". When making the saw cut on the skin side of the weep hole after crack initiation on the tank side of the weep hole, the crack on the tank side became too large. It is very difficult to control crack growth in an integrally stiffened panel. Small variables, such as exact location of the weep hole, small imperfections in the material, and small alignment differences of the panel in the grips and machine can make a significant difference. It was found that the best way to pre-crack the panels was to make a saw cut on the skin side of the weep hole and fatigue until crack initiation, then make a saw cut on the tank side of the weep hole.

Table 4.1 gives information about exact crack location and size after pre-cracking. Several definitions are necessary to define the location of the different crack fronts. Fig.4.1 and Fig.4.2 show the different definitions. When looking at the top of the stiffener, the crack in the skin on the left side of the

stiffener is called L and the crack in the skin on the right side of the stiffener is called R. When looking at the web of the stiffener from view A, the crack on the skin side of the weep hole is called LL (Left side of stiffener-Left side of weep hole), the crack on the stiffener side of the weep hole is called LR (Left side of stiffener-Right side of weep hole). When looking at the web of the stiffener from view B, the crack on the stiffener side of the weep hole is called RL (Right side of stiffener-Left side of weep hole), the crack on the skin side of the weep hole is called RR (Right side of stiffener, Right side of weep hole). The crack size in the stiffener is measured from the inside of the skin towards the top of the stiffener. As soon as cracks have grown into the skin, they are measured from the left and right side of the stiffener. The total crack size will be the summation of L, R and 4.66 mm (thickness of stiffener).

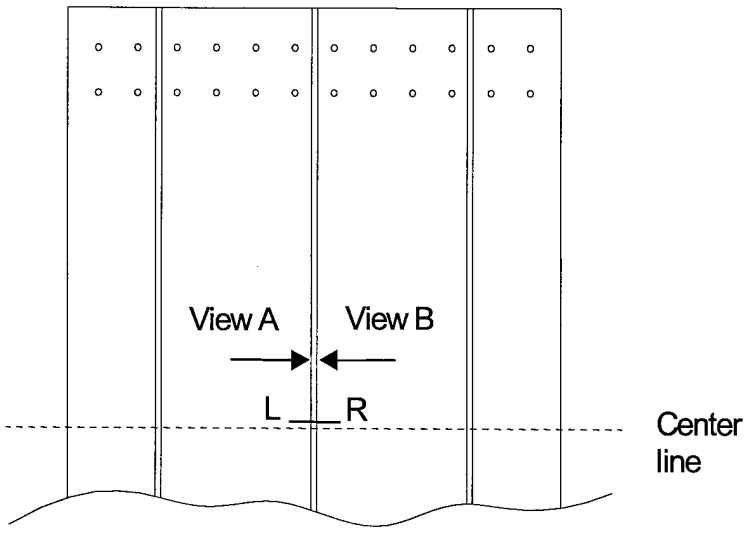

Fig.4.1: Front view of stiffened panel, crack in skin visible.

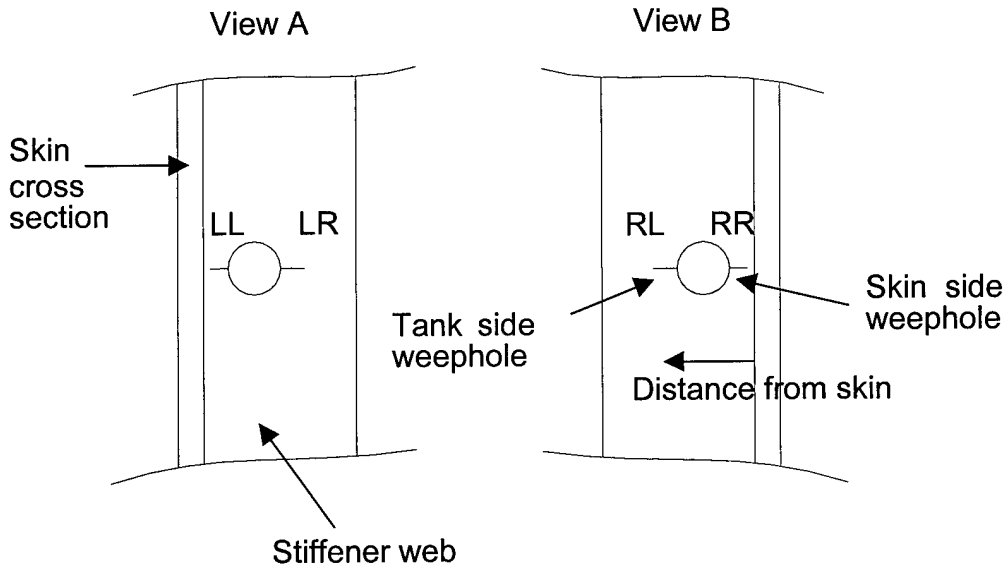

Fig.4.2: Left and right view of stiffener web with crack definitions.

Specimen #	L (mm from left side stiffener)	R (mm from right side stiffener)	LL (mm from inside skin)	LR (mm from inside skin)	RL (mm from inside skin)	RR (mm from inside skin)
N1	Tested up to failure					
N2	Tested up to failure					
N3	1.0	0.5	0	13.5	13.0	0
N4	1.0	2.25	0	13.25	13.0	0
N5	3.5	4.25	0	13.75	14.5	0
N6	3.5	3.75	0	14.25	14.0	0
N7	14.5	15.0	0	14.5	15.0	0
N8	15.0	15.0	0	14.0	13.5	0
Extra test	14.7	14.6	0	16.75	16.5	0
W1	0	0	0	14.25	14.5	0
W2	0	0	0	14.0	13.75	0
W3	16.0	14.0	0	15	15.5	0
W4	3.0	3.0	0	16.0	16.0	0
W5	3.0	3.0	0	14.0	14.0	0
W6	11.0	11.0	0	16.0	16.0	0
W7	8.5	9.0	0	14.75	14.75	0

Table 4.1: Location of crack tips after pre-cracking.

The fact that LL and RR are 0 in all cases means that there is a crack from the weep hole down to the intersection with the skin. Values different from 0 for L and R mean that the crack has grown from the stiffener into the skin. As can be seen in Table 4.1, there is some variety in crack sizes between the different

panels. Some panels have the desired stiffener cracks with still no crack growth in the skin, some other panels developed crack growth in the skin before the crack in the stiffener on the stiffener side of the weep hole reached the desired crack size.

4.2 SPECTRUM TESTS ON NARROW PANELS

The reason for testing unpatched specimens is to obtain a baseline for the crack growth rates for unpatched specimens. Both N3 and N4 are tested under C-141 spectrum loading without a patch. N3 is tested with the C-141 spectrum including compressive loads up to –100 MPa, N4 is tested with a modified C-141 spectrum where the compressive loads are replaced by zero MPa. It is more realistic to test panels with the compressive loads because compressive loads can decrease the crack growth life. Compressive loads can decrease the crack growth-reducing effect of plastic zones that were formed by high tensile loading [9,10]. These plastic zones created by tensile loads will increase the crack opening stress, reducing crack growth rates. By leaving the compressive loads out of the spectrum and replace them by 0, the results will become unconservative. However, the compressive loads are omitted from the spectrum for research purposes and the test results are not used to qualify the bonded repairs that are in service, and are therefore allowable.

Fig.4.3 shows the crack growth curves for N3 and N4. The crack length shown in Fig.4.3 is the sum of the crack on the left (L) and on the right (R) of the stringer, increased by the stiffener width of 4.66 mm. Note that the horizontal axis represents 60 blocks, which is the equivalent of one C-141 life.

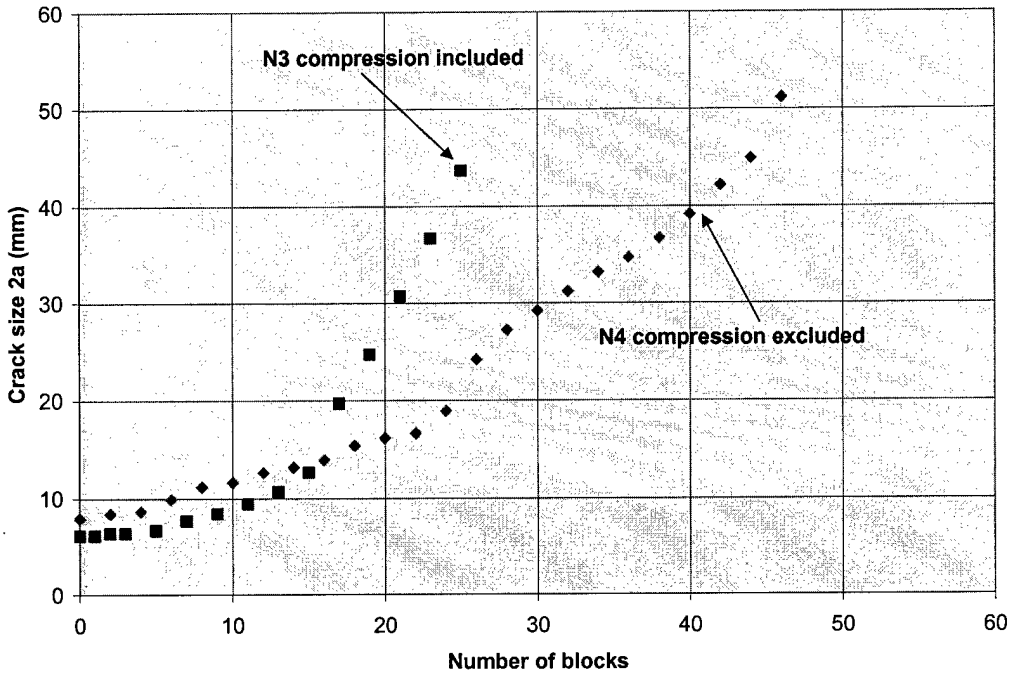

Fig.4.3: Crack growth curves of skin crack for narrow specimens loaded by C-141 spectrum with and without compressive loads.

As can be seen in Fig.4.3, N3 shows higher crack growth rates than specimen N4. This is a direct cause of the compressive loads that reduce the crack growth-reducing effect of plastic zones that are formed in tension, and thus reduce the crack growth rates.

Fig.4.4 shows the crack growth curves of the stiffener cracks in N3 and N4. The total crack size is the average value of the crack on the left and on the right side of the stiffener. Note that the starter crack in the stiffeners had already grown into the skin and the crack size in Fig.4.4 is the total stiffener crack starting at the inside of the skin and growing towards the top of the stiffener (maximum crack size is therefore 22.24 mm). As can be seen, the specimen with the compressive loads included in the spectrum shows larger crack growth rates than the specimen that was loaded by the spectrum without compressive loads.

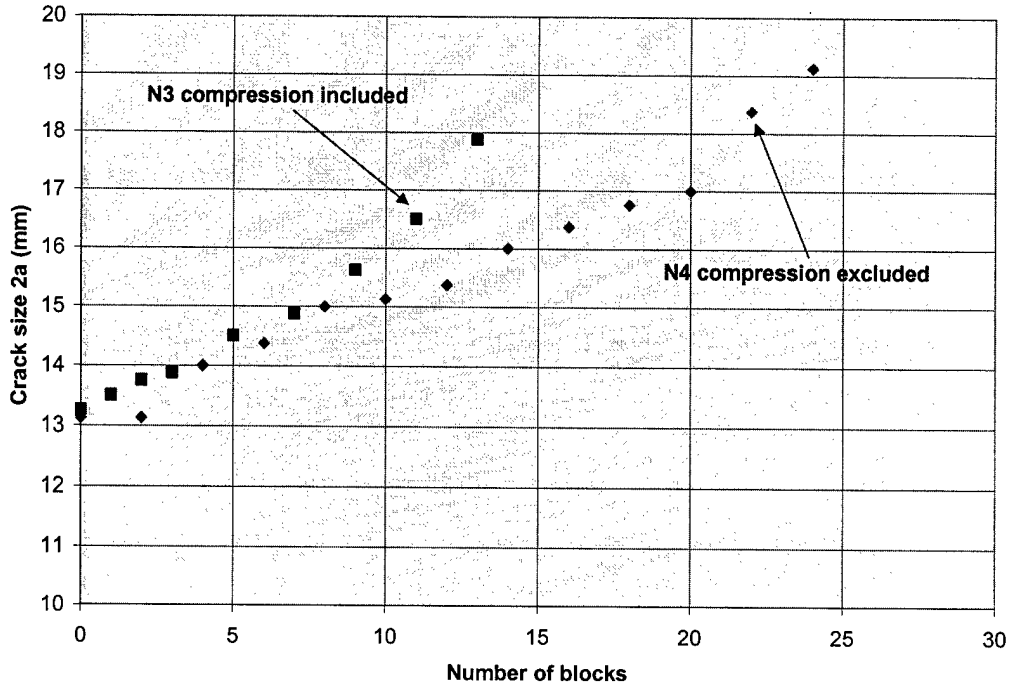

Fig.4.4: Crack growth curves of stringer crack for narrow specimens loaded by C-141 spectrum with and without compressive loads.

Although the differences between the two spectra used are significant for unpatched panels, it is expected that the differences will be less significant for patched specimens since tensile overloads cannot cause large plastic zones under patches because the patches reduce the stress intensity factor. Therefore, the presence of compressive loads will not make a large difference by reducing the effect of the plastic zones formed by tensile loads since these plastic zones will not be present or will be smaller to begin with.

4.3 SPECTRUM TESTS ON WIDE PANELS

As was the case with the narrow panels, two wide unpatched panels were tested with the two different spectra. However, as was expected from the static analysis, specimen W1 failed when tested with the C-141 spectrum including the compressive loads up to –100 MPa. Therefore it was decided to use a C-141 spectrum with maximum compressive loads of –40 MPa on panel W3.

For uncracked panels the static analysis showed that the wide and the narrow panels are loaded in a similar way and show similar strains. In the case of a crack reaching the edge of the narrow panel or the outer stiffeners of the wide panel, a difference in crack growth behavior can be expected. The free edge of the narrow panel could increase crack growth rates whereas the outer stiffeners will start to carry more load with increasing skin crack and could therefore

temporarily reduce crack growth rates in the skin. However, cracks are not grown up to the free edges of the narrow panel during these tests.

Fig.4.5 shows the skin crack measured on the stiffener side of the panel for the two narrow panels N3 and N4, and for the two wide panels W2 and W3. The total crack size is the sum of the crack on the left and on the right side of the stiffener, increased by the stiffener width. As can be seen, the crack growth curve of panel W2, loaded with the spectrum without compressive loads, shows lower crack growth rates than specimen N4, also loaded without compressive loads. This can be explained by the finite-width effect of panel N4 and the reinforcing presence of the outer stringers in panel W2. Crack growth rates are similar up to a total crack size of approximately 20 mm.

It can also be seen from Fig.4.5 that the starter crack of panel W3 is significantly larger than the starter cracks from the other panels. Because of this, direct comparison of crack growth becomes difficult. It can be seen that the slope of W3 is close to linear whereas the other panels show more parabolic crack growth curves in the beginning of these tests, followed by more linear crack growth at a larger crack size.

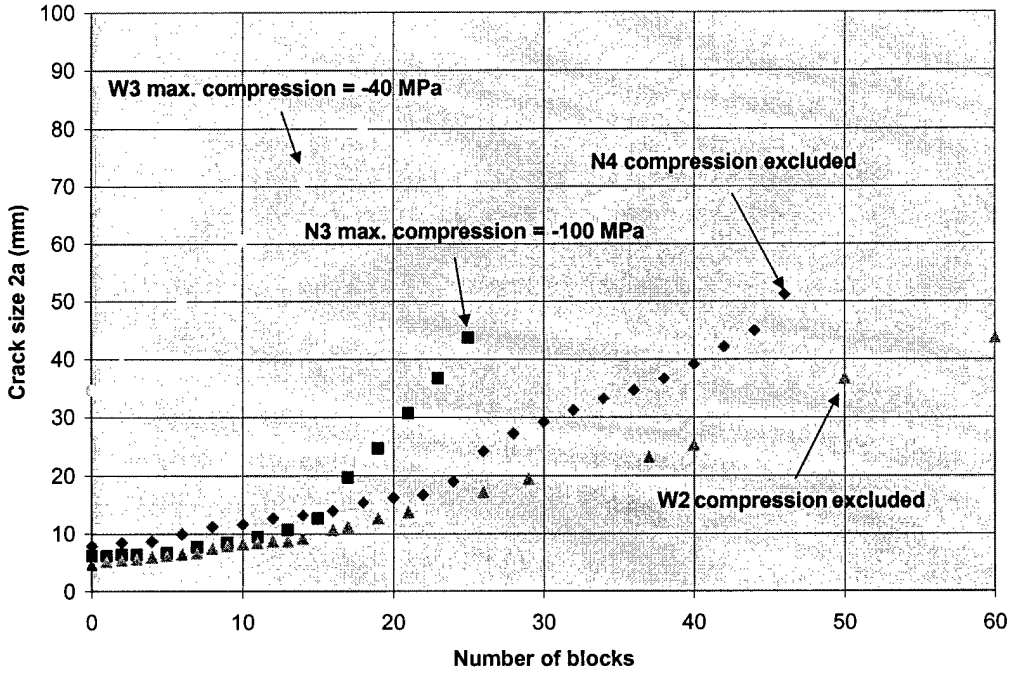

Fig.4.5: Crack growth curves of skin cracks for narrow and wide panels loaded by C-141 spectrum with and without compressive loads.

Fig.4.6 shows the crack growth curves for the stiffener cracks in N3, N4, W2 and W3. Again, the total crack size is the average value of the crack lengths on the left and right sides of the stiffener. Note that the starter crack in the stiffeners had

already grown into the skin, and the crack size in Fig.4.6 is the total stiffener crack starting at the inside of the skin and growing towards the top of the stiffener (maximum crack size is therefore 22.24 mm).

Again, the starter crack length for the stiffener crack of W3 was larger than for the other three specimens and therefore the initial crack growth is larger, resulting in shorter crack growth life of the stiffener. It should also be noted that the starter crack in the skin of W3 was larger, resulting in a panel that was less stiff and increasing the crack growth rates in the stiffener as well.

Chapter 6 will compare crack growth rates and give a more and a more detailed analysis.

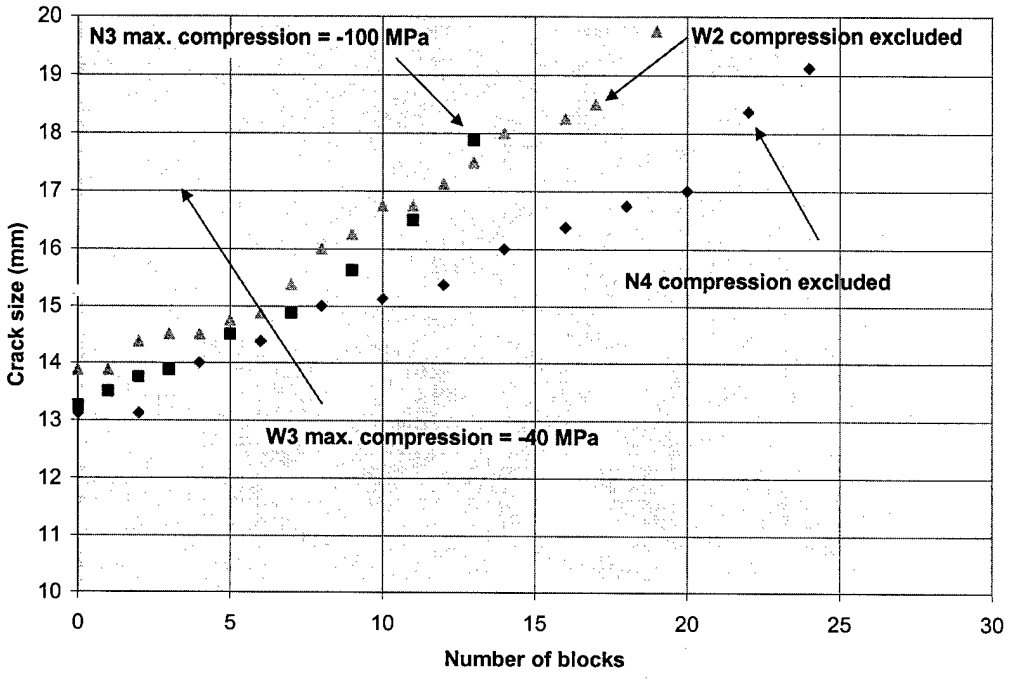

Fig.4.6: Crack growth curves of stringer crack for narrow and wide specimens loaded by C-141 spectrum with and without compressive loads.

5. SPECTRUM TESTS ON PATCHED PANELS

5.1 CRACK GROWTH MONITORING

As was the case with the unpatched panels, it is fairly easy to measure crack growth on the inside of the skin (tank/stiffener side) for the patched panels. However, because of the double sided patches on the stiffener it is not possible to observe crack growth in the stiffener itself using a microscope. Two available methods have been considered: C-scanning and Eddy-current method.

A difficulty with the C-scan is that the transmitter-receiver cannot cover the entire patch area close to the skin. The dimensions of the C-scan equipment in combination with the panel dimensions do not allow this. If the C-scan equipment could scan the entire height of the stiffener, the C-scans would not be able to show small crack size differences, the C-scan is scanning the debond and the reflection of the crack and not the crack itself. Therefore the C-scan equipment is not considered suitable for observing crack growth in the stiffener under the patches.

In order to penetrate the patches using Eddy-current, the probe dimensions need to be relatively large, limiting the resolution. Massar [7] predicted total crack growth of the patched stiffener crack of less than 0.4 mm per lifetime. It will be impossible to measure crack growth on this order using the Eddy-current method.

The only solution to measuring crack growth is to remove the stiffener patches at certain intervals, but this is not desirable; removal can cause damage to the panel and the conditions will change every time new patches are bonded to the stiffener. Because of these difficulties, the crack lengths in the patched stiffeners will not be monitored during testing.

5.2 SPECTRUM TESTS ON NARROW PATCHED PANELS

5.2.1 Spectrum tests on narrow patched panels

Four patched narrow panels were tested: two panels with boron-epoxy patches (N5 and N6) and two panels with Glare patches (N7 and N8). Fig.5.1 shows the crack growth curves for panel N5 and N6, repaired with boron-epoxy patches. As can be seen, both crack growth curves appear to be similar, showing no significant difference in crack growth behavior. In other words, the omission of the compressive loads for N5 does not seem to result in slower crack growth as was the case for the unpatched panels N3 and N4. Apparently, the influence of plasticity under bonded repairs can be neglected in this case. This can be explained as follows. The relatively high tensile loads are expected to cause insignificant plastic zones at the crack tip due to the large reduction in stress intensity factor underneath the patch. Because of the relatively small plastic

zones, compared to an unpatched situation, the compressive stresses cannot cause a large difference in crack growth rates by decreasing the effect of the plastic zones formed by tensile loads.

Fig.5.2 shows the crack growth curves for the narrow panels repaired with Glare patches, N7 and N8, combined with the results of specimens N5 and N6. As can be seen from this graph, there does not appear to be a significant difference in crack growth behavior between the specimen loaded by a spectrum including compressive loads, N7, and the specimen without compressive loads, N8. The explanation that was given for the panels with boron-epoxy patches is also valid in this case.

From Fig.5.2 it can be seen that there is no significant difference in crack growth behavior between the specimens with boron-epoxy patches and the specimens with Glare patches. Note that there is a difference in initial crack size between the two different patching materials, more on this can be found in paragraph 5.2.2. Possible splitting of the boron-epoxy patches does not seem to be of any concern, and the differences in the coefficients of thermal expansion between boron-epoxy and Glare seem to be overruled by other effects. In the past, using unstiffened thin skin specimens, specimens with boron-epoxy showed larger crack growth rates than similar specimens repaired with Glare patches. It was believed that this difference was caused by the difference in the coefficients of thermal expansion between both patch materials. The mismatch in CTE between aluminum and Glare is smaller than between aluminum and boron-epoxy, resulting in lower residual thermal tensile stresses when using Glare patches. Furthermore, when using patches with the same extensional stiffness, the Glare patches will be thicker than the boron-epoxy patches. Although, when considering secondary bending, this causes a larger deflection of the neutral axis, the Glare patches will also have a higher bending stiffness compared to the boron-epoxy patches, possibly resulting in overall lower bending stresses. These two effects could account for the lower crack growth rates when using Glare instead of boron-epoxy patches on thin unstiffened aluminum panels.

However, in this case, thick stiffened panels were tested and this could explain why Glare does not outperform boron-epoxy. The possible advantage of the higher bending stiffness of the thicker Glare patches is not present since bending over the crack is restricted by the stiffener on the panel. Furthermore, since the Glare patches are thick, shear lag in the patches can occur. The inner layers of the Glare patches might be highly loaded whereas the outer layers are hardly loaded, resulting in a patch that is effectively less stiff, possibly resulting in higher crack growth rates. Future research is planned to look into the effects of shear lag and bending behavior when using thick Glare patches.

During the tests the patched stiffeners did not fail in any of the specimens; they easily withstood one full life. If the patched structure is assumed to be

non-inspectable, the minimum required life is twice the remaining life of the aircraft. Therefore, assuming that the C-141's are at 75 percent of their life, only half a life time has to be accomplished. The patched structures have this capability. Fig.5.3 compares the crack growth curves of the patched panels with the unpatched panels N3 and N4. As can be seen, the reduction in crack growth after patching is significant.

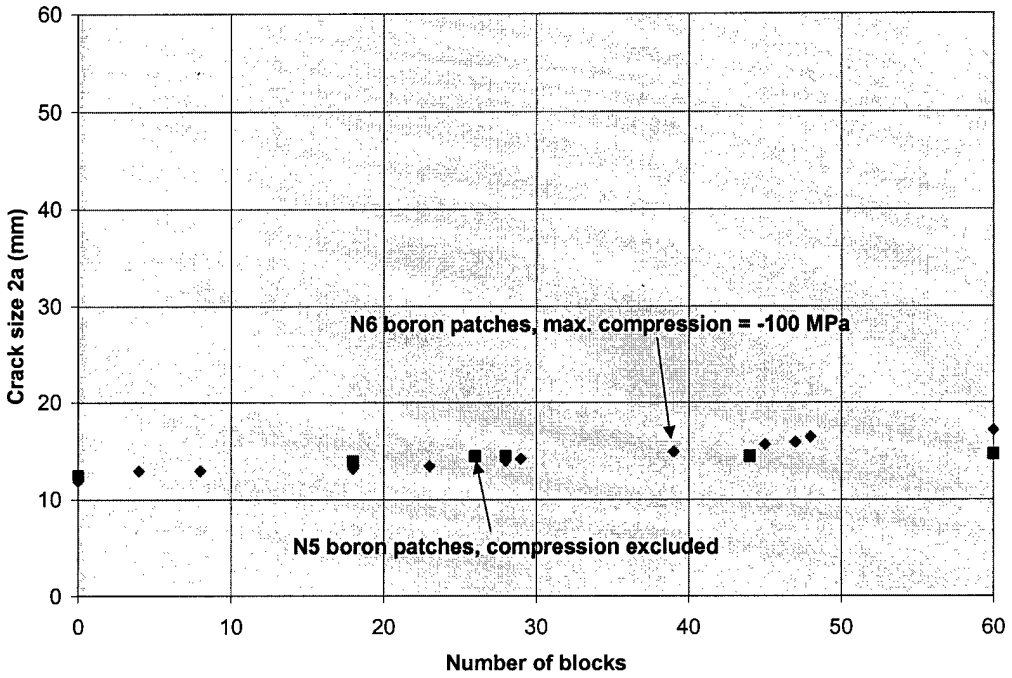

Fig.5.1: Crack growth curves of skin crack for narrow panels with boron-epoxy patches loaded by C-141 spectrum with and without compressive loads.

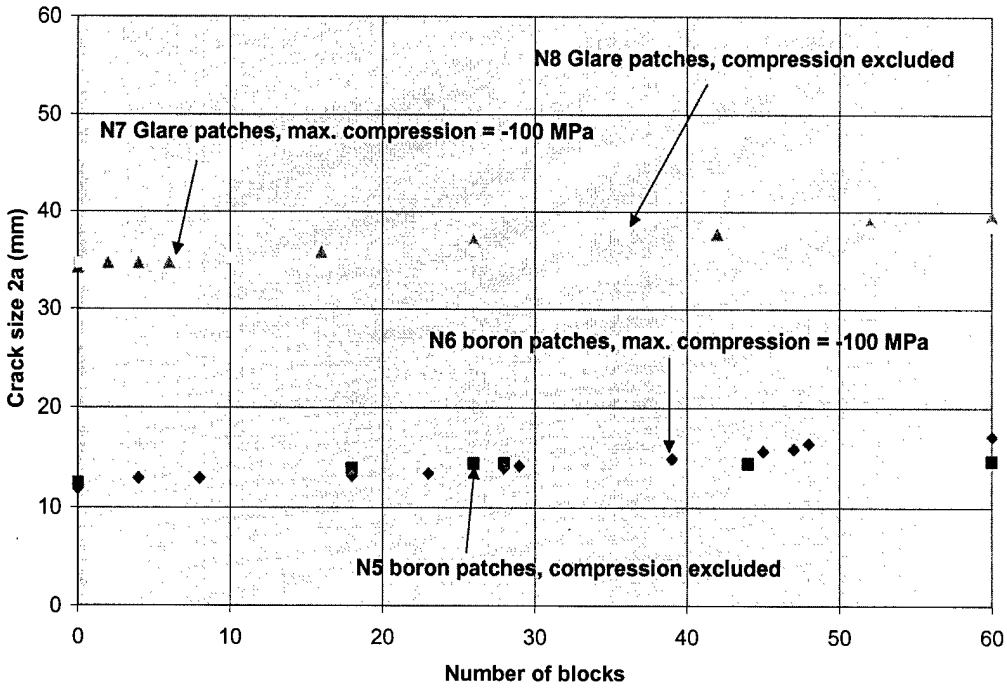

Fig.5.2: Crack growth curves of skin crack for narrow panels with boron-epoxy and Glare patches, loaded by C-141 spectrum with and without compressive loads.

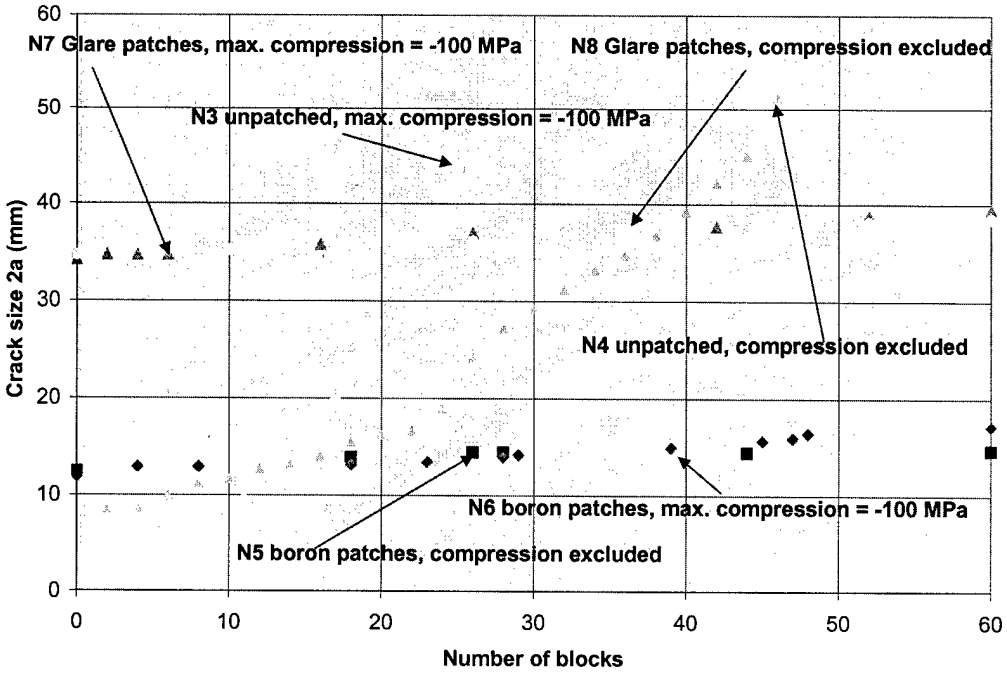

Fig.5.3: Crack growth curves of patched panels compared to unpatched panels.

5.2.2 Extra test to verify influence of different initial crack sizes

As was mentioned in paragraph 5.2.1, the panels with boron-epoxy patches showed similar crack growth behavior compared to the panels with Glare patches. However, as can be seen from Fig.5.2, the panels with boron-epoxy patches had significantly smaller initial cracks than the panels with Glare patches. This was purely coincidental, it was the intention to have similar starter cracks for all panels but during pre-cracking of the integral panels it was very difficult to control the crack size.

Before a comparison can be made between the crack growth rates of the panels with boron-epoxy patches and the panels with Glare patches, it is necessary to verify that crack growth underneath a bonded repair is constant, as is predicted by the Rose model. Therefore, one additional test was done. A narrow panel was pre-cracked in the same way as the other specimens until an initial crack size comparable to the panels with Glare patches was reached. This panel was then patched with boron-epoxy patches and loaded by a C-141 spectrum without the compressive loads.

The results for this extra test can be seen in Fig.5.4 (yellow triangular markers), together with the results for panels N5 through N8. As can be seen, the crack growth behavior of this extra panel with boron-epoxy patches is similar to the panel with Glare patches that was subjected to the same loading and with a similar starter crack size (N8). As can also be seen, the crack growth for this extra test is similar to the crack growth for panel N5, also with boron-epoxy patches and subjected to the C-141 spectrum without compressive loads but with a significant smaller starter crack. More crack growth information for this specimen will be given in chapter 6.

As can be concluded, the difference in starter crack size does not influence the crack growth rate significantly, as can be expected from the Rose model which predicts a constant stress intensity underneath the patch, independent of crack size, and, for the panels tested, crack growth for panels with boron-epoxy patches and Glare patches is similar. Possible explanations for this behavior were already given in paragraph 5.2.1.

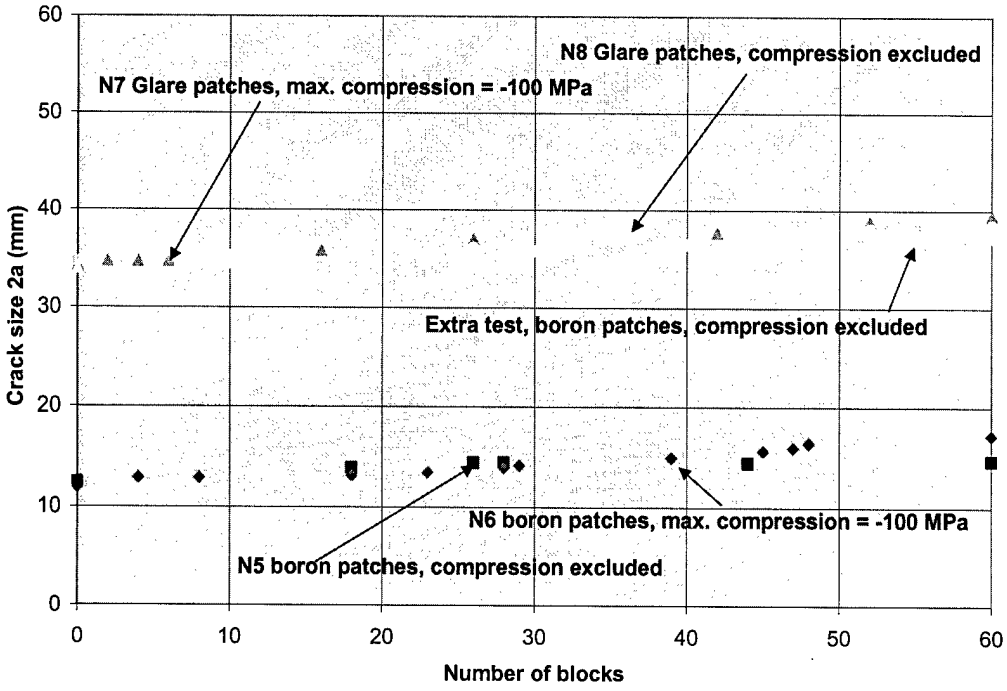

Fig.5.4: Crack growth curve of extra test (boron patches) loaded by C-141 spectrum without compressive loads, compared to specimens N5 through N8.

5.3 SPECTRUM TESTS ON WIDE PATCHED PANELS

As was the case with the narrow panels, four patched wide panels were tested. Two panels with boron-epoxy patches (W4 and W5), and two panels with Glare patches (W6 and W7). Panel W6 can be seen in Fig.5.5 and Fig.5.6.

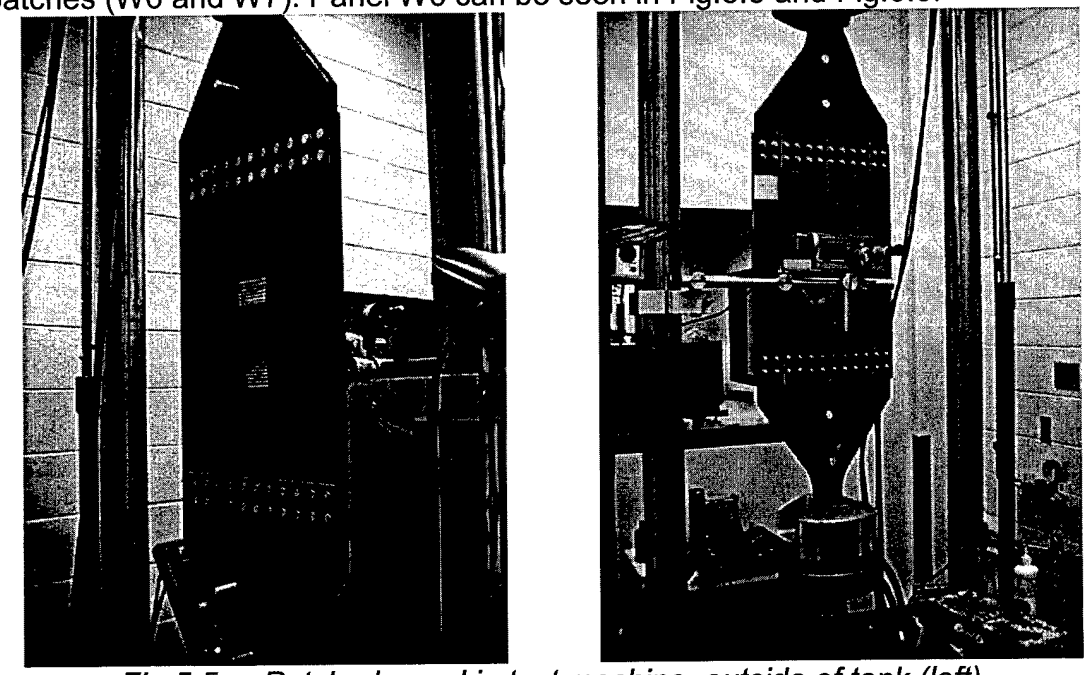

Fig.5.5: Patched panel in test machine, outside of tank (left) and inside of tank (right).

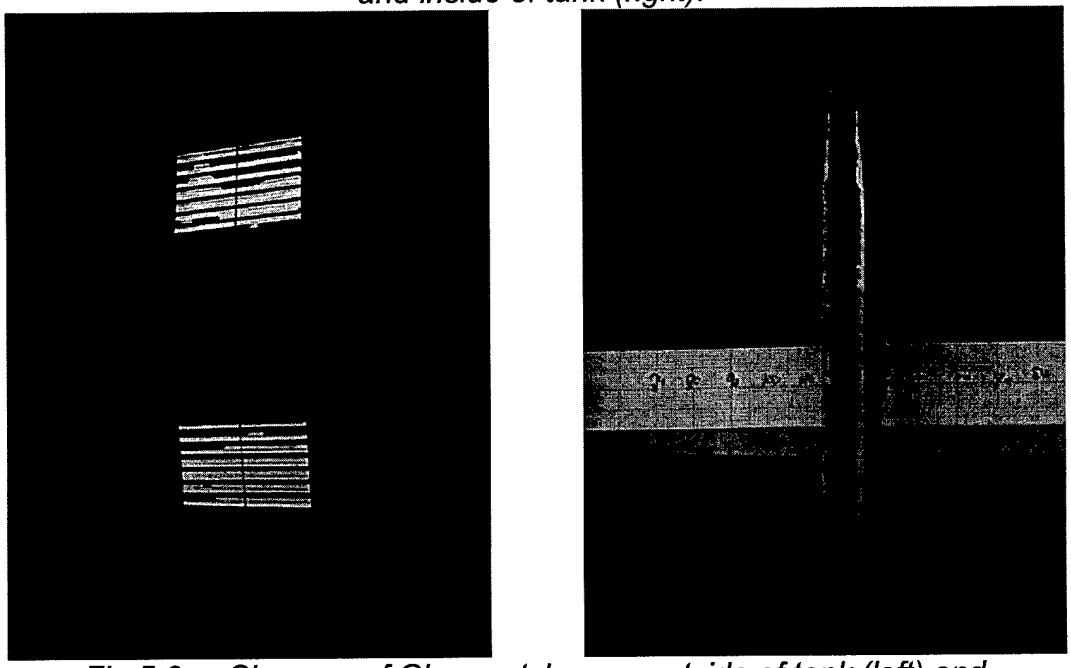

Fig.5.6: Close-up of Glare patches on outside of tank (left) and on stiffener on inside of tank (right).

Fig.5.7 shows the crack growth curves for panels W4 and W5 repaired with boron-epoxy patches. As was the case for the narrow panels repaired with boron-epoxy patches, both crack growth curves appear to be similar, showing no significant difference in crack growth behavior. In other words, the omission of the compressive loads for W5 does not result in significant slower crack growth, as was the case for the unpatched panels W2 and W3. Apparently, the influence of plasticity under bonded repairs can be neglected or is not present here. The explanation for the similar crack growth behavior for the two different spectra, with and without the compressive loads, is the same as was given for the narrow panels in paragraph 5.2.1.

Fig.5.8 shows the crack growth curves for the wide panels repaired with Glare patches, W6 and W7, combined with the specimens W4 and W5 repaired with boron-epoxy. As can be seen from this graph, there seems to be no significant difference in crack growth behavior between the specimen loaded by a spectrum including compressive loads, W6, and the specimen without compressive loads, W7. As was the case with the narrow panels, there appears to be no significant difference in crack growth behavior between the specimens with boron-epoxy patches and the specimens with Glare patches. Possible explanations for this were given in paragraph 5.2.1.

During the tests the center stiffeners did not fail in any of the specimens; they easily withstood one full life. If the patched structure is assumed to be non-inspectable, the minimum required life is twice the remaining life of the aircraft. Therefore, assuming that the C-141's are at 75 percent of their life, only half a life time has to be accomplished. The patched structures have this capability.

Fig.5.9 compares the crack growth curves of the patched panels with the unpatched panels W2 and W3. As can be seen, the reduction in crack growth after patching is large.

Chapter 6 will consider the crack growth rates of the patched as well as the unpatched specimens in more detail.

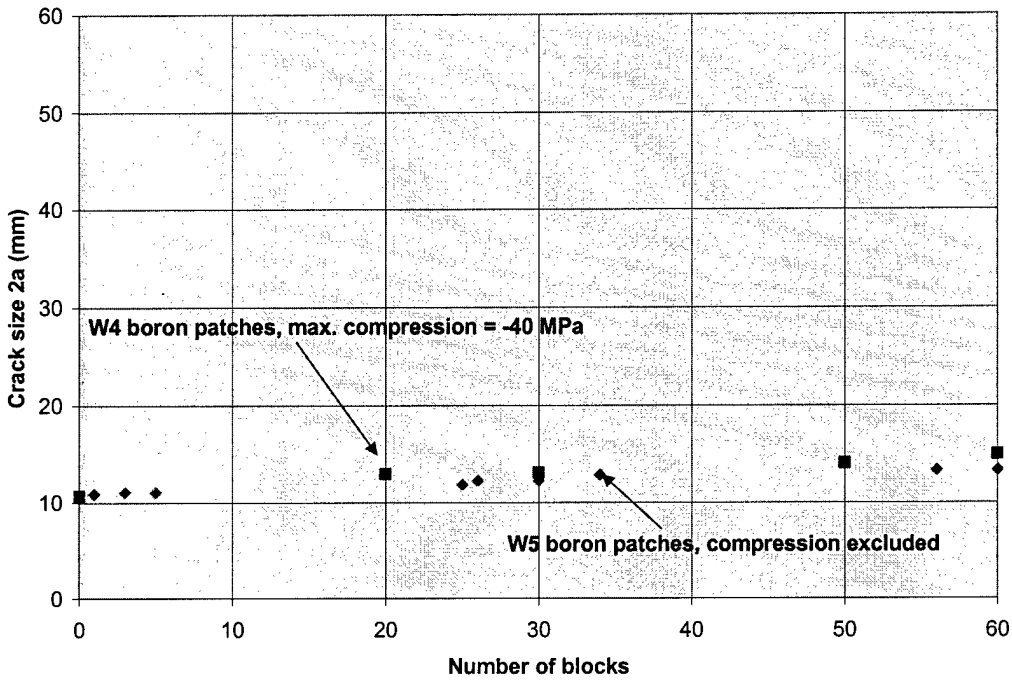

Fig.5.7: Crack growth curves of skin crack for wide panels with boron-epoxy patches loaded by C-141 spectrum with and without compressive loads.

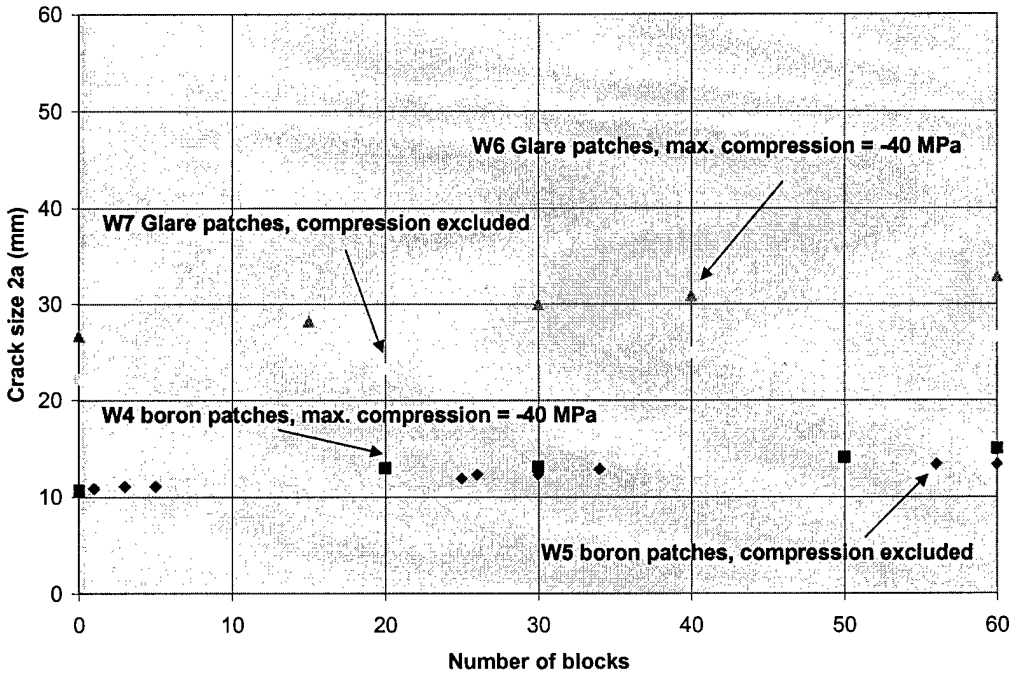

Fig.5.8: Crack growth curves of skin crack for wide panels with boron-epoxy and Glare patches, loaded by C-141 spectrum with and without compressive loads.

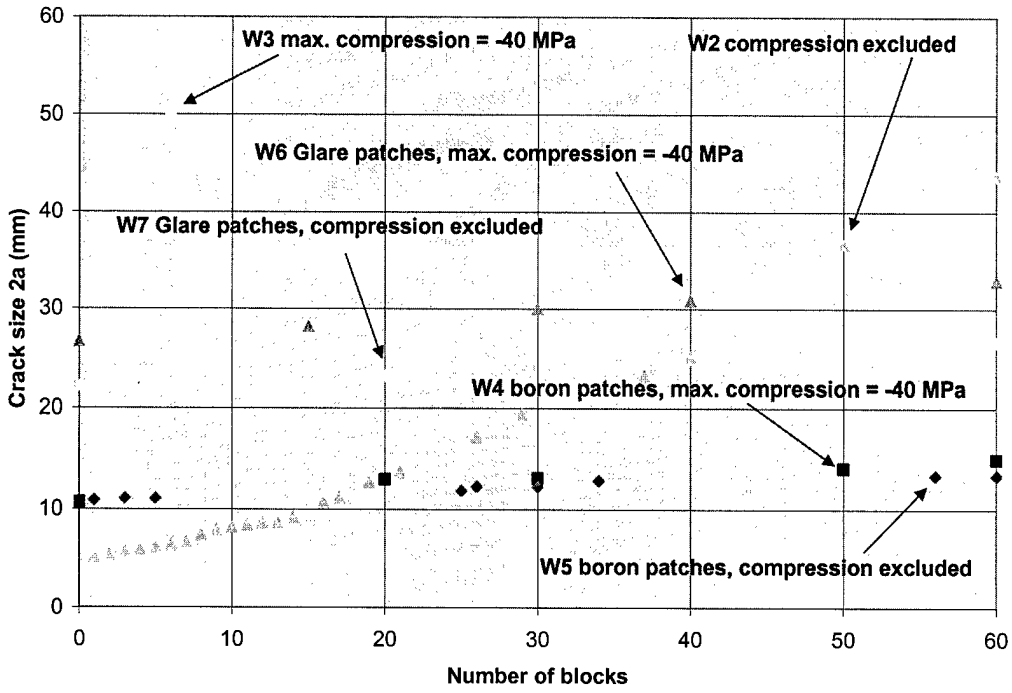

Fig.5.9: Crack growth curves of patched panels compared to unpatched panels.

6. CRACK GROWTH ANALYSIS

Chapter 4 and 5 showed the crack growth curves of both the unpatched and the patched specimens. It is possible to draw preliminary conclusions from these graphs, but a more thorough analysis is useful. This analysis will be given in this chapter as well as some background information on flight loads simulation, necessary for this analysis.

6.1 BACKGROUND INFORMATION ON SPECTRUM CONSTRUCTION

When performing a constant amplitude fatigue test it is fairly simple to analyze crack growth data in more detail. da/dN vs. ΔK curves and da/dN vs. a curves can be easily made since every load cycle is identical. This makes it simple to calculate the stress intensity factor, K, for each cycle at each crack size. When performing variable amplitude tests, each cycle can be different, and each cycle causes a different amount of damage or crack growth. Due to this variable character it is impossible to correctly construct the types of curves mentioned above.

However, there are some ways to evade these problems. To do this, two important assumptions have to be made: 1. all blocks within a spectrum should be considered identical and 2. the actual usage of an aircraft should be kept as close as possible to the statistical predictions made in the design phase of an aircraft. The following section will consider these two assumptions in more detail.

6.1.1 Assumptions

There are several ways to obtain variable amplitude data which can be tested on real aircraft structures or used as input for a crack growth prediction program such as AFGROW [11].

As was mentioned in Chapter 2, the spectrum data that was supplied by Warner-Robins ALC is based on statistical data. The spectrum data is obtained by statistical determination of the cyclic loading that the aircraft structure will experience during its service life. The task of the designers is to limit the uncertainties involved in the prediction of the expected loads. This can be done by careful analysis of the different missions (also called a mission profile or flight) for which the aircraft is designed. The design usage of an aircraft is defined by a mixture of design missions, also known as a mission profile set or a block.

The C-141 spectrum is divided into 60 blocks and each C-141 block represents 504.5 flight hours. Repeating these blocks sufficiently will result in the total life of an aircraft. Each block contains the same number and types of flights (mission profiles) in exactly the same order. However, the exact number and magnitude of cycles within a flight depend on the point in time in the aircraft life at which this flight occurs, due to statistical occurrences of cycles. Fractional occurrences are

summed and when an occurrence value of 1 is reached they are placed in the spectrum. Hence there can be a different number of cycles in each flight and thus in each block. It must be realized however that the differences between the different blocks are small. Therefore, it may be assumed that a block contains a constant amount of cycles, causing approximately the same amount of damage. Earlier spectrum tests on the C-5A fuselage aft crown repair showed that this assumption is justified; crack growth is nearly linear [12].

In the previous paragraphs only statistical loads were considered, as well as the method for constructing spectra for the purpose of crack growth predictions. For these predictions to be useful it is important that the actual aircraft is used in a way that is close to the assumed usage in the design phase. In order to assume that an aircraft is used in a relatively constant way throughout its life time, it is very important to manage the fleet well. For military aircraft, fatigue load monitoring has evolved from the simple counting accelerometer to new sophisticated recorder systems and complex data processing and analysis procedures. The larger air forces in the world have adopted the following load monitoring procedures [13] :

- Control point definition. By performing fatigue analysis and full scale tests, critical points are indicated in the structure. The most critical points are selected as control points. By monitoring these points, stress spectra are developed for these locations.
- Flight load survey. A fully strain-gaged and instrumented aircraft is used for flight load measurements to establish relationships between structural loads and various flight parameters.
- Service load spectra survey. A limited number of aircraft is equipped with extensive recording equipment to determine average stress spectra for the control points belonging to a specific task or for each mission type.
- Individual aircraft tracking (I.A.T.). Individual aircraft tracking involves each aircraft in the fleet and they are monitored for one or a few parameters. It is then possible to adapt the maintenance schedule to the individual usage severity.

I.A.T. can be necessary if the average load experience per mission type differs from aircraft to aircraft. This can be the case if an aircraft is always flown by the same pilot with a certain style or if a certain aircraft performs better than other planes, mainly caused by different performances of the engines. In the modern air forces, pilots do not fly the same aircraft all the time and engines are changed frequently, and thus the differences between certain aircraft for a specific mission can be ignored.

Second reason for the I.A.T. can be differences in the mission mixture, caused by the selection of specific aircraft for certain missions. This can occur if a particular mission requires a specific configuration that is only available on one or some of the aircraft. By careful managing of the fleet and, for example, changing

squadron composition, having a particular plane reach the end of its fatigue life while other planes are still in perfect condition (because of a less severe mission mixture) can be avoided. Keeping this in mind, it seems justified to assume that an aircraft is used in a relatively constant way throughout it's service life.

6.2 CRACK GROWTH RATES

As became clear from the previous paragraphs, it is not possible to construct da/dN vs. ΔK or da/dN vs. a curves when performing spectrum tests. It was also explained in the previous paragraphs that it is justified to consider a block within a spectrum as a constant amount of cycles, attributing a constant amount of damage to the structure. This makes it possible to construct da/d(Block) vs. a curves for the specimens tested.

All the crack growth data can be seen in Appendix B, together with curve fits made for the crack growth curves that were shown in Chapter 4 and 5. By taking the first derivative of the a vs. Block curves, it is possible to construct the da/d(Block) vs. a curves, shown in this chapter. Appendix B gives these curves for each of the specimens in more detail.

6.2.1 Narrow panels

Fig.6.1 shows the crack growth rates per block at each crack size for the skin cracks of the two narrow unpatched panels N3 and N4. As can be seen, the crack growth rates for specimen N3 are significantly higher than for N4. This is caused by the compressive loads in the spectrum that decrease the effect of plastic zones at the crack tip formed by tensile loads, and therefore reduce crack growth rates.

Fig.6.2 shows the crack growth rates for the stiffener cracks for both N3 and N4. Again it is clear that the stiffener crack in N3 grows at a higher rate than the stiffener crack in N4, caused by the presence of compressive loads in the spectrum.

Fig.6.3 shows the crack growth curves for the skin cracks in the four patched narrow panels as well as for the extra panel with boron-epoxy patches. From this graph it appears that there is a large difference in crack growth rates between the different specimens, but it should be noted that the scale on the vertical axis covers only a small range of crack growth rates. It can be seen clearly that the specimens had different starter cracks and it can also be seen that specimens loaded with spectra including compressive loads show higher crack growth rates than similar specimens loaded by a spectrum where the compressive loads are replaced by zero. It should further be noted that for the specimens with Glare patches, crack growth rates are somewhat higher for both the spectrum with and without the compressive loads but this is exaggerated by the scale on the vertical axis. It can further be noted that the extra panel with the boron patches shows

similar crack growth rates compared to specimen N8 with Glare patches and similar initial crack size.

Fig.6.4 combines the specimens with and without patches. From this graph it becomes very clear that the crack growth is significantly reduced by the presence of the patches and that the differences in crack growth rates between the different patched specimens are insignificant.

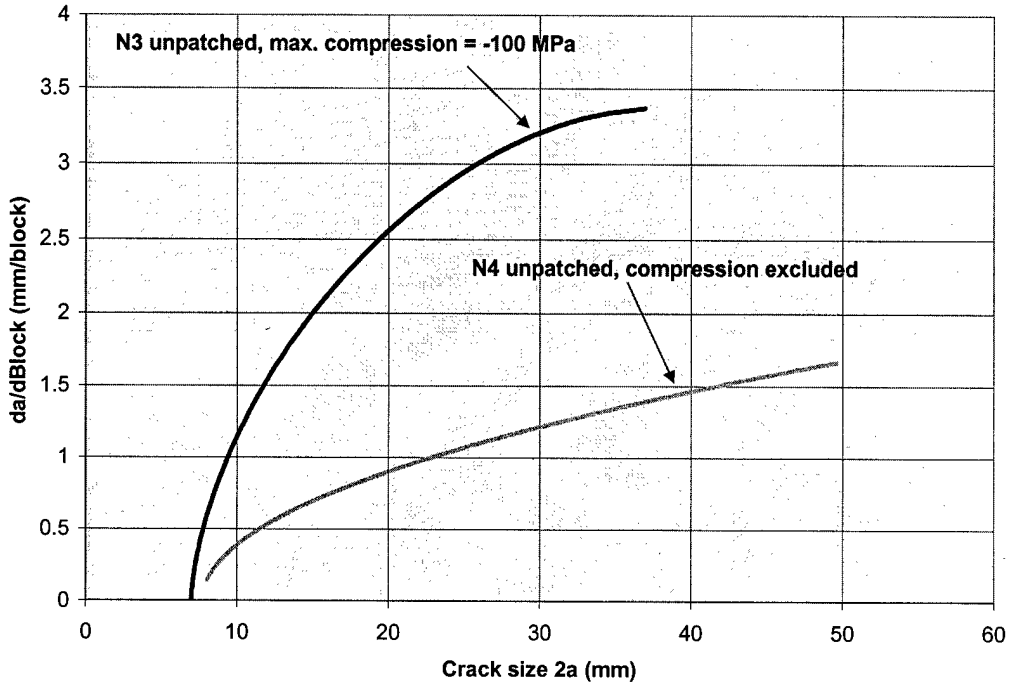

Fig.6.1: Crack growth rates (mm per block) versus crack size for skin cracks in narrow unpatched panels.

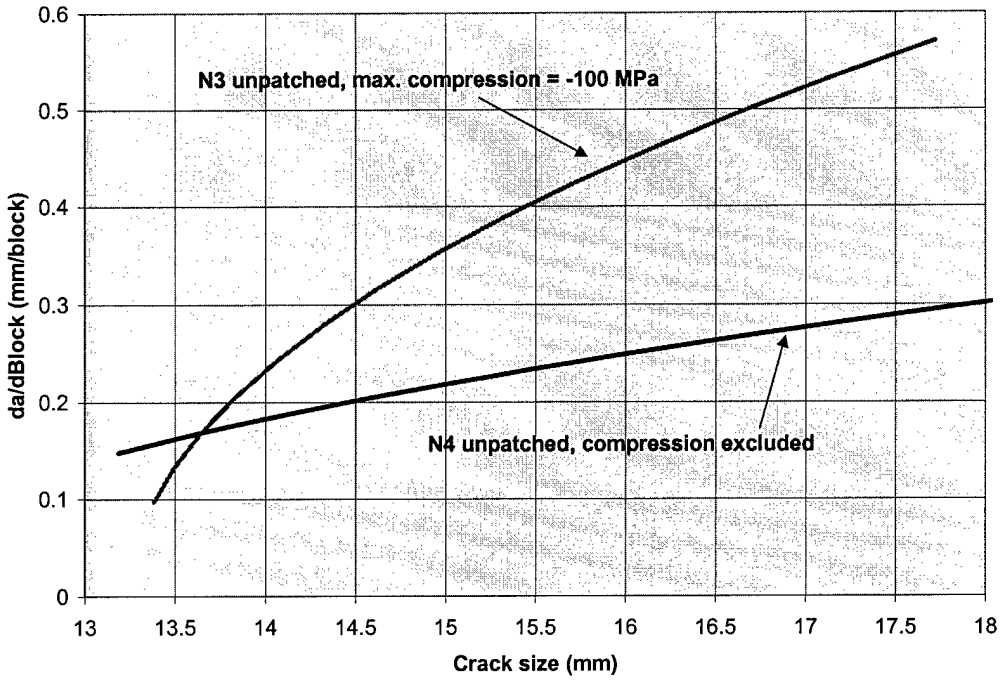

Fig.6.2: Crack growth rates (mm per block) versus crack size for stiffener cracks in narrow unpatched panels.

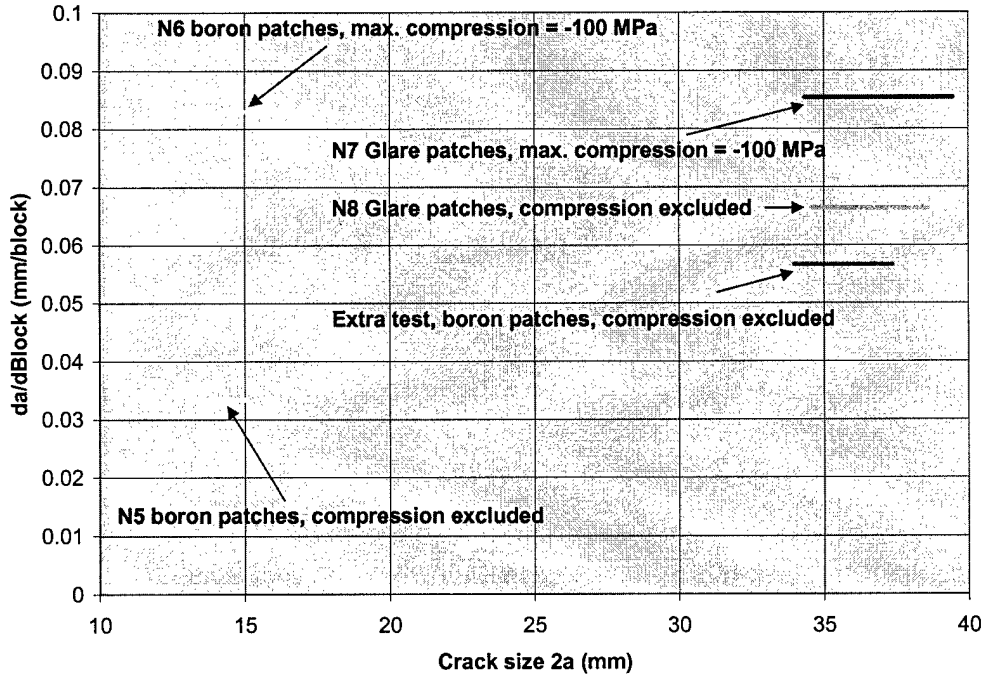

Fig.6.3: Crack growth rates (mm per block) versus crack size for skin cracks in narrow patched panels.

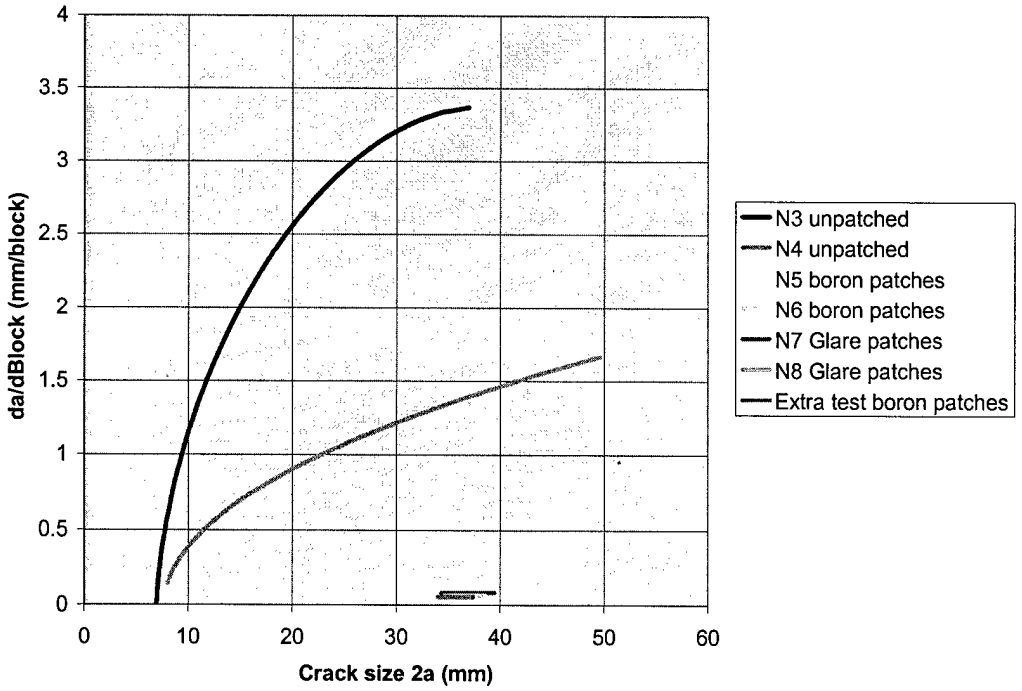

Fig.6.4: Crack growth rates (mm per block) versus crack size for skin cracks in narrow unpatched and patched panels.

6.2.2 Wide panels

As can be seen in Fig.6.5 the wide unpatched specimen only loaded by a positive spectrum, W2, has significantly lower crack growth rates in the skin than the specimen that was also loaded by compressive loads, W3. The same explanation applies as the explanation given for the narrow panels in the previous paragraph and in paragraph 5.2.1.

Fig.6.6 shows the crack growth rates for the stiffener cracks for specimens W2 and W3. It is clear that the stiffener crack in W3 grows at a higher rate, but there are two explanations for this: compressive loads and starter crack size. The starter cracks in the skin as well as in the stiffener were larger in W3, resulting in a specimen with less stiffness, causing higher crack growth rates. This combined with the compressive loads in the spectrum results in a significantly higher crack growth rate for W3 compared to W2.

Fig.6.7 shows the crack growth rates for the skin cracks of the wide patched specimens. Again the differences between the specimens appear to be large. But note that the scale on the vertical axis only covers a small range of crack growth rates. Specimens loaded only in tension show lower crack growth rates than the specimens with identical patches loaded by a spectrum including compression loads.

Fig.6.8 combines the results for the skin cracks of the patched and unpatched panels and it can be seen that the patched cracks grow at a significantly lower rate than the unpatched cracks in W2 and W3. Note that crack growth rates for the skin cracks for patched specimens are constant as can be expected from the Rose model.

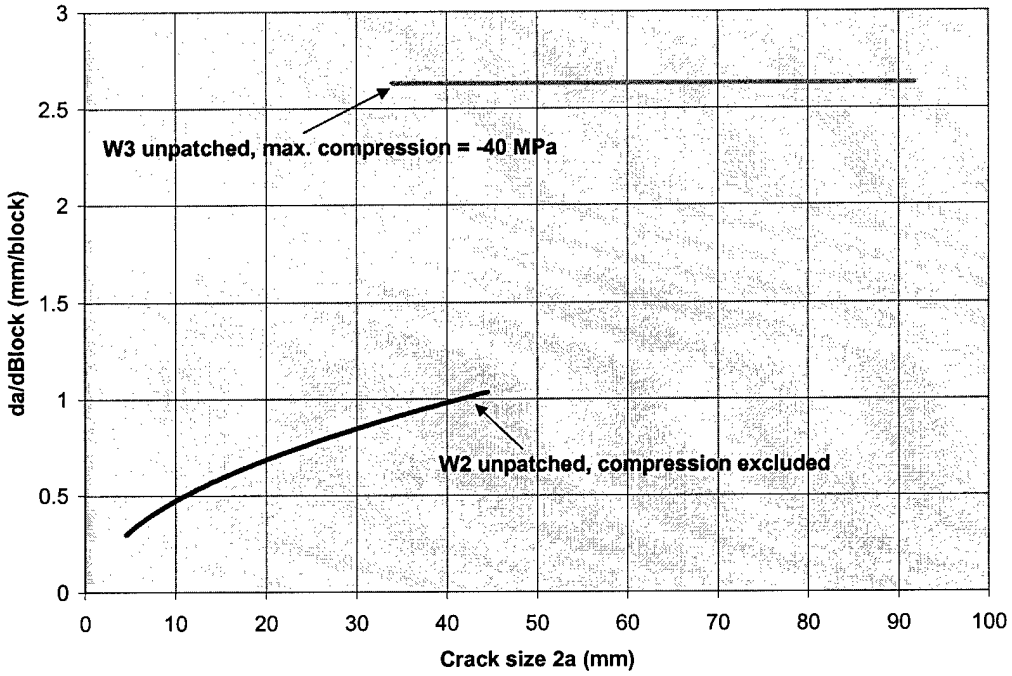

Fig.6.5: Crack growth rates (mm per block) versus crack size for skin cracks in wide unpatched panels.

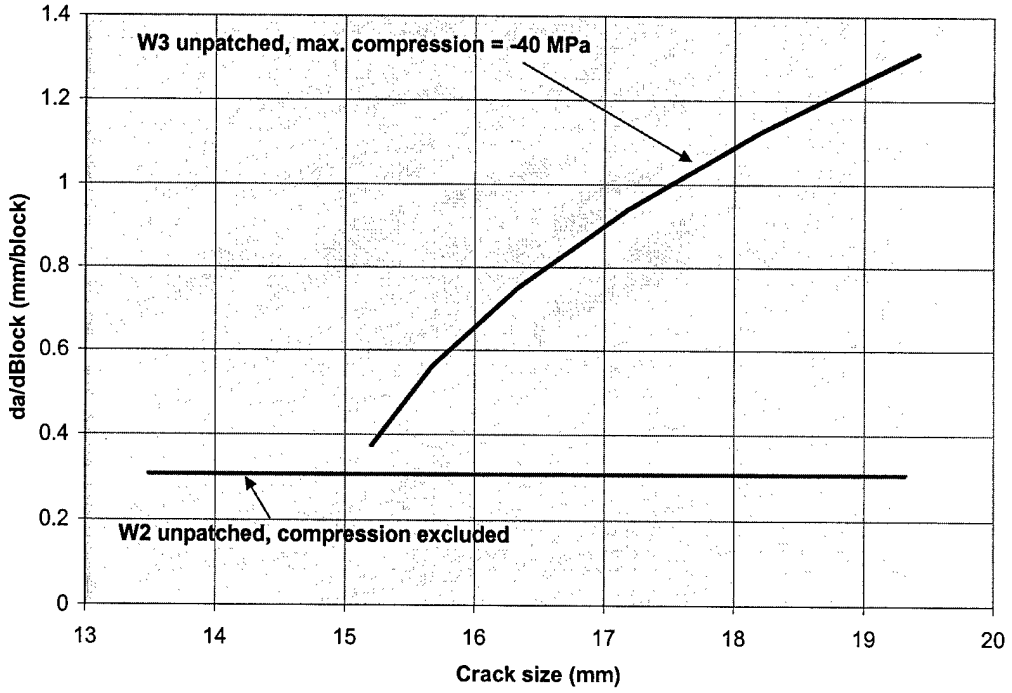

Fig.6.6: Crack growth rates (mm per block) versus crack size for stiffener cracks in wide unpatched panels.

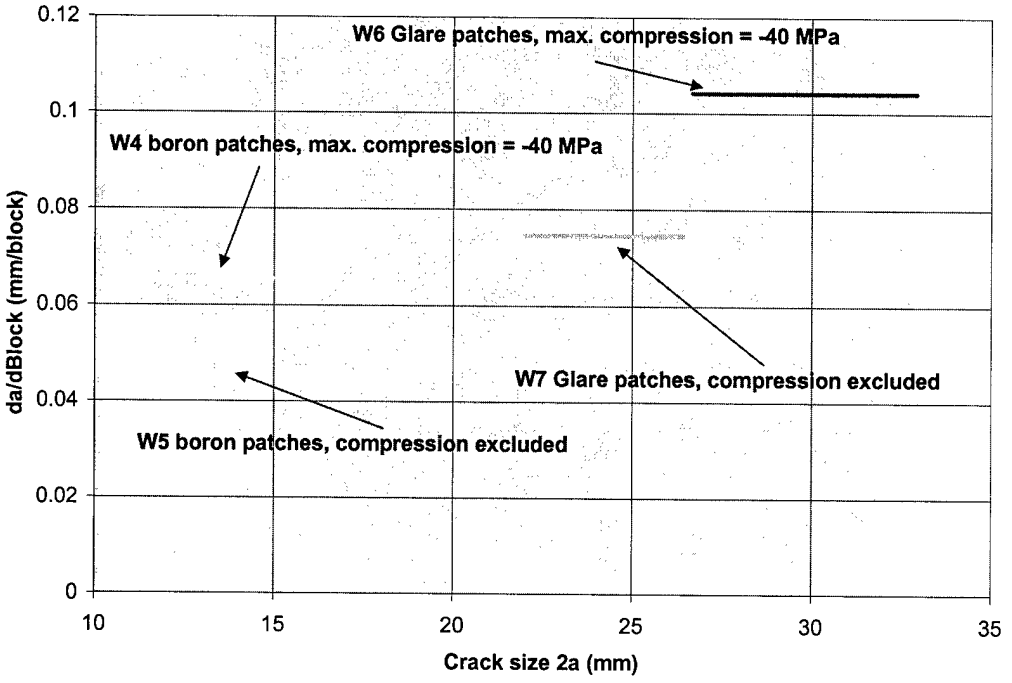

Fig.6.7: Crack growth rates (mm per block) versus crack size for skin cracks in wide patched panels.

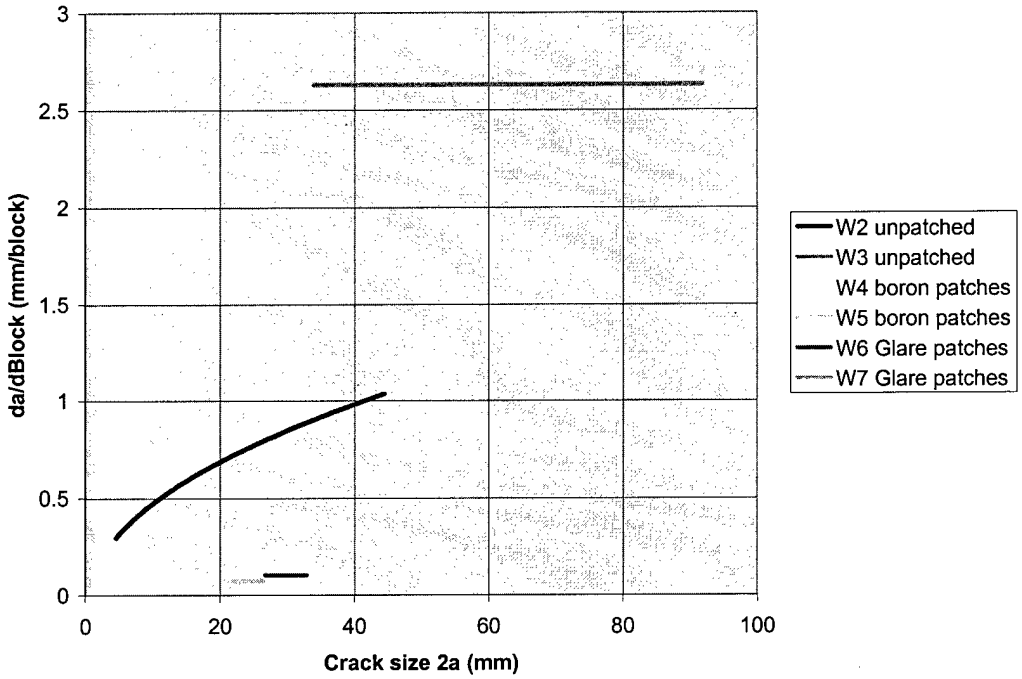

Fig.6.8: Crack growth rates (mm per block) versus crack size for skin cracks in wide unpatched and patched panels.

6.2.3 Comparison of wide and narrow panels

Due to the compression limitations of the wide panels, as was discussed in Chapter 3, it is only possible to compare the wide and narrow panels when loaded by the spectra that omit compressive loads.

One interesting subject, when comparing narrow to wide specimens, is the possibility of load attraction. Load attraction can occur when a stiff inclusion is present in a less stiff surrounding structure. Loads from the surrounding structure are drawn into the stiffer zone. In case of a patched crack this results into additional load attraction to the repaired area compared to the situation prior to repair. For this reason patches with a moderate extensional stiffness are preferred over high extensional stiffness patches. Load attraction is a known effect in unstiffened panels but it is interesting to see if, and to what extend load attraction will occur in stiffened panels.

Fig.6.9 shows the crack growth rates for the skin cracks of the wide and narrow panels that were loaded under the C-141 spectrum with only tensile loads. As can be seen, the crack growth rates for the patched panels are all of the same order of magnitude. When considering load attraction into the patched area, it would be expected that the wide panels would show higher crack growth rates since there is more surrounding structure on both sides of the patch from which load can be attracted into the patched area, whereas the narrow panel has

almost no surrounding structure next to the patch from where load could be transferred into the patched area. However, no significant difference in crack growth rates can be seen from the comparison of the patched wide and the narrow panels, and apparently load attraction does not play a significant role in these panels. Therefore, it appears to be valid to use the narrow panels for fatigue crack growth experiments of patched cracks.

A possible explanation for the lack of load attraction is that the narrow panels can be considered as the center section of the wide panels. Although the center section of the panels are stiffer due to the presence of the patches, the outer sections of the wide panels are also stiff due to the outer stiffeners. Instead of load from the surrounding skin of the central stiffener going into the patched area, it is possible that this load is still attracted by the outer stiffeners, reducing the loads attracted into by the patched area. Therefore, the difference between the wide and narrow panels could be minimal so that there is no noticeable difference in crack growth rates.

Another possible explanation could be caused by the presence of the central stiffener. In case of the narrow panel, the stiffener material could be considered to widen the actual width of the panel by spreading the stiffener material over the width of the panel, and allowing load attraction from the stiffener into the patched skin area. Therefore, the narrow panels should not be considered being narrow without the possibility of load attraction, and the expected difference will not be present.

Fig.6.9 also shows the comparison of crack growth rates for the unpatched narrow and wide panels tested in tension. As can be seen, the narrow specimen shows somewhat higher crack growth rates than the wide panel. One possible explanation could be the effect of humidity. Since both panels were not tested at the same time, changes in humidity could affect crack growth. Currently, research is being done into the effects of temperature and humidity on crack growth, both on patched as well as unpatched specimens.

Fig.6.10 shows the crack growth rates for the stiffener cracks of the wide and narrow panels only loaded in tension. Note that the vertical scale covers a small range compared to Fig.6.9. Again there is a difference in crack growth rates for the wide and narrow panel for which difference in humidity could be an explanation.

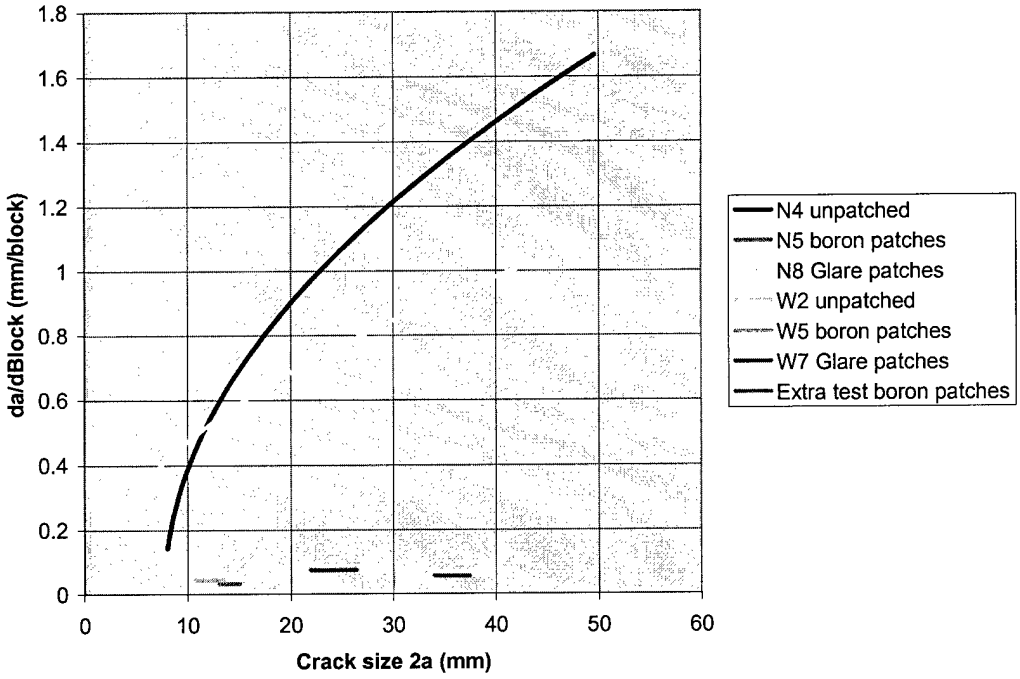

Fig.6.9: Crack growth rates (mm per block) versus crack size for skin cracks in wide and narrow patched panels loaded by positive spectrum.

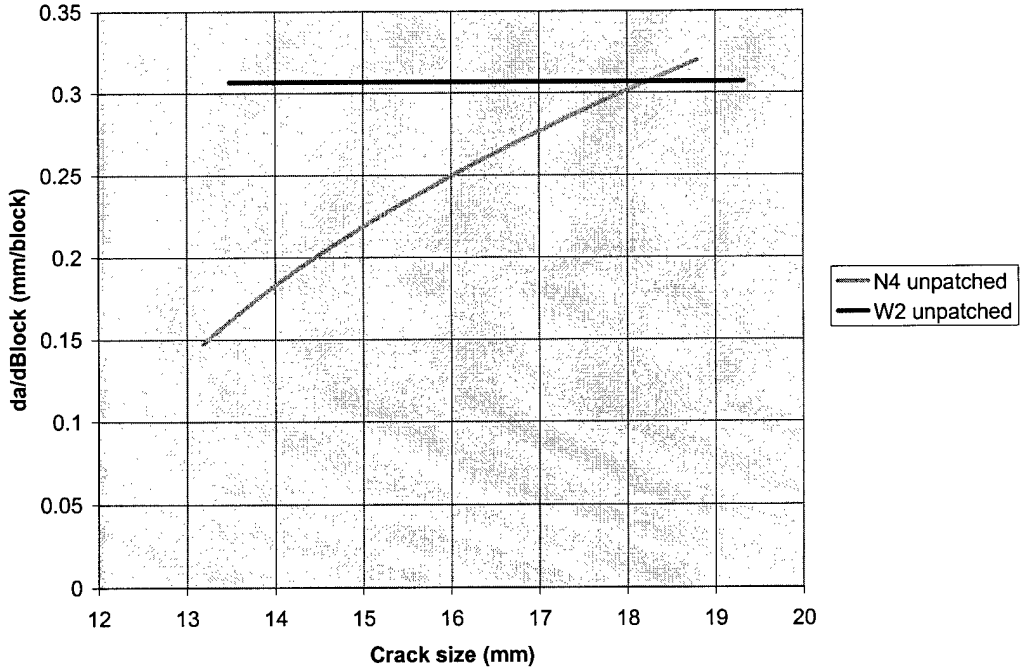

Fig.6.10: Crack growth rates (mm per block) versus crack size for stiffener cracks in wide and narrow unpatched panels loaded by positive spectrum.

6.3 CRACK GROWTH VERIFICATION

As was mentioned in the introduction, the data in this report will be used for verification of the new and/or improved models that will be incorporated into CalcuRep2000. However, CalcuRep2000 will not be a crack growth prediction program. Through input and output files the user can combine the repair results with the crack-growth program of choice, such as AFGROW [11].

One of the new capabilities of CalcuRep2000 will be the spectrum capability. The spectrum capability and compatibility of the program is greatly improved by the capacity of using input stress files, and output stress-intensity (K), or ΔK files. The size of these files is unlimited, therefore many calculations can be executed in one step. The output file from CalcuRep2000 could be used as a lookup table for a crack growth prediction code.

By using the spectrum files that were used for the testing of the specimens as input files in CalcuRep2000, output files containing K values or ΔK values will be generated by the program. Since these files will be in Excel format, compatibility is possible with, for example, AFGROW. It will be straightforward to generate these stress intensity files for each block of the spectra used in this report. Using a crack growth prediction code, the crack extension can be calculated for each block. After processing one block, the crack extension can be added to the starter crack and a new crack length is obtained, which will be the "starter crack" for the next block being processed.

Performing these calculations would be fairly simple but, at this point, not yet possible since CalcuRep2000 is still in its development phase. It is expected to be ready in the summer of 2000. The data in this report is ready for usage in combination with CalcuRep2000 and a crack growth prediction code of choice in order to verify the new and improved models that will be incorporated into the new program.

7. CONCLUSIONS

7.1 STATIC ANALYSES

The strain gage results for the wide and narrow panels show that the grips introduce the loads satisfactory as far as distributing the load over the panel is concerned. By measuring the strains on both sides of the skin, it becomes clear that there is no variation of stress throughout the thickness of the skin. By measuring the strains on top of the stiffener, it is evident that the load introduction into the stiffeners occurs over a short distance. It also becomes clear from the strain gage results that the gages on top of the stiffener show consistently lower strains than the gages on the outside of the skin, adjacent to the stiffeners. This difference in strain is caused by secondary bending of the panel since the panels are not loaded on the neutral line by the grips but are only gripped at the skin. Although there is secondary bending, all gages show linear results in tension.

Comparison of the strains in the wide panel and the narrow panel shows that the strains in the narrow panel are similar to the strains in the wide panel. It should be kept in mind that the panels did not have cracks. The stress distribution can and did change when cracks are present in the stiffener and skin.

When comparing FE-calculated load cases to strain gage results, it can be seen that the average absolute error decreases with increasing applied load for both the wide and the narrow panel. The average error for the narrow panel is lower than the average error for the wide panel but is mainly caused by a large deviation in one of the strain gages on the wide panel.

Testing the narrow panel in compression shows that the skin and stiffener buckle; the gage readings are not linear over the range of loading. The skin of the narrow panel buckles in a twisting mode, during which the stiffener is still able to carry more load. Gages on the stiffener show that there is some buckling in the stiffener but the stiffener is still able to carry load with increasing applied stress. The non-linear behavior is due to the nature of the panel dimensions, which are not equivalent to the actual C-141 wing panel dimensions. Although the narrow panel can carry the maximum compressive load in the C-141 spectrum, the buckling characteristics of the narrow panel require reducing the maximum compressive spectrum load. Compressive testing of the wide panels resulted in compressive failure. The load versus displacement curve of the wide panel becomes non-linear at approximately -50 MPa. A possible explanation for the compressive failure of the wide panel is the fact that the total length of the specimen, including grips, is larger for the wide panel compared to the narrow panel and therefore reducing the critical buckling load of the panel. To be able to test the wide panels under spectrum loading including compressive loads, it was decided to reduce the maximum compressive load to –40 MPa.

7.2 SPECTRUM TESTS ON UNPATCHED PANELS

7.2.1 Narrow panels

Two different spectra are used for testing; the original C-141 spectrum including compressive loads (-100 MPa for narrow panels and –40 MPa for wide panels), and a modified spectrum where the compressive loads are replaced by zero. Testing of two narrow unpatched panels shows significantly larger crack growth rates in both skin and stiffener for the specimen loaded by the spectrum including compressive loads. This is caused by the compressive loads in the spectrum that decrease the effect of plastic zones at the crack tip formed by tensile loads, and therefore reduce crack growth rates.

7.2.2 Wide panels

When testing a wide panel with a spectrum including the compressive loads up to –100 MPa, failure of the panel occurred in compression. This was expected from the static analysis. It was decided to use a spectrum with maximum compressive loads of –40 MPa on the wide panels. The specimen loaded by a spectrum with only tensile loads had significantly lower crack growth rates in both skin and stiffener, compared to the specimen that was loaded by a spectrum including compressive loads. The same explanation applies as the explanation given for the narrow panels in the previous paragraph.

Due to the compression limitations of the wide panels, it is only possible to compare the wide and narrow panels loaded by the spectra that omit the compressive loads. The unpatched narrow specimen showed somewhat higher crack growth rates for the skin crack compared to the wide panel, whereas the crack growth rate in the stiffener in the narrow specimen was smaller than for the wide panel. These differences in crack growth rates could be caused by humidity since the narrow and wide panel were not tested at the same time.

7.3 SPECTRUM TESTS ON PATCHED PANELS

7.3.1 Narrow panels

Four patched narrow panels were tested: two panels with boron-epoxy patches and two panels with Glare patches. Comparing specimens loaded by spectra including compressive loads to specimens loaded only by a tensile spectrum showed only marginal differences. The omission of compressive loads has no significant effect on crack growth under patches. This can be explained by the fact that high tensile loads hardly cause significant plastic zones at the crack tip due to the large reduction in stress intensity factor underneath the patch. Because of the relatively small plastic zones, the compressive stresses cannot cause a large difference in crack growth rates by decreasing the effect of plastic zones formed by tensile loads, that are not present to begin with.

Furthermore, it was found that there is no significant difference in crack growth behavior between the specimens with boron-epoxy patches and the specimens with Glare patches. Possible splitting of the boron-epoxy patches does not seem to be of any concern, and the differences in the coefficients of thermal expansion between boron-epoxy and Glare seem to be overruled by other effects. Two possible explanations were given: 1. the restriction of bending over the crack by the stiffener, canceling the possible advantage of the higher bending stiffness of a Glare patch, compared to a boron-epoxy patch with the same extensional stiffness 2. shear lag in the thicker Glare patches, resulting in higher loading of the bottom layers and allowing more crack opening. Future research is planned to look into the effects of shear lag and bending behavior when using thick Glare patches.

Since the panels with Glare and boron-epoxy patches had significantly different initial crack sizes, one extra test was done to verify the influence of the difference in starter crack size on crack growth. As could be expected from the Rose model, it was found that the difference in starter crack size does not influence the crack growth rates significantly.

Comparing crack growth rates of narrow patched and unpatched panels shows that the crack growth is significantly reduced by the presence of the patches and the stiffeners did not fail in any of the patched specimens. The repair easily withstood one full C-141 life.

7.3.2 Wide panels

Four wide patched panels were tested: two with Glare patches and two with boron-epoxy patches. There was no significant difference in crack growth rates between the specimens loaded by a spectrum including compressive loads and by a spectrum without compressive loads. The explanation that was given for the narrow panels also applies for the wide panels.

As was the case with the narrow panels, there appears to be no significant difference in crack growth behavior between the specimens with boron-epoxy patches and the specimens with Glare patches. Possible splitting of the boron-epoxy patches does not seem to be of any concern, and the differences in the coefficients of thermal expansion between boron-epoxy and Glare seem to be overruled by other effects. The same explanations that were given for the narrow panels apply: 1. the restriction of bending over the crack by the stiffener, canceling the possible advantage of the higher bending stiffness of a Glare patch, compared to a boron-epoxy patch with the same extensional stiffness 2. shear lag in the thicker Glare patches, resulting in higher loading of the bottom layers and allowing more crack opening.

By comparing the crack growth rates for the skin cracks of the patched and unpatched panels, it can be seen that the patched cracks grow at a significantly lower rate than the unpatched cracks. During the tests the center stiffeners did not fail in any of the specimens and the repair easily withstood one full life.

Comparison of the crack growth rates of the patched narrow and wide panels, tested under the C-141 spectrum with only tensile loads, showed that the crack growth rates for the skin cracks were all of the same order of magnitude. When considering load attraction into the patched area, it would be expected that the wide panels would show higher crack growth rates since there is more surrounding structure on both sides of the patch from which load can be attracted into the patched area, whereas the narrow panel has almost no surrounding structure next to the patch from where load could be transferred into the patched area. However, no significant difference in crack growth rates can be seen from the comparison of the patched wide and the narrow panels, and apparently load attraction does not play a significant role in these panels. Therefore, it appears to be valid to use the narrow panels for fatigue crack growth experiments of patched cracks.

The data that was obtained during this research can be readily used for verification of the new and/or improved models in CalcuRep2000 when it will be ready in 2000. It will be straightforward to generate stress intensity files for each block by using these spectrum files as input files in CalcuRep2000. Output files containing K values or ΔK values can be generated and, by using a crack growth prediction code, the crack extension can be calculated for each block, and direct comparison with the results in this report will be possible.

REFERENCES

1. For CalcuRep software go to: http://www.usafa.af.mil/ Follow links to Academics, Dean of the Faculty, Engineering Mechanics (DFEM), CAStLE. A password is required for downloading the software.

2. Rose, L.R.F. (1988). *Theoretical analysis of crack patching,* in : *Bonded repair of aircraft structures pp. 77-106,* Baker, A.A., Jones, R., editors. Martinus Nijhoff Publishers, Dordrecht, The Netherlands.

3. Guijt, C., Krul, D., Greer, J., Mazza, J. (1999). *New design tools for bonded repairs.* 1999 USAF Aircraft Structural Integrity Program Conference, San Antonio, Texas.

4. D.R.C Siwpersad (1996). *Bonded Glare patches for the repair of cracked aluminum fuselages.* Master Thesis, Delft University of Technology.

5. Hall, K.B. (1993), *Spectra development analysis.* Lockheed, Excerpt section 4.2 LG93ER0022, pp. 4-23 through 4-88.

6. C-141 data supplied by Warner Robins ALC.

7. Massar, J.J.A. (1999), *Crack growth predictions of bonded repairs by means of Finite Element Models.* Master Thesis, Delft University of Technology.

8. Verhoeven, S. (1997), *Preparation of the spectrum testing of bonded Glare repairs for the C-5A Galaxy, a study of the interaction effects of peak loads on bonded repairs and a proposal for the modification of C-5A aft crown spectrum data.* TZ Report, Delft University of Technology.

9. Padmadinata, U.H. (1990), *Investigation of crack-closure prediction models for fatigue in aluminum alloy sheet under flight-simulation loading.* Report LR-619, Delft University of Technology.

10. Schijve, J. (1974), *Fatigue damage accumulation and incompatible crack front orientation.* Eng. Frac. Mech., Vo.6, pp. 245 through 252.

11. AFGROW software can be downloaded from: http://fibec.flight.wpafb.af.mil/fibec/afgrow.html

12. Verhoeven, S. (1998), *In-Service effects on crack growth under bonded composite repairs.* Master Thesis, Delft University of Technology.

13. Jonge, J.B. (1989), *Assessment of service load experience.* National Aerospace Laboratory NLR, Report NLR TP 89097.

14. Fredell, R.S. (1994), *Damage tolerant repair techniques for pressurized aircraft fuselages*. PhD thesis, Delft University of Technology.

APPENDIX A: SURFACE PREPARATIONS

A.1 GRIT BLAST-SILANE PRE-TREATMENT

The grit blast-silane procedure contains the following steps:

- Prepare silane solution. Concentration should be at least 1%, but not exceed 2%. Hydrolyze for 1 hour. Best to use within the next hour but can be used up to 2.5 hours after mixture.
- Clean surface with acetone or MEK until completely clean.
- Scotch Brite surface using de-ionized water (tap or distilled also allowed). Use SB 07447+ (red/fine). Rinse with tap water, use gloves to clean.
- Dry surface and clean with acetone or MEK.
- Grit blast surface with aluminum oxide (50 micron). Use Argon or liquid Nitrogen (40 psi), prevent "zebra stripes". Blow excess grit off, using only gas. Keep between grit blasting and silane preferably 0.5 hour, maximum of 1 hour.
- Brush with silane for at least 10 minutes. Keep wet during silane application, blow off excess silane. Cure in oven for 60 minutes at 200-220 degrees F (preferably just under 212 degrees F).
- Cool panels to maximum of 90 degrees F, preferably room temperature.
- Primer should be at room temperature for usage.
- Apply primer. Thickness should be between 0.1 and 0.2 mils. Let panel with primer dry for 30 minutes to let MEK evaporate.
- Cure primer for one hour at 250 degrees F or 90 minutes at 200 degrees F.
- Before bonding patch, clean primer surface using acetone.

A.2 PAA PRE-TREATMENT

By using an electric current through the adherend via a conductive acid medium, H_3PO_4 for PAA, a stable adherent oxide layer of approximately 0.5 μm is produced. The resulting surface will have a rough, interlocked appearance, see Fig.A.1.

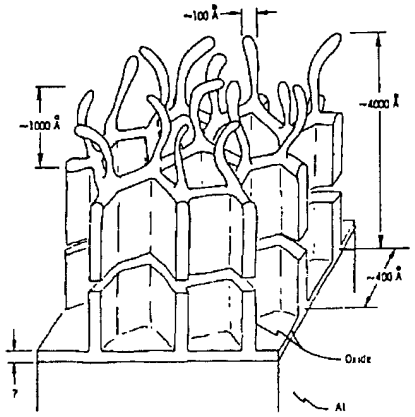

Fig.A.1: Idealized structure of phosphoric acid anodic coating, providing a chemically roughened surface and mechanical interlocking [14].

The PAA (phosphoric acid anodizing) process works as follows:

- Degrease panel in P3RST alkaline degreaser for 30 minutes at 60-65 degrees Celsius.
- Rinse in tap water for 5 minutes.
- Etch in chromic acid (30-55 g/l) and sulfuric acid (150-275 g/l) at 60-65 degrees Celsius for 20 minutes to remove the old oxide layer which was formed uncontrolled.
- Rinse in tap water for 5 minutes.
- Anodize panel at room temperature in the electrolyte (H_3PO_4 100g/l) under 15 volts for 25 minutes. Remove from bath while voltage is still on panel to prevent deterioration of oxide layer after turning off the power. Oxide layer is approximately 0.5 μm thick. This new oxide layer is in a stable form.
- Rinse in tap water for 5 minutes.
- Cytec primer BR-127 should be at room temperature for usage. The primer gives good wetting of the surface of the adherend and because it is epoxy based, it can chemically bond to the adhesive. The primer also prevents corrosion of the bond line by the presence of an amount of chromates in the primer.
- Apply primer. Thickness should be between 0.1 and 0.2 mils. Let panel with primer dry for 30 minutes to let MEK evaporate.
- Cure primer for one hour at 250 degrees F or 90 minutes at 200 degrees F.
- Before bonding patch, clean primer surface using acetone.

APPENDIX B: CRACK GROWTH DATA

This appendix will give all the crack growth information of the specimens tested. Black markers in the graphs indicate the measured data, whereas red lines are the results of curve fitting. Crack size versus Number of blocks as well as da/Block versus crack size will be shown in this appendix. Equations of curve fits used are given as well as the measured data in tabular form.

B.1 SPECIMEN N3

Specimen information

Narrow panel, no patches, maximum compression loads of -100 MPa included in spectrum.

Blocks	Total crack size skin inside tank (mm)	Crack size in stiffener (mm)
0	6.16	13.25
1	6.16	13.5
2	6.41	13.75
3	6.41	13.875
5	6.66	14.5
7	7.66	14.875
9	8.41	15.625
11	9.41	16.5
13	10.66	17.875
15	12.66	[illegible]
17	19.66	
19	24.66	
21	30.66	
23	36.66	
25	43.66	
	[illegible]	

Curve fit for skin crack

4th Degree Polynomial Fit: y=a+bx+cx^2+dx^3+ex^4
Coefficient Data:
a = 5.6613907
b = 0.82471315
c = -0.18026576
d = 0.014923456
e = -0.00026398

Curve fit for stiffener crack

Quadratic Fit: y=a+bx+cx^2
Coefficient Data:
a = 13.38305
b = 0.096670138
c = 0.018240468

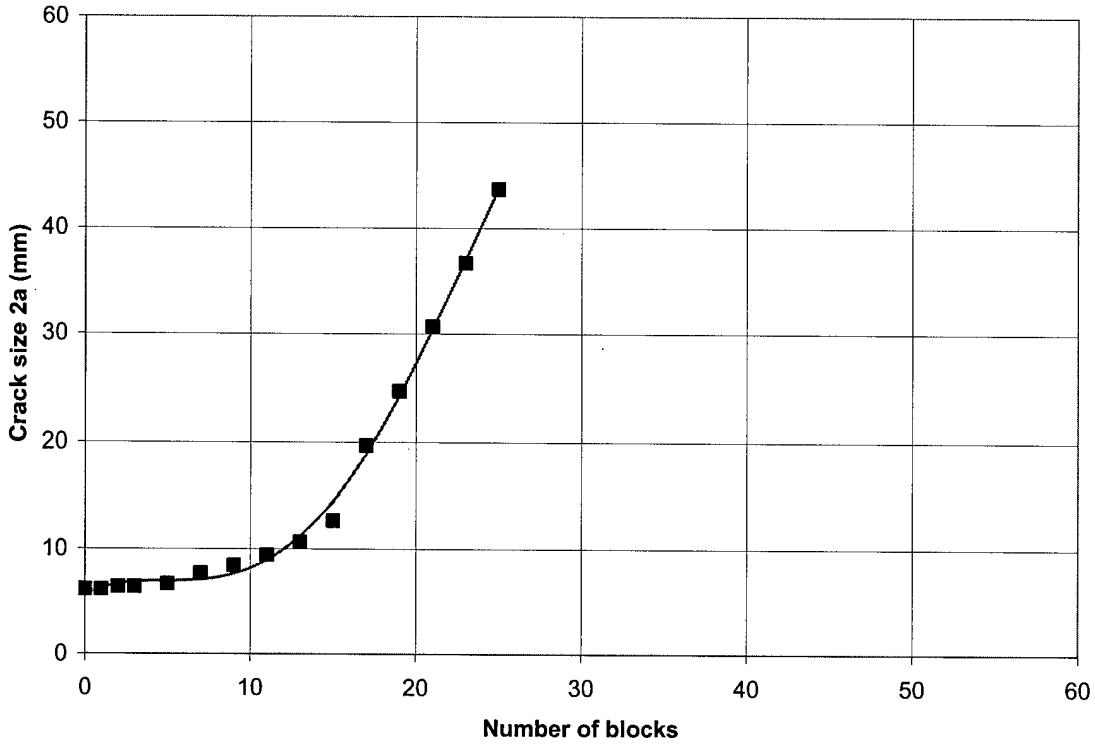

Fig.B.1: Crack size versus number of blocks for skin crack in N3.

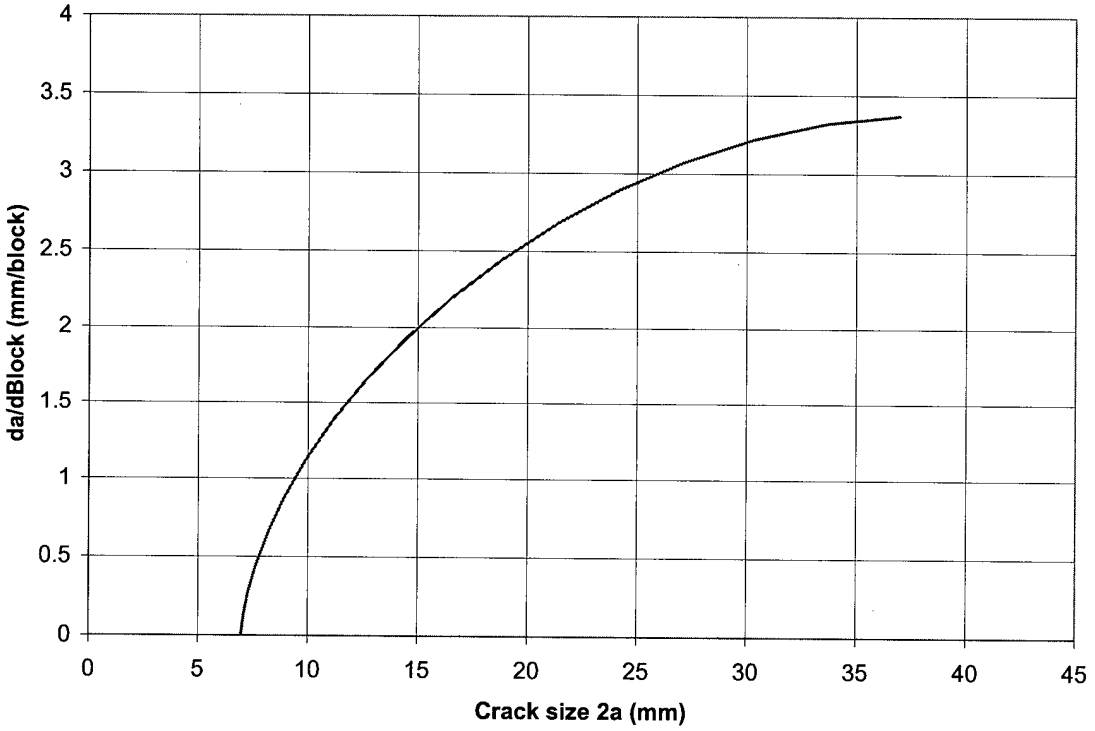

Fig.B.2: Crack growth rates versus crack size for skin crack in N3.

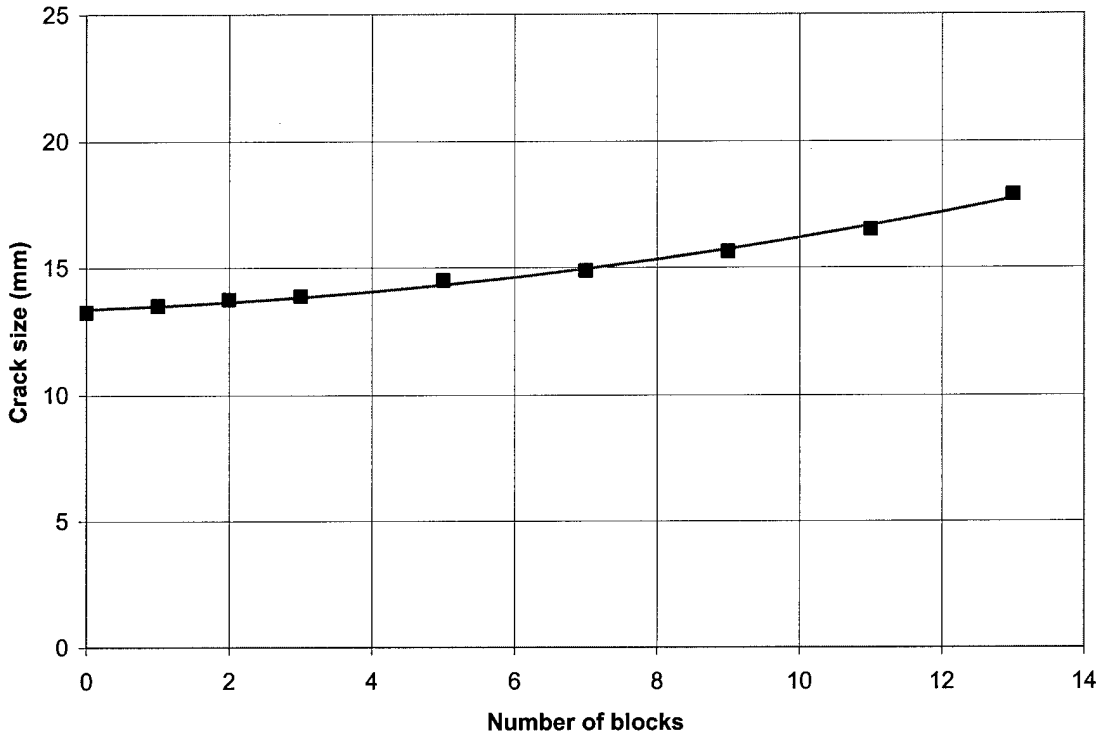

Fig.B.3: Crack size versus number of blocks for stiffener crack in N3.

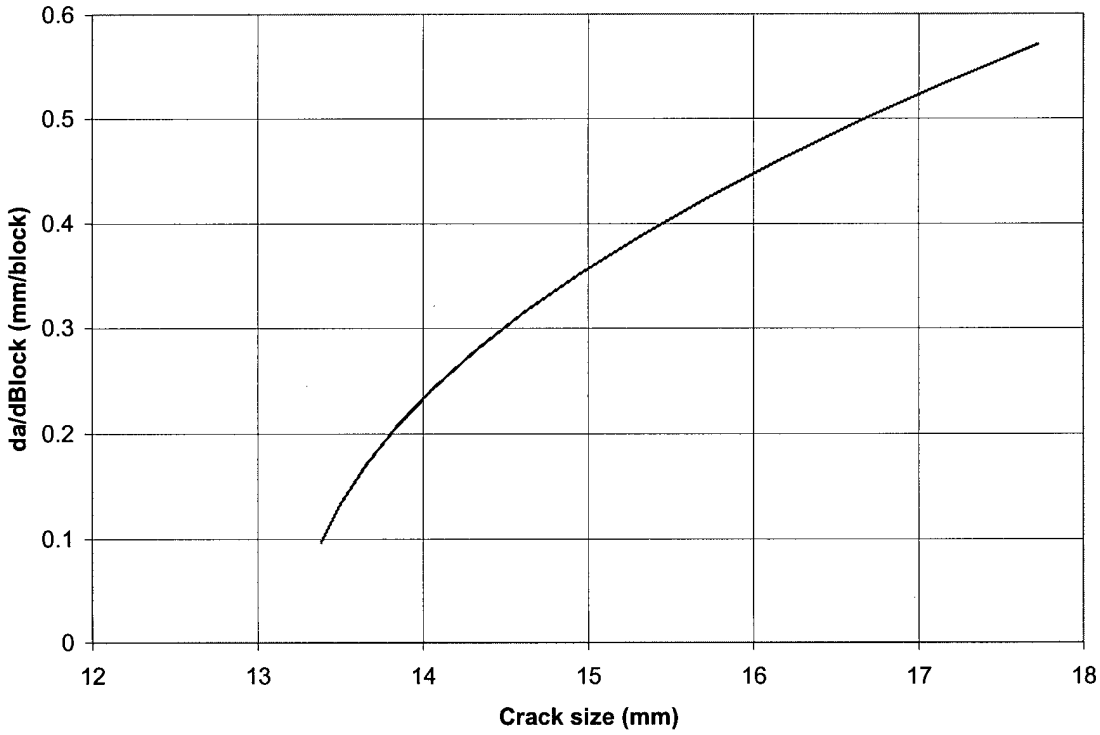

Fig.B.4: Crack growth rates versus crack size for stiffener crack in N3.

B.2 SPECIMEN N4

Specimen information

Narrow panel, no patches, no compression loads in spectrum.

Blocks	Total crack size skin inside tank (mm)	Crack size in stiffener (mm)
0	7.91	13.125
2	8.41	13.125
4	8.66	14
6	9.91	14.375
8	11.16	15
10	11.66	15.125
12	12.66	15.375
14	13.16	16
16	13.91	16.375
18	15.41	16.75
20	16.16	17
22	16.66	18.375
24	18.91	19.125
26	24.16	FAILURE
28	27.16	
30	29.16	
32	31.16	
34	33.16	
36	34.66	
38	36.66	
40	39.16	
42	42.16	
44	44.91	
46	51.16	
	FAILURE	

Curve fit for skin crack

Quadratic Fit: y=a+bx+cx^2
Coefficient Data:
a = 8.0600962
b = 0.14181989
c = 0.016556609

Curve fit for stiffener crack

Quadratic Fit: y=a+bx+cx^2
Coefficient Data:
a = 13.186813
b = 0.14735265
c = 0.00359016

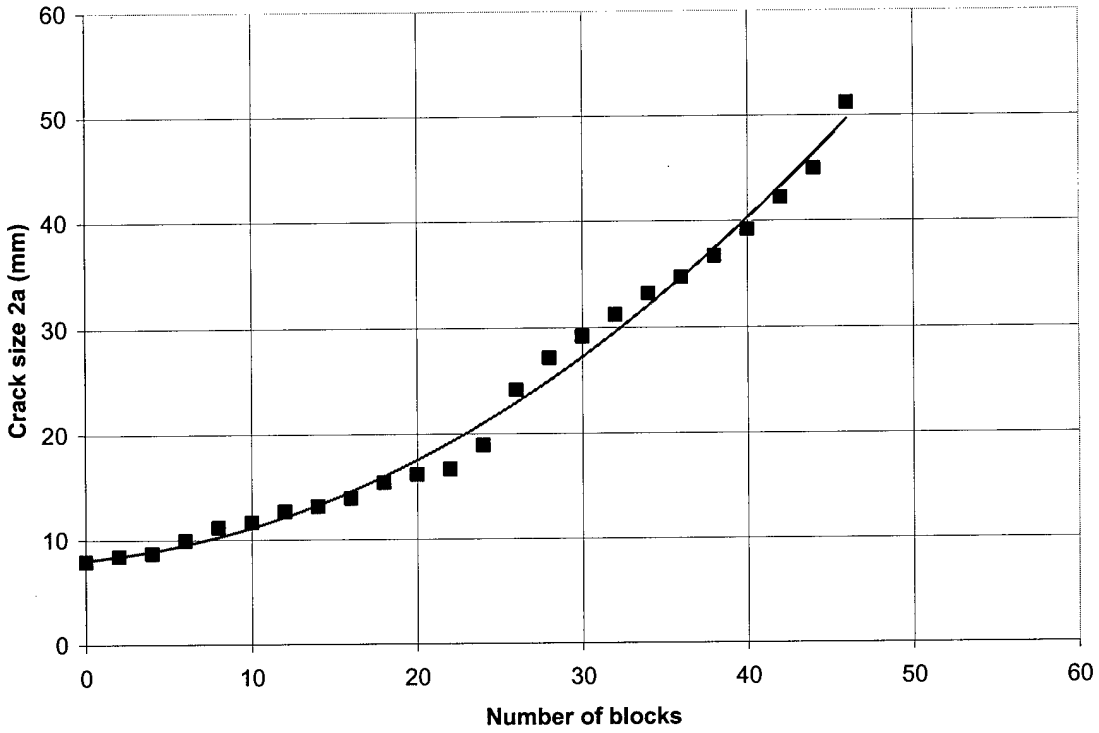

Fig.B.5: Crack size versus number of blocks for skin crack in N4.

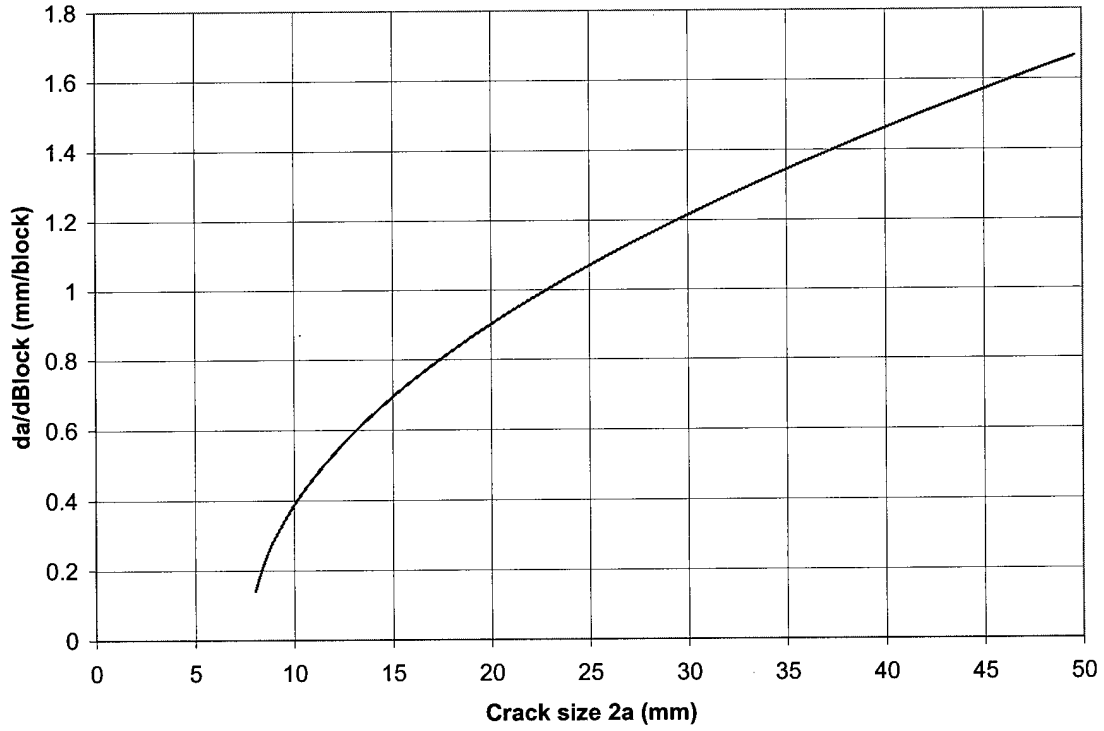

Fig.B.6: Crack growth rates versus crack size for skin crack in N4.

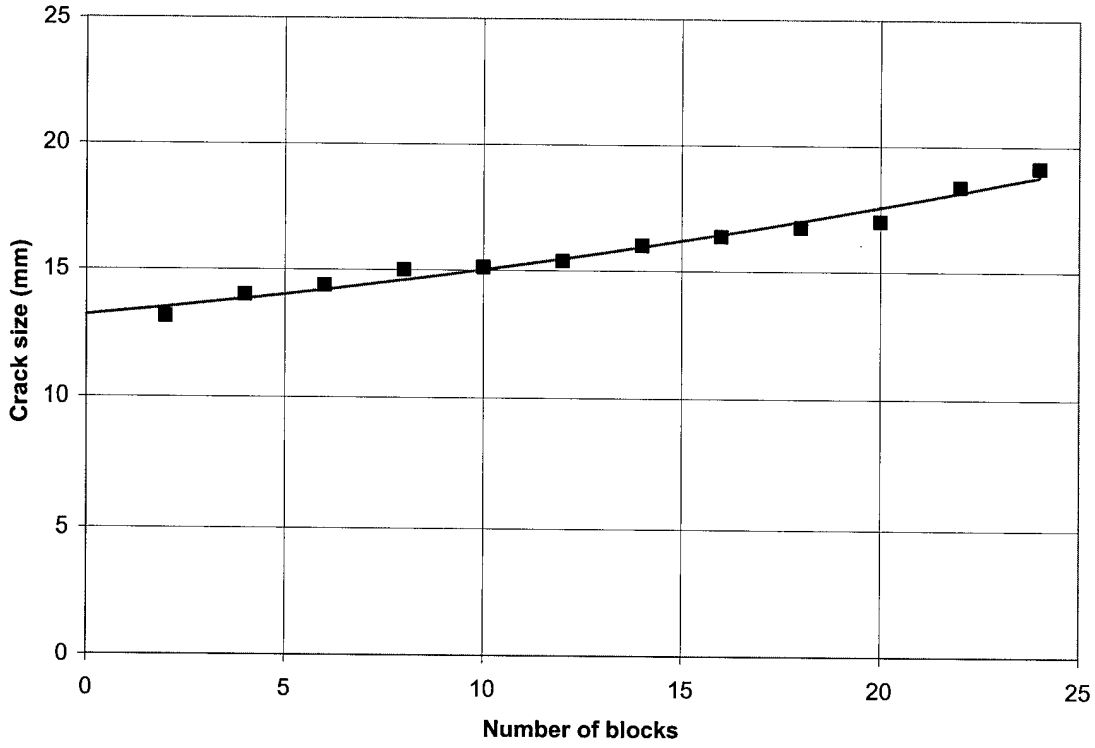

Fig.B.7: Crack size versus number of blocks for stiffener crack in N4.

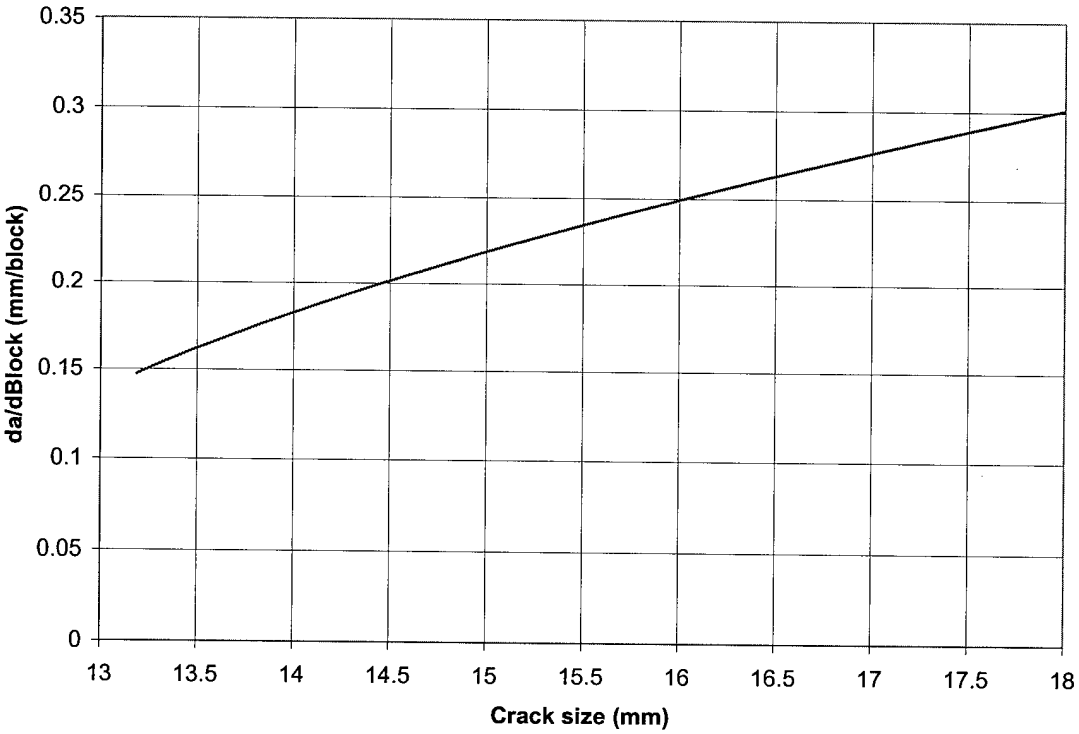

Fig.B.8: Crack growth rates versus crack size for stiffener crack in N4.

B.3 SPECIMEN N5

Specimen information

Narrow panel, boron-epoxy patches, no compression loads in spectrum.

Blocks	Total crack size skin inside tank (mm)
0	12.41
18	13.91
26	14.41
28	14.41
44	14.41
60	14.66

Curve fit for skin crack

Linear Fit: y=a+bx
Coefficient Data:
a = 13.056014
b = 0.033374536

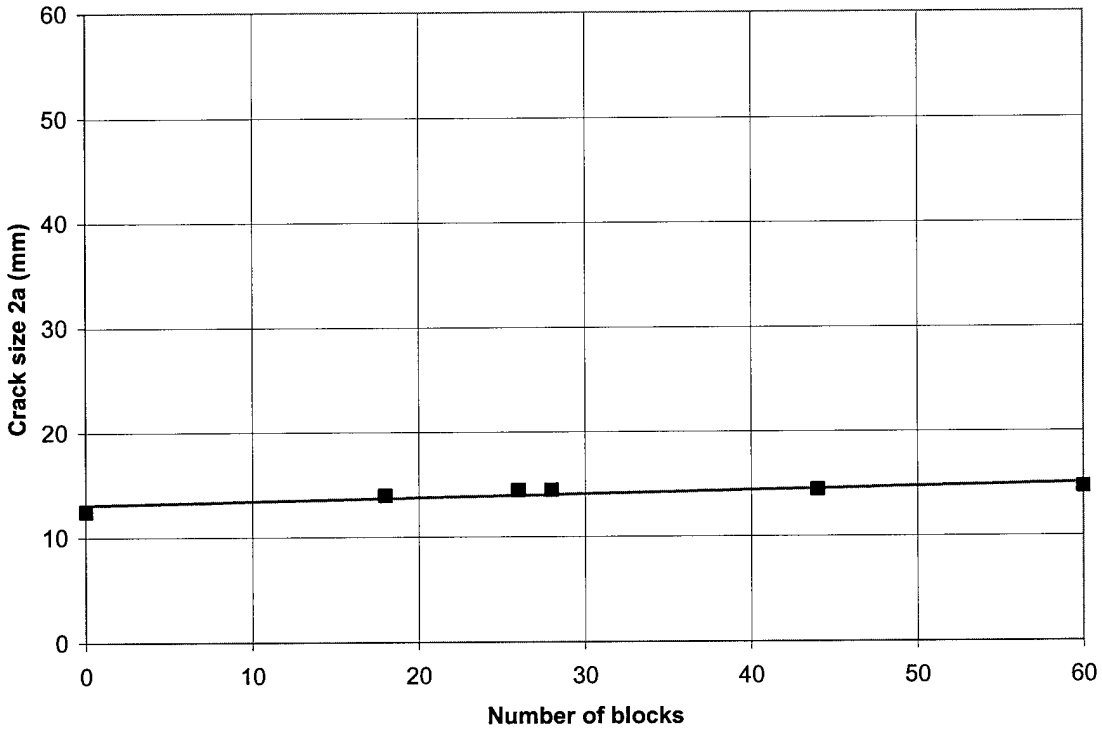

Fig.B.9: Crack size versus number of blocks for skin crack in N5.

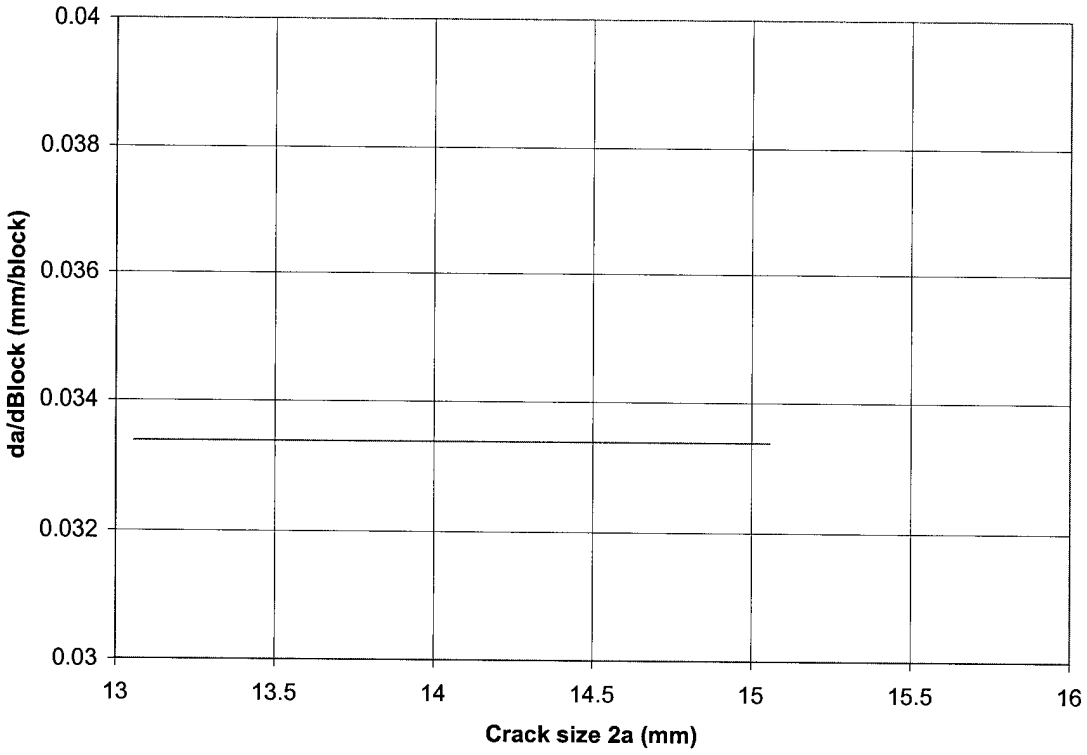

Fig.B.10: Crack growth rates versus crack size for skin crack in N5.

B.4 SPECIMEN N6

Specimen information

Narrow panel, boron-epoxy patches, maximum compression loads of -100 MPa included in spectrum.

Blocks	Total crack size skin inside tank (mm)
0	11.91
4	12.91
8	12.91
18	13.16
23	13.41
28	13.91
29	14.16
39	14.91
45	15.66
47	15.91
48	16.41
60	17.16

Curve fit for skin crack

Linear Fit: y=a+bx
Coefficient Data:
a = 11.958081
b = 0.082874004

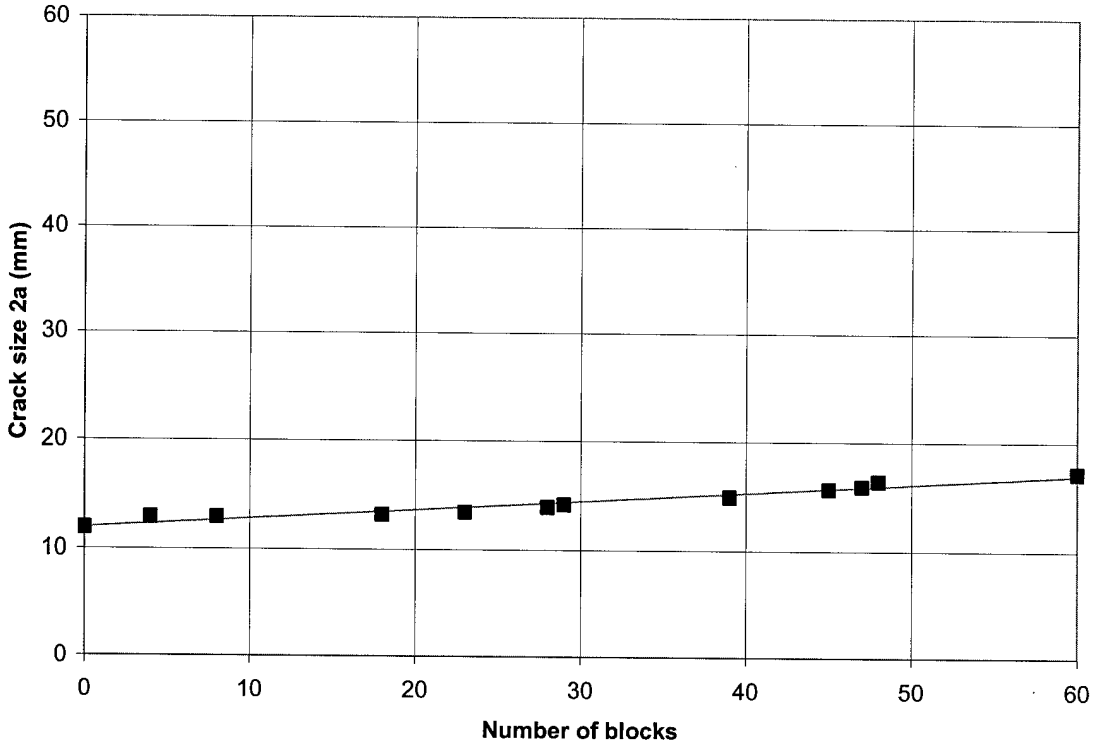

Fig.B.11: Crack size versus number of blocks for skin crack in N6.

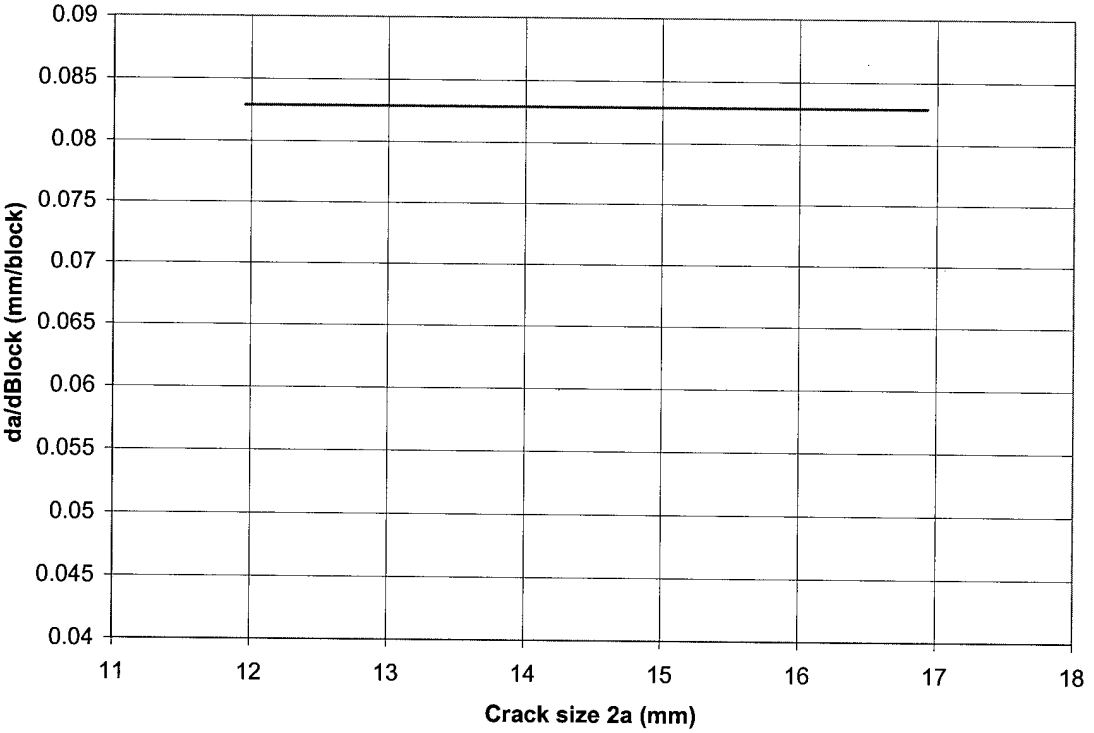

Fig.B.12: Crack growth rates versus crack size for skin crack in N6.

B.5 SPECIMEN N7

Specimen information

Narrow panel, Glare patches, maximum compression loads of -100 MPa included in spectrum.

Blocks	Total crack size skin inside tank (mm)
0	34.16
2	34.66
4	34.66
6	34.66
16	35.76
26	36.96
42	37.66
52	38.76
60	39.46

Curve fit for skin crack

Linear Fit: y=a+bx
Coefficient Data:
a = 34.332385
b = 0.085329498

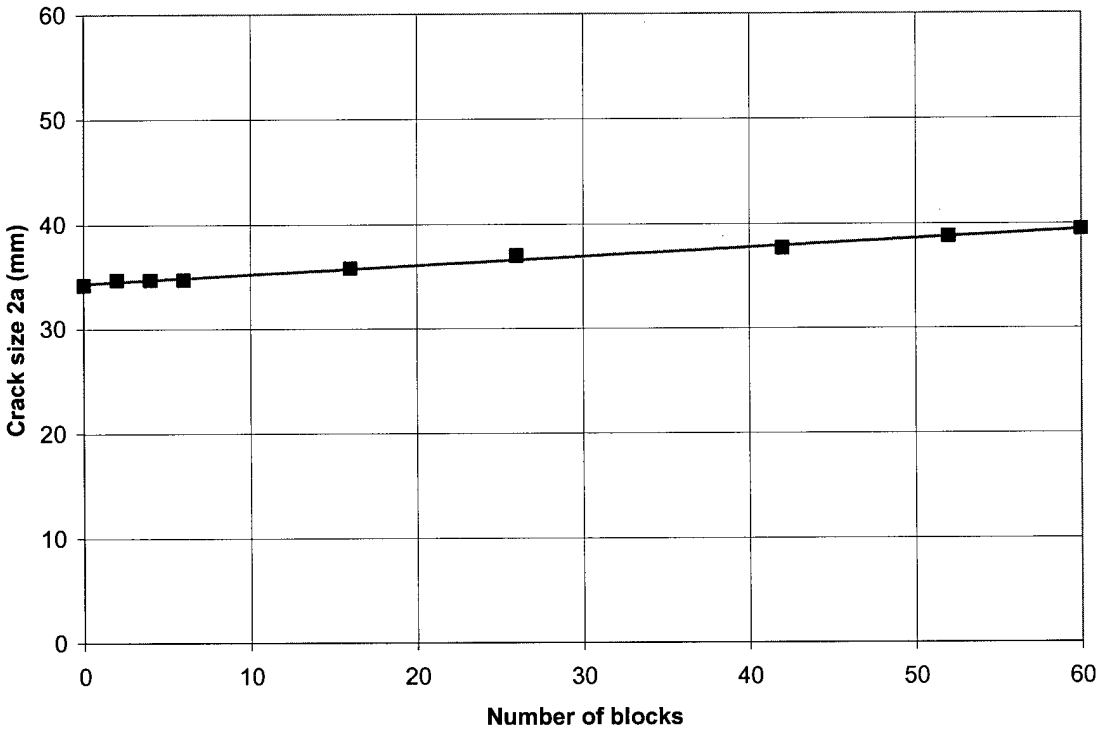

Fig.B.13: Crack size versus number of blocks for skin crack in N7.

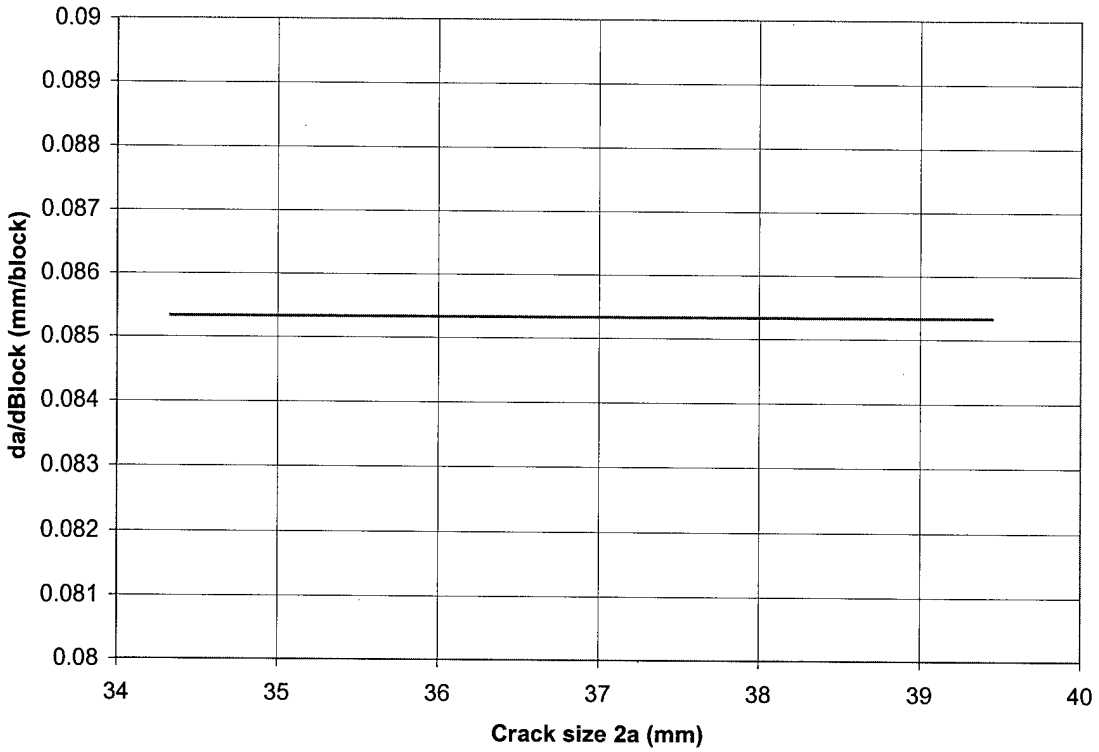

Fig.B.14: Crack growth rates versus crack size for skin crack in N7.

B.6 SPECIMEN N8

Specimen information

Narrow panel, Glare patches, no compression loads in spectrum.

Blocks	Total crack size skin inside tank (mm)
0	34.66
10	35.16
26	36.06
36	37.36
52	38.06
60	38.46

Curve fit for skin crack

Linear Fit: y=a+bx
Coefficient Data:
a = 34.589951
b = 0.066414634

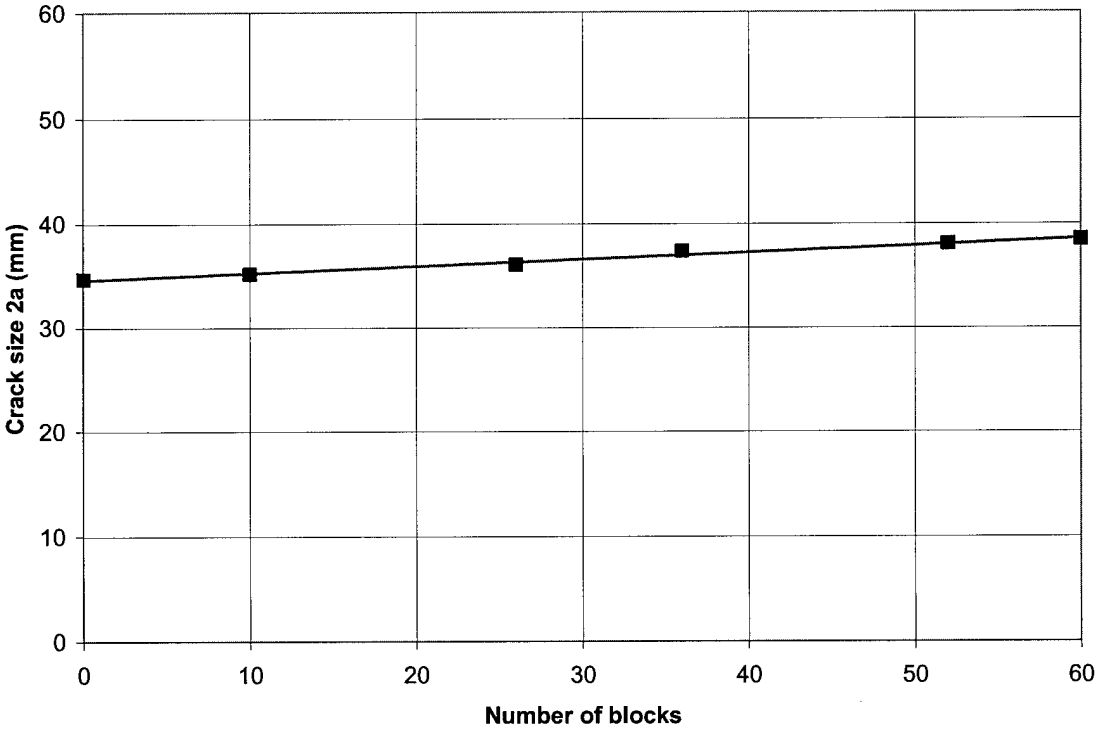

Fig.B.15: Crack size versus number of blocks for skin crack in N8.

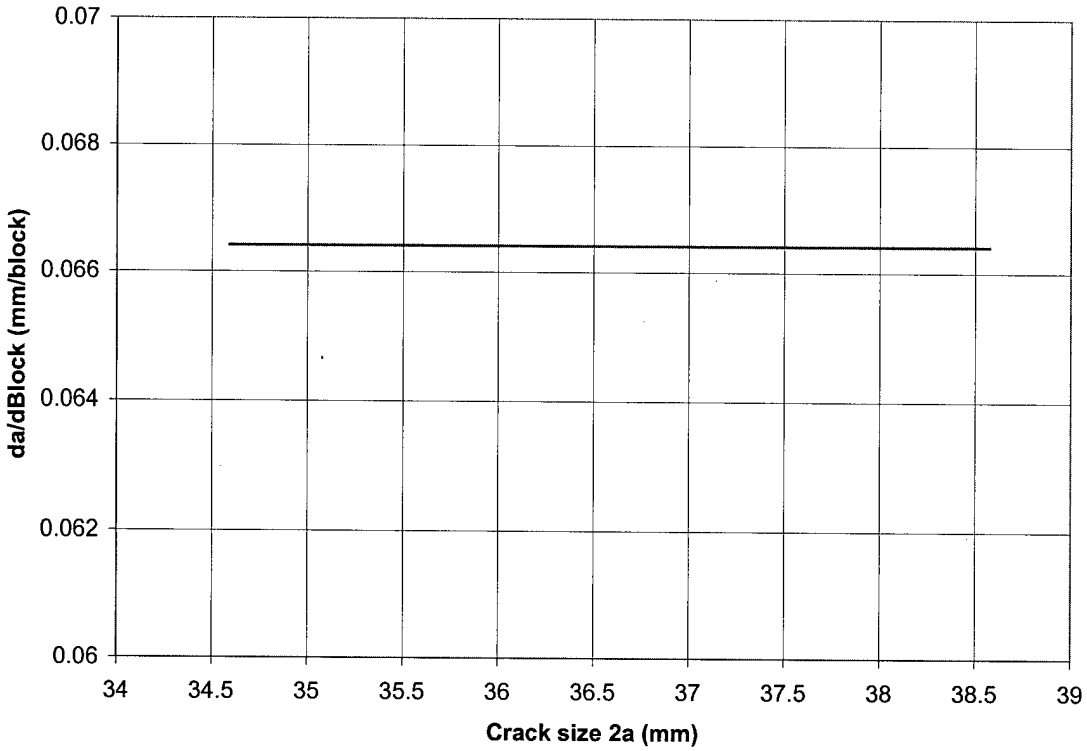

Fig.B.16: Crack growth rates versus crack size for skin crack in N8.

B.7 EXTRA SPECIMEN

Specimen information

Narrow panel, boron-epoxy patches, no compression loads in spectrum.

Blocks	Total crack size skin inside tank (mm)
0	33.96
10	34.46
15	34.86
25	35.36
27	35.46
29	35.66
30	35.76
40	36.46
55	37.06
60	37.26

Curve fit for skin crack

Linear Fit: y=a+bx

Coefficient Data:

a = 33.98278

b = 0.056605496

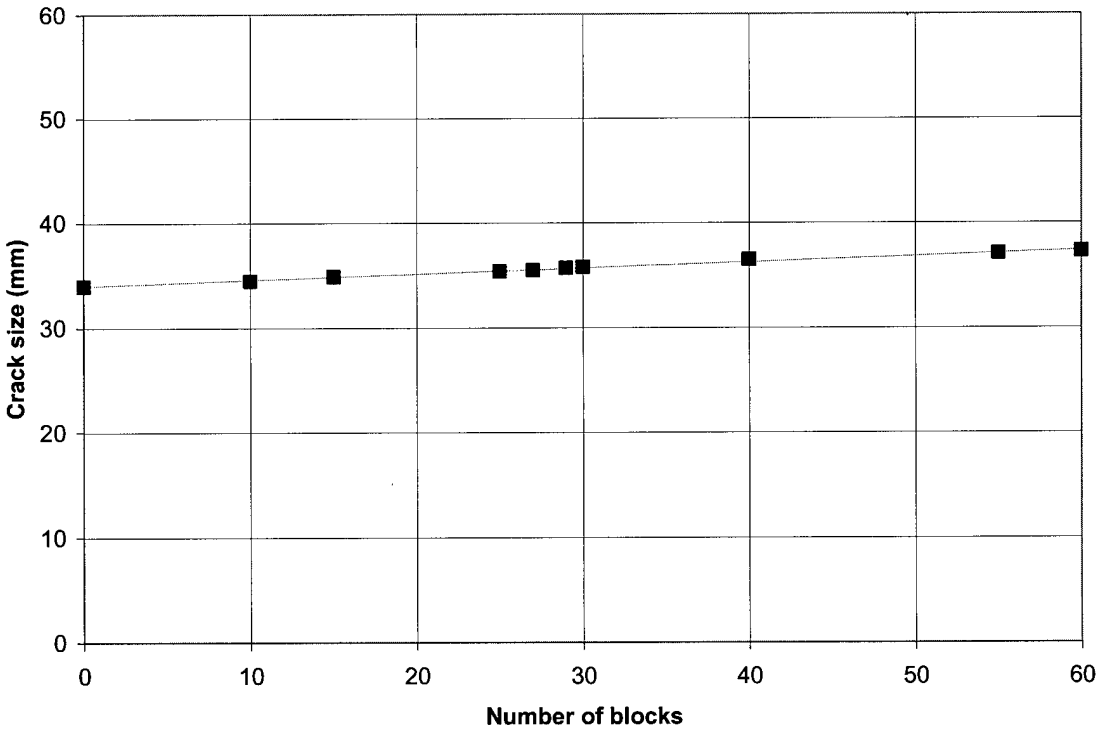

Fig.B.17: Crack size versus number of blocks for skin crack extra specimen.

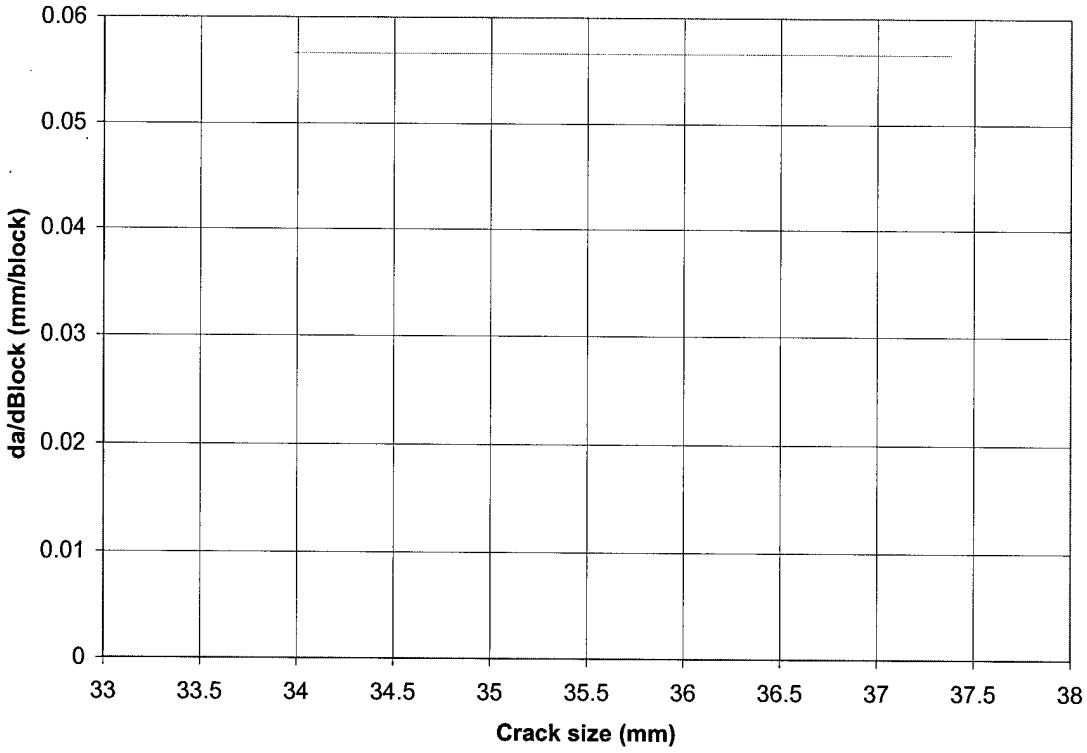

Fig.B.18: Crack growth rates versus crack size for skin crack extra specimen.

B.8 SPECIMEN W2

Specimen information

Wide panel, no patches, no compression loads in spectrum.

Blocks	Total crack size skin inside tank (mm)	Crack size in stiffener (mm)
0	4.66	13.875
1	5.16	13.875
2	5.41	14.375
3	5.66	14.5
4	5.91	14.5
5	6.16	14.75
6	6.41	14.875
7	6.66	15.375
8	7.41	16
9	7.91	16.25
10	8.16	16.75
11	8.41	16.75
12	8.66	17.125
13	8.66	17.5
14	9.16	18
16	10.66	18.25
17	11.16	18.5
19	12.66	19.75
21	13.66	
26	17.16	
29	19.41	
37	23.16	
40	25.16	
50	36.66	
60	43.66	

Curve fit for skin crack

Quadratic Fit: y=a+bx+cx^2
Coefficient Data:
a = 4.5309834
b = 0.29726436
c = 0.006149551

Curve fit for stiffener crack

Linear Fit: y=a+bx
Coefficient Data:
a = 13.489123
b = 0.30697955

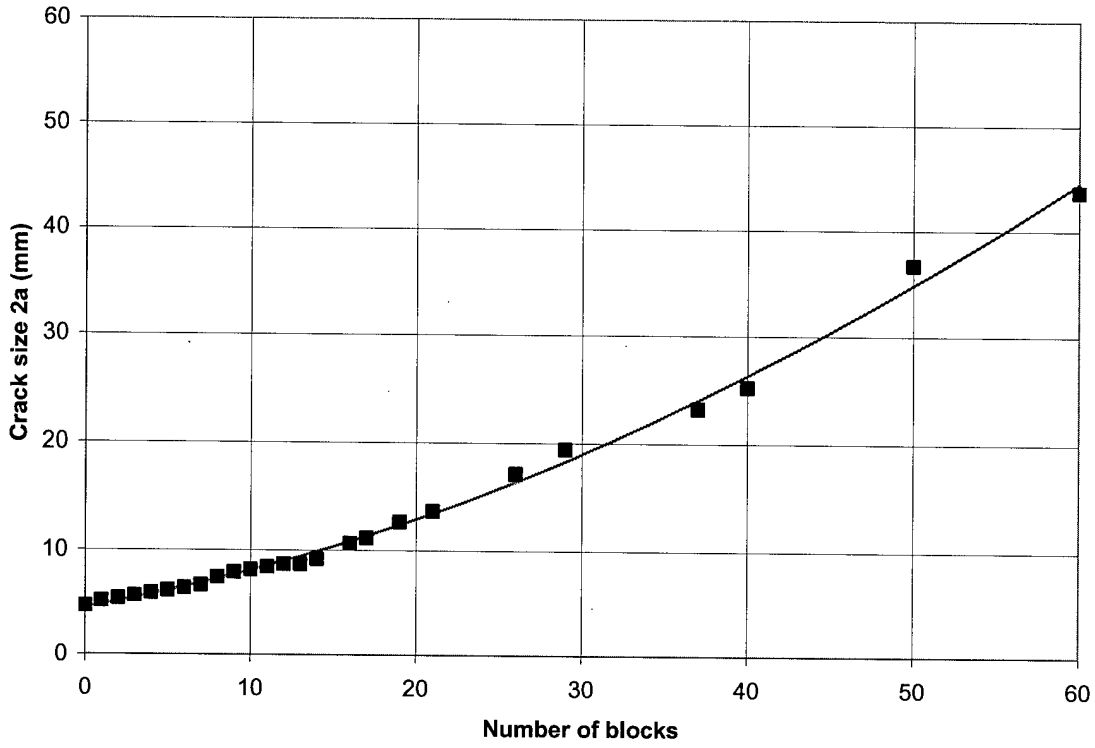

Fig.B.19: Crack size versus number of blocks for skin crack in W2.

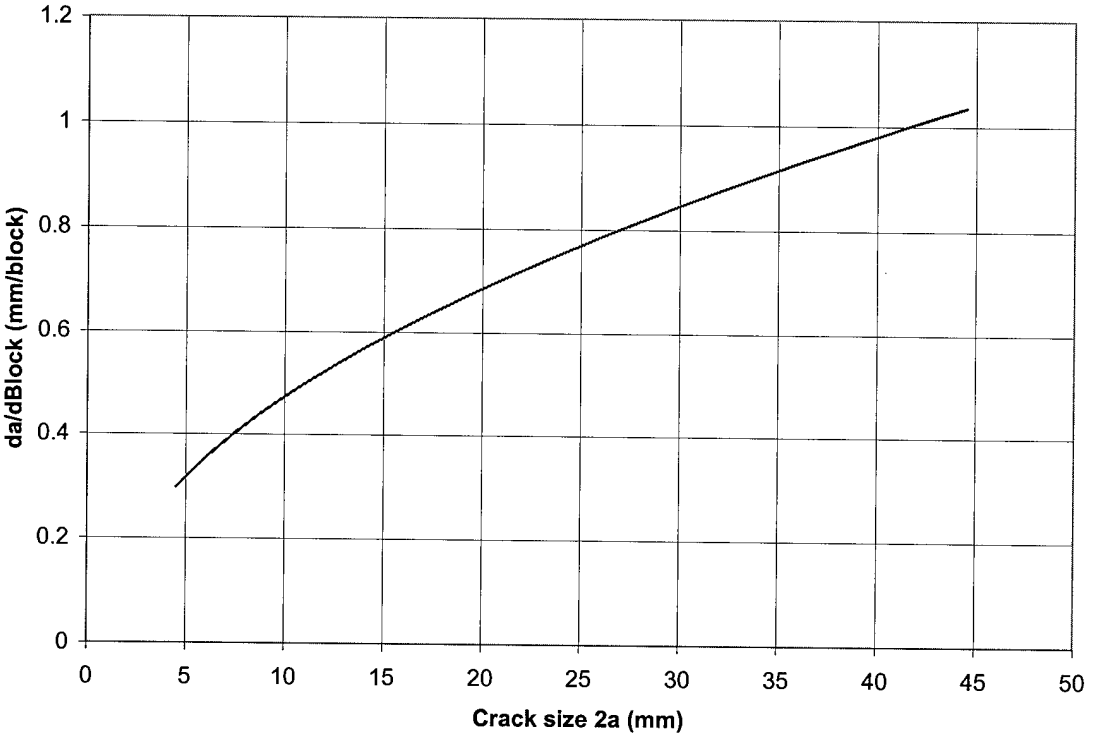

Fig.B.20: Crack growth rates versus crack size for skin crack in W2.

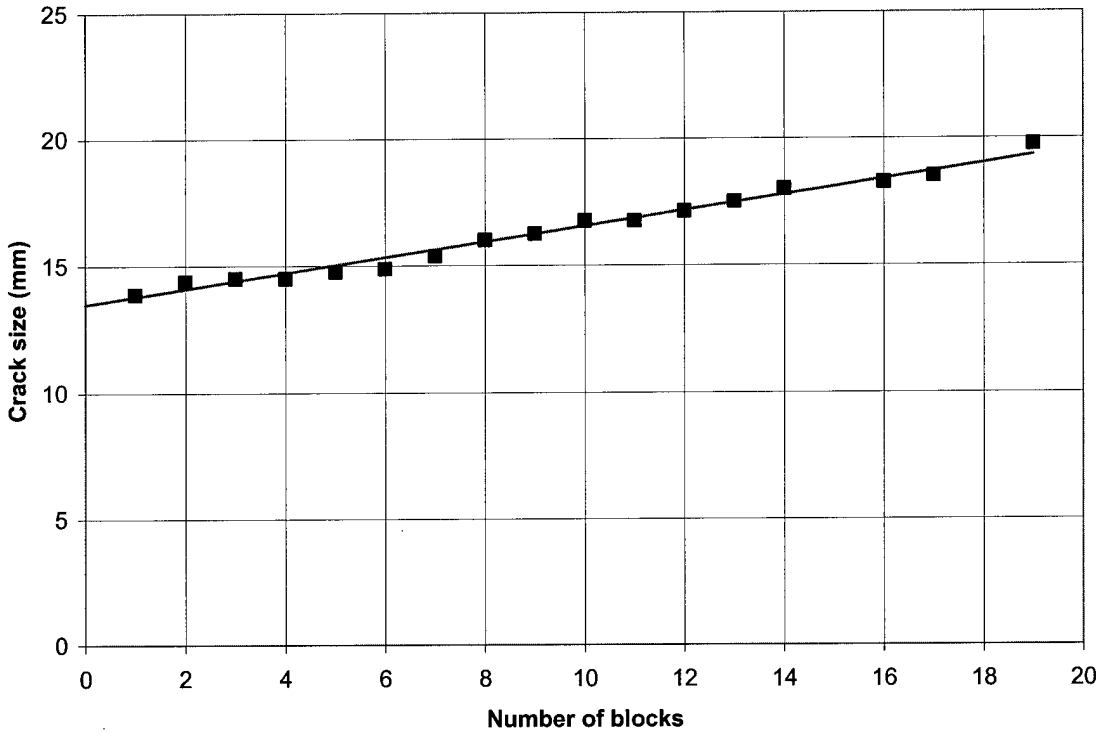

Fig.B.21: Crack size versus number of blocks for stiffener crack in W2.

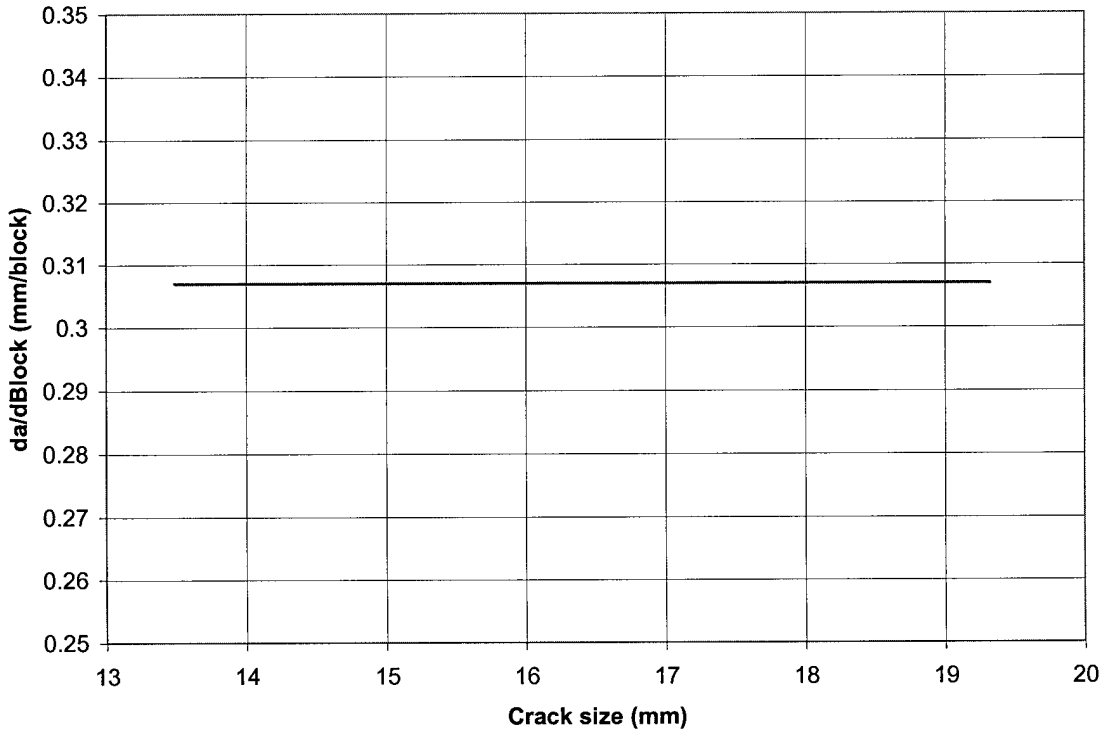

Fig.B.22: Crack growth rates versus crack size for stiffener crack in W2.

B.9 SPECIMEN W3

Specimen information

Wide panel, no patches, maximum compression loads of -40 MPa included in spectrum.

Blocks	Total crack size skin inside tank (mm)	Crack size in stiffener (mm)
0	34.66	15.25
1	36.76	15.625
2	38.96	16.25
3	41.46	17.25
4	44.06	18.25
5	46.06	19.375
6	50.06	FAILURE
8	55.56	
10	60.56	
14	70.86	
18	80.36	
22	92.36	

Curve fit for skin crack

Linear Fit: y=a+bx
Coefficient Data:
a = 33.926744
b = 2.6300975

Curve fit for stiffener crack

Quadratic Fit: y=a+bx+cx^2
Coefficient Data:
a = 15.205357
b = 0.37410714
c = 0.09375

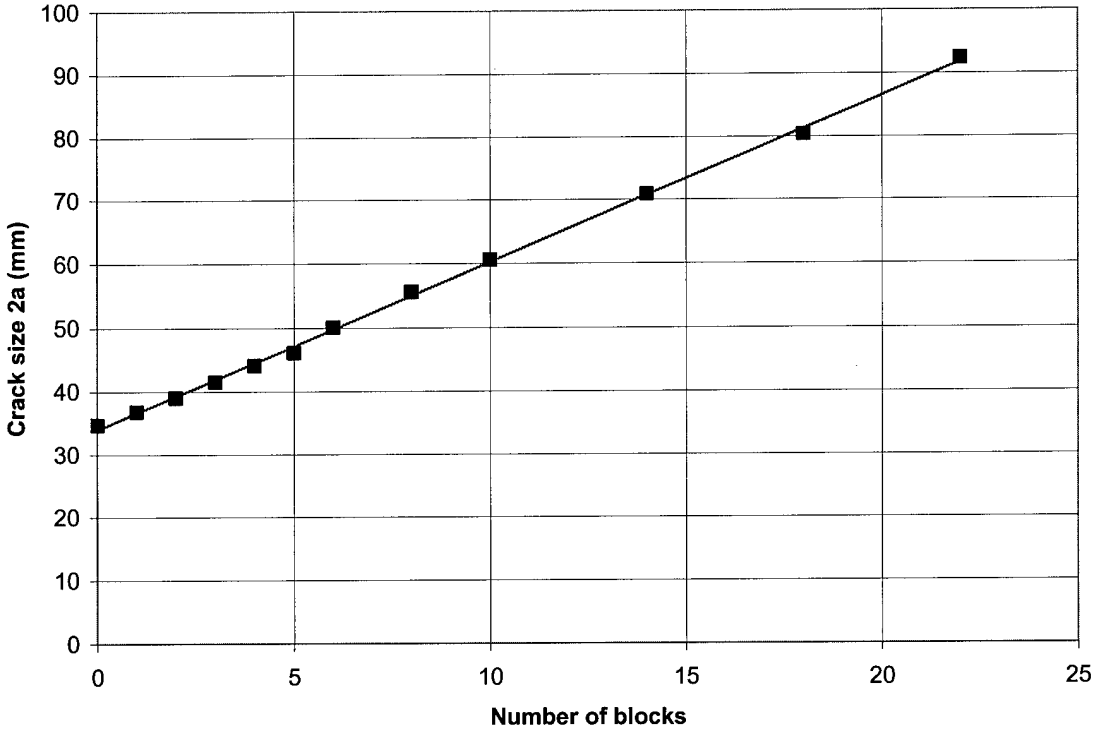

Fig.B.23: Crack size versus number of blocks for skin crack in W3.

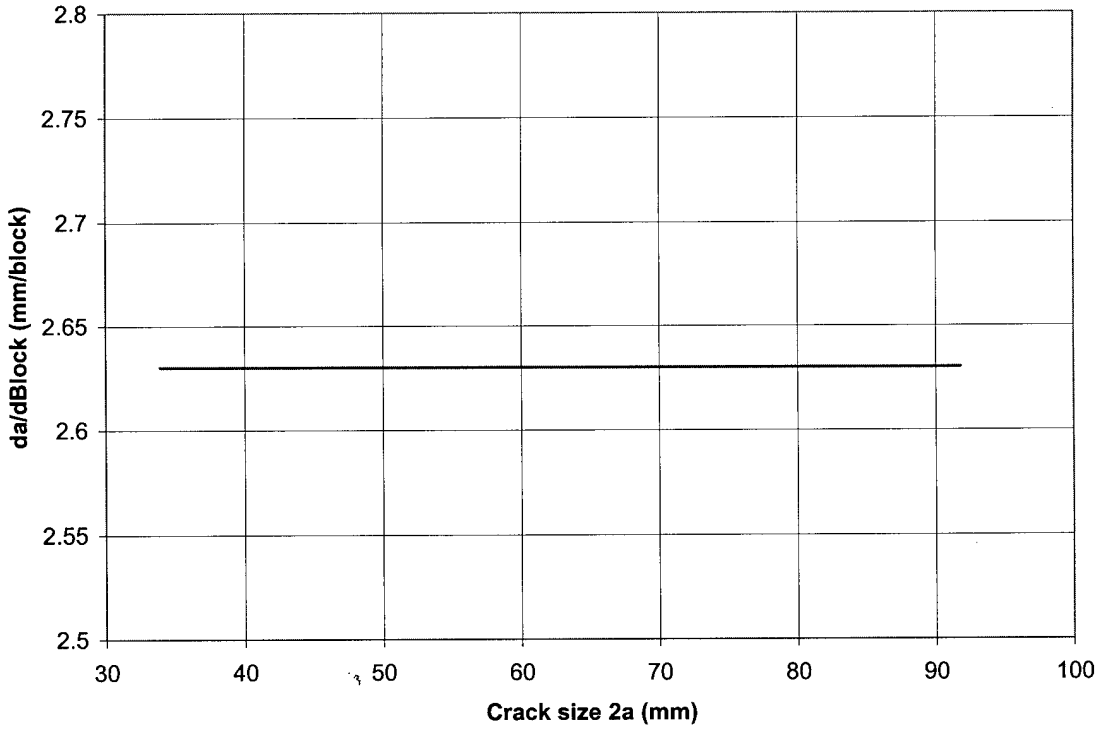

Fig.B.24: Crack growth rates versus crack size for skin crack in W3.

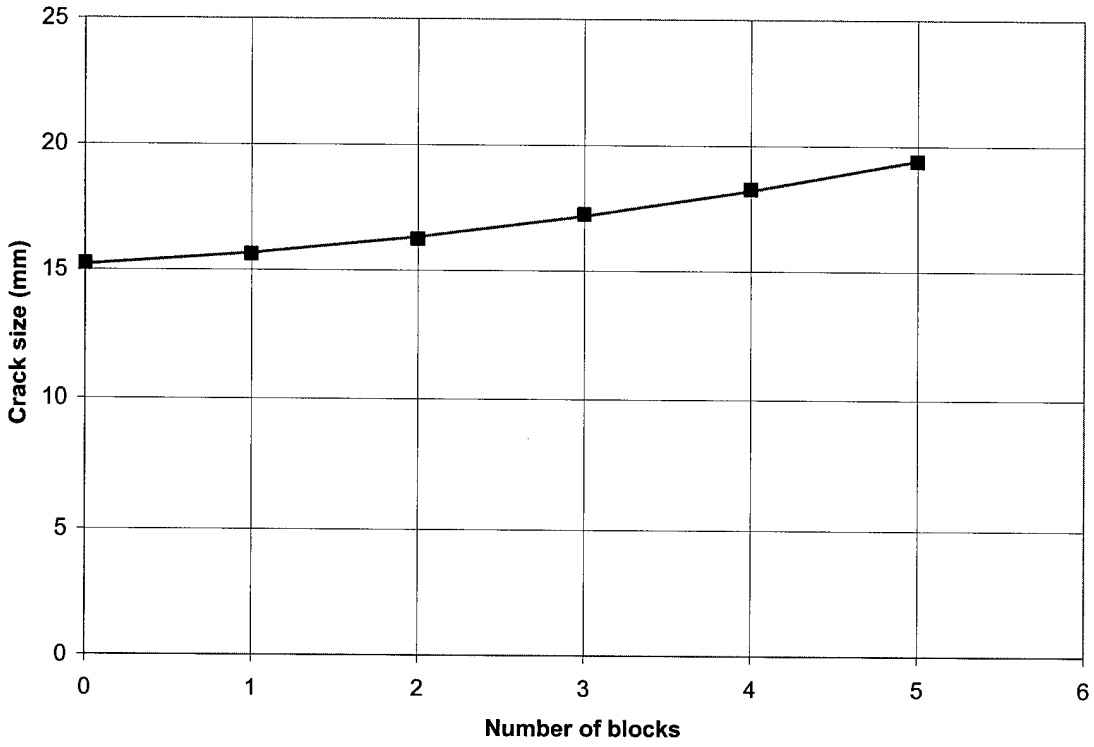

Fig.B.25: Crack size versus number of blocks for stiffener crack in W3.

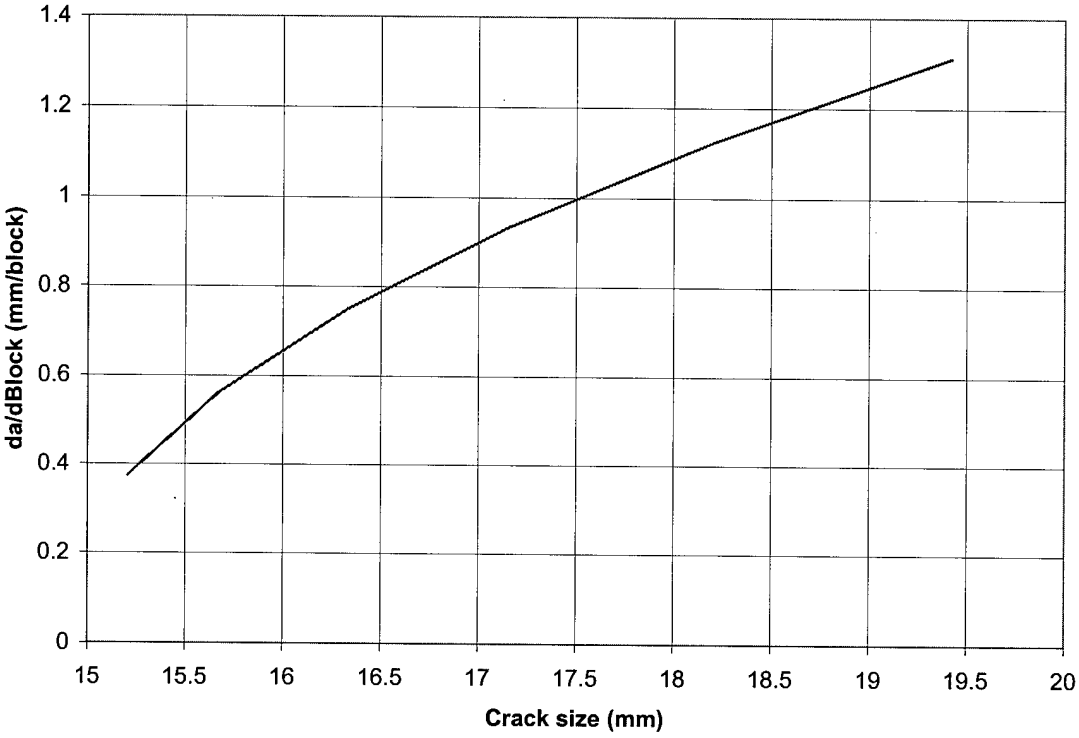

Fig.B.26: Crack growth rates versus crack size for stiffener crack in W3.

B.10 SPECIMEN W4

Specimen information

Wide panel, boron-epoxy patches, maximum compression loads of -40 MPa included in spectrum.

Blocks	Total crack size skin inside tank (mm)
0	10.66
20	12.96
30	13.06
50	14.06
60	14.96

Curve fit for skin crack

Linear Fit: y=a+bx
Coefficient Data:
a = 11.045965
b = 0.065438596

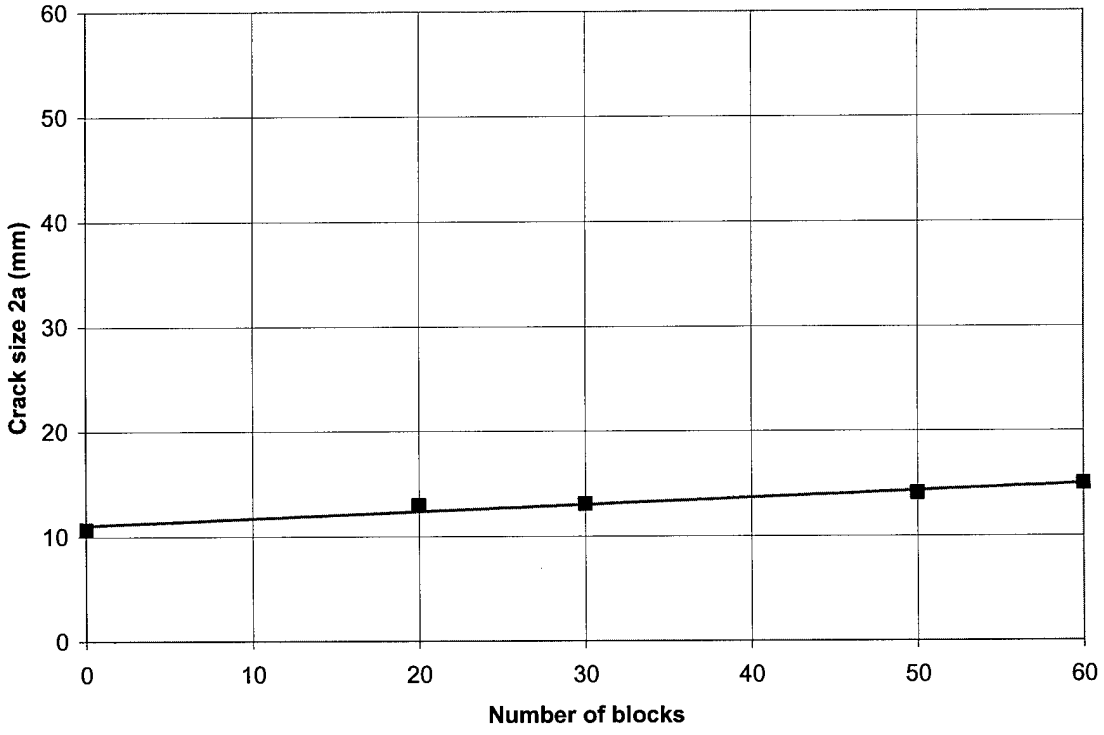

Fig.B.27: Crack size versus number of blocks for skin crack in W4.

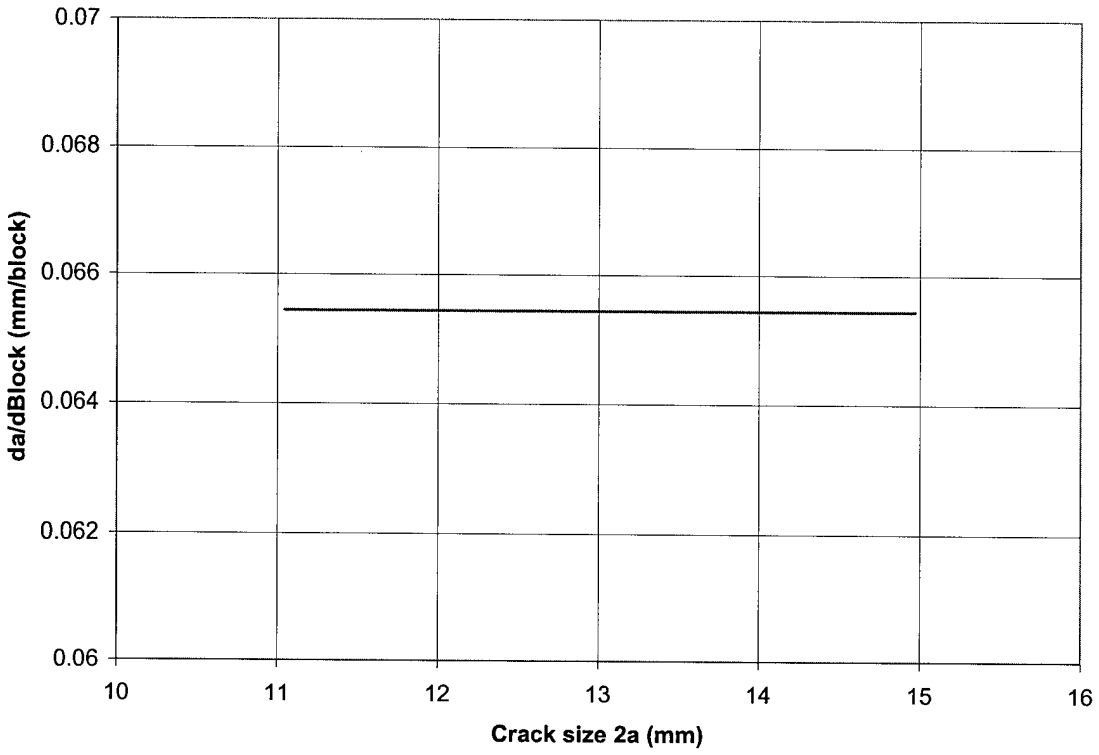

Fig.B.28: Crack growth rates versus crack size for skin crack in W4.

B.11 SPECIMEN W5

Specimen information

Wide panel, boron-epoxy patches, no compression loads in spectrum.

Blocks	Total crack size skin inside tank (mm)
0	10.66
1	10.86
3	11.06
5	11.06
25	11.86
26	12.26
30	12.26
34	12.86
56	13.36
60	13.36

Curve fit for skin crack

Linear Fit: y=a+bx
Coefficient Data:
a = 10.866593
b = 0.045558608

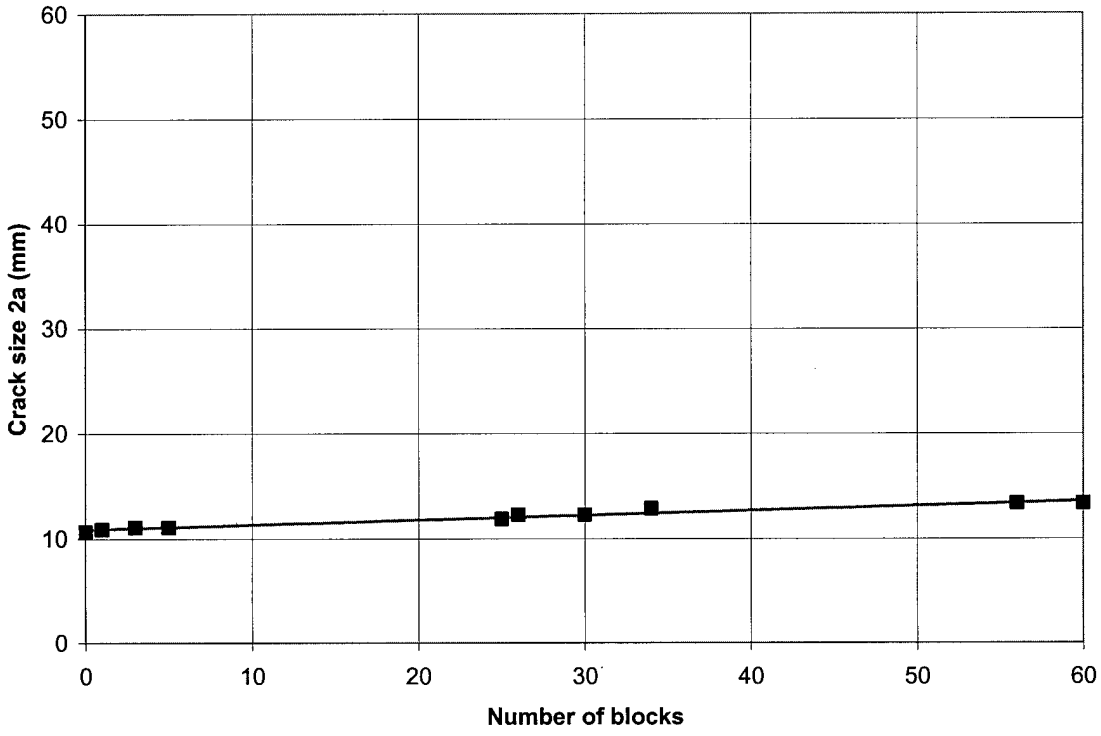

Fig.B.29: Crack size versus number of blocks for skin crack in W5.

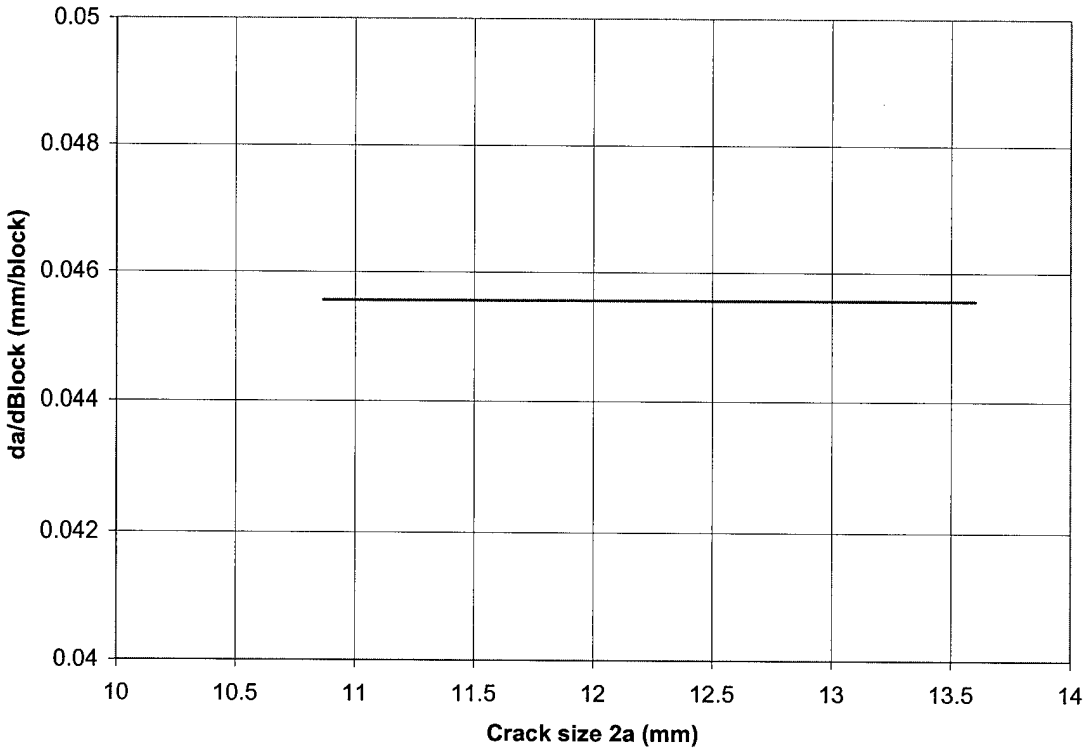

Fig.B.30: Crack growth rates versus crack size for skin crack in W5.

B.12 SPECIMEN W6

Specimen information

Wide panel, Glare patches, maximum compression loads of -40 MPa included in spectrum.

Blocks	Total crack size skin inside tank (mm)
0	26.66
15	28.16
30	29.96
40	30.86
60	32.86

Curve fit for skin crack

Linear Fit: y=a+bx
Coefficient Data:
a = 26.680991
b = 0.10410377

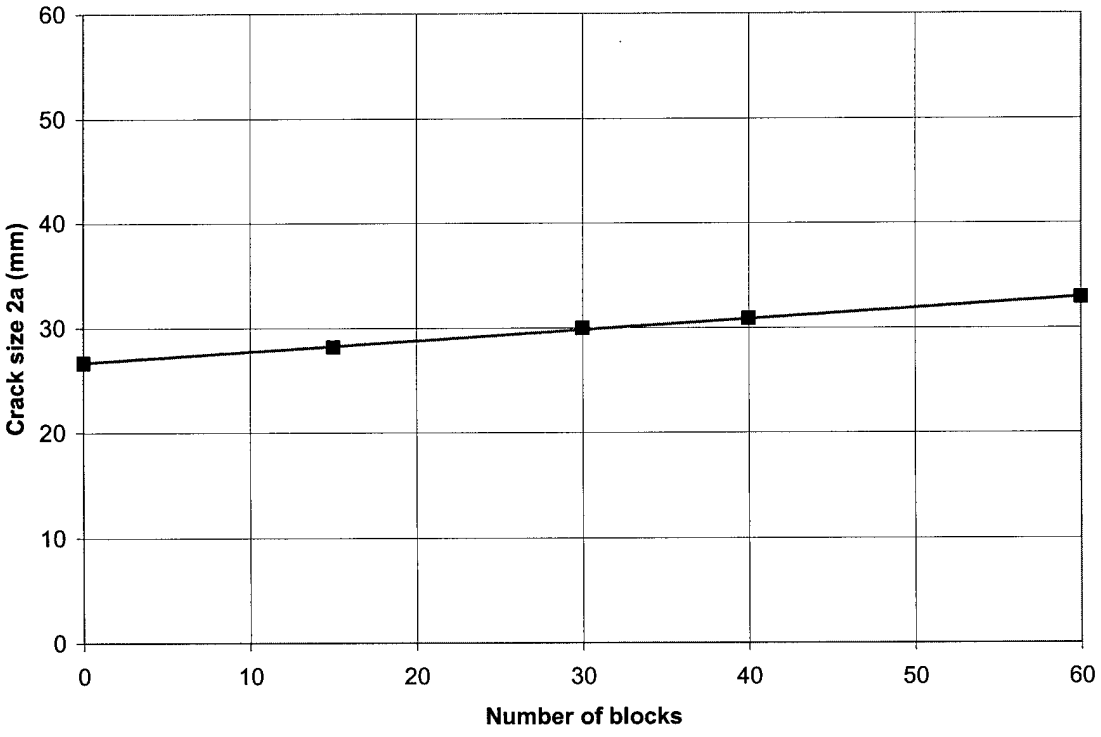

Fig.B.31: Crack size versus number of blocks for skin crack in W6.

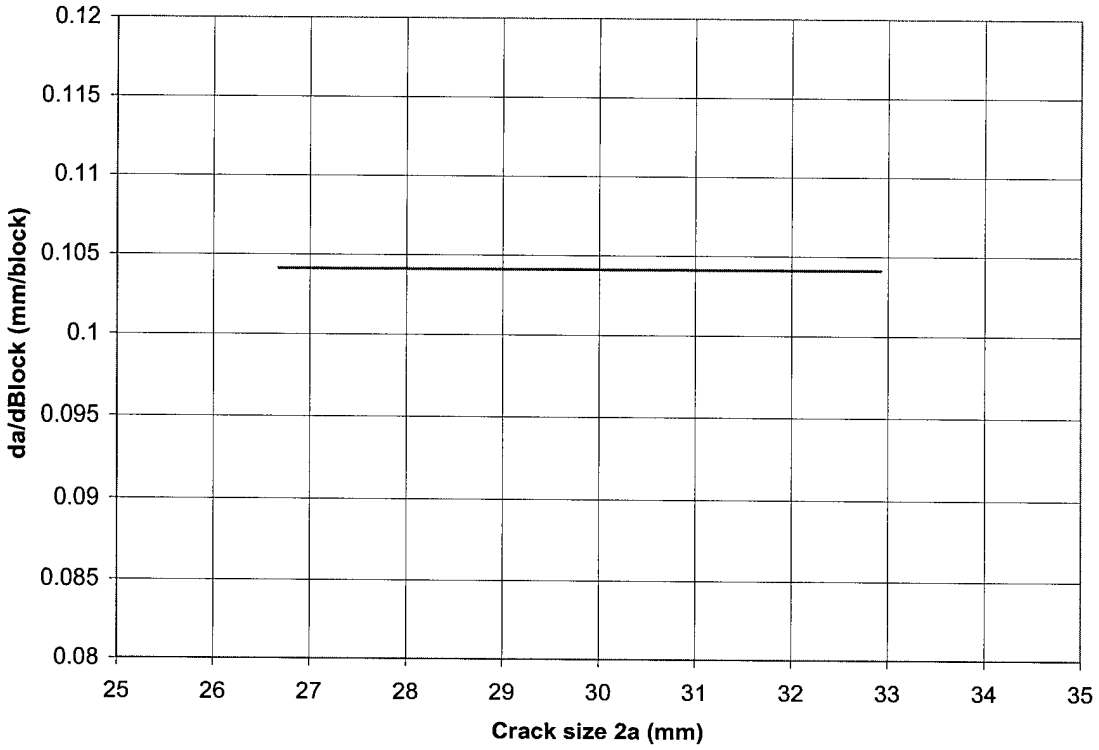

Fig.B.32: Crack growth rates versus crack size for skin crack in W6.

B.13 SPECIMEN W7

Specimen information

Wide panel, Glare patches, no compression loads in spectrum.

Blocks	Total crack size skin inside tank (mm)
0	22.16
20	23.16
40	24.86
60	26.56

Curve fit for skin crack

Linear Fit: y=a+bx
Coefficient Data:
a = 21.95
b = 0.0745

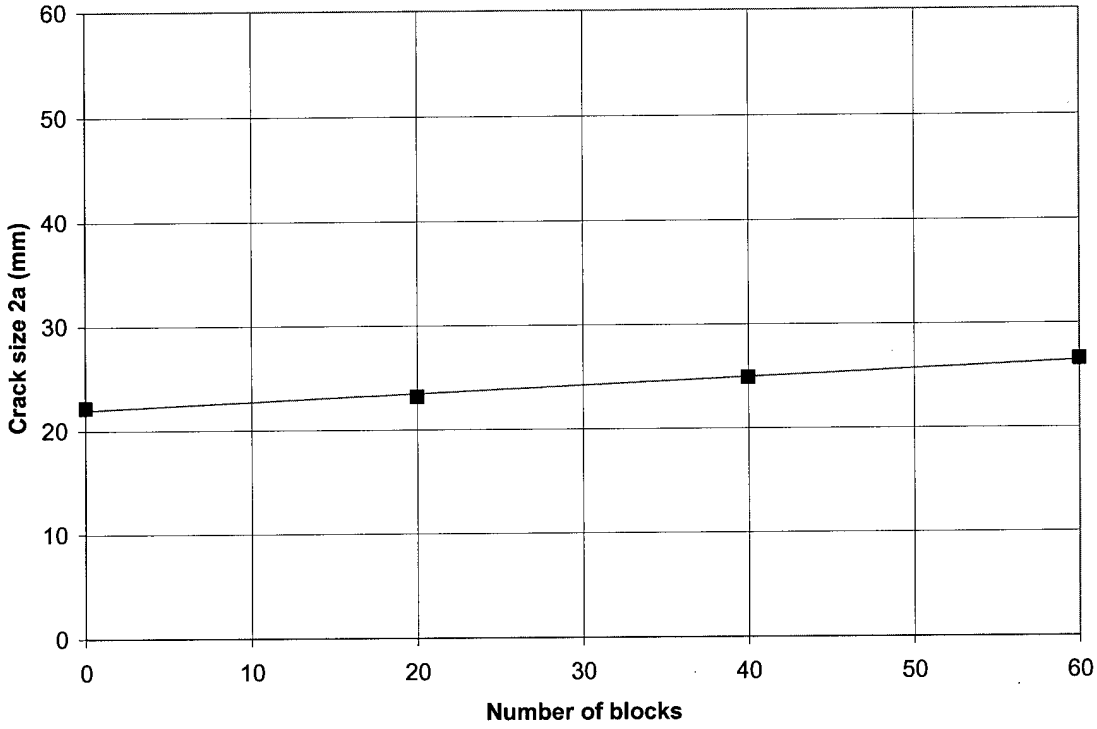

Fig.B.33: Crack size versus number of blocks for skin crack in W7.

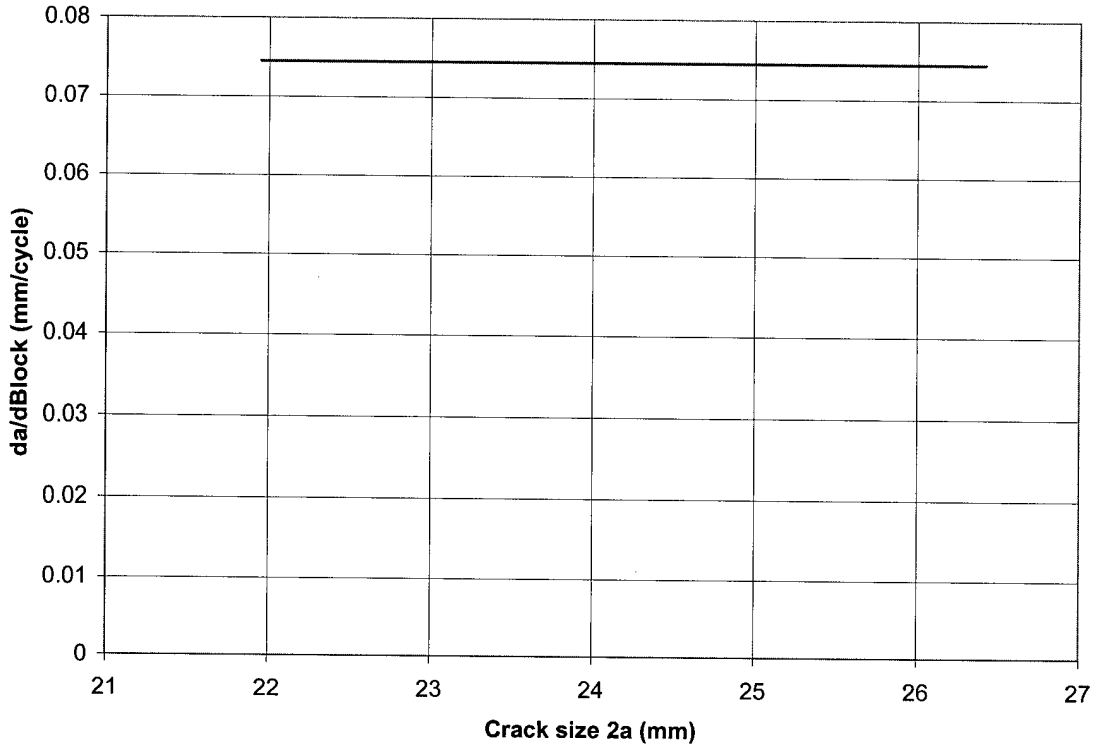

Fig.B.34: Crack growth rates versus crack size for skin crack in W7.